SPATIOTEMPORAL DYNAMICS OF INORGANIC PHOSPHATE DISTRIBUTION

IN ARABIDOPSIS THALIANA ROOTS

A Dissertation

by

ABIRA SAHU

Submitted to the Office of Graduate and Professional Studies of
Texas A&M University
in partial fulfillment of the requirements for the degree of

DOCTOR OF PHILOSOPHY

Chair of Committee,	Wayne Versaw
Committee Members,	L. Rene Garcia
	Thomas D. McKnight
	Brian D. Shaw
Head of Department,	Thomas D. McKnight

August 2020

Major Subject: Biology

ABSTRACT

Inorganic phosphate (Pi) is an essential nutrient that plants must acquire from soil via their roots and then distribute to all other organs, cells, and subcellular organelles to sustain growth and development. However, Pi limits worldwide crop productivity due to its low bioavailability. Because Pi mined for fertilizers is a finite and nonrenewable resource, a comprehensive understanding of how plants acquire, store, recycle, and distribute this nutrient is urgently needed to develop crops that maintain high yields with minimal Pi input. In this work, I used genetically encoded Forster Resonance Energy Transfer (FRET)-based biosensors and confocal microscopy to measure Pi concentrations in *Arabidopsis thaliana* roots with high spatial and temporal resolution. I found distinct spatial patterns for Pi uptake, recycling, and vacuolar sequestration. These processes were distinguished through the novel use of cyanide and mutant comparisons. Cyanide blocked Pi assimilation into ATP to reveal a rapid increase in cytosolic Pi concentration due to metabolic recycling. Additional gains in cytosolic Pi levels were detected upon addition of exogenous Pi and I attributed these to uptake. Similar experiments conducted with a vacuolar Pi transport mutant, *pht5;1*, (defect in vacuolar uptake) suggested that less Pi sequestration occurs in cells of the transition zone than in cells of the flanking developmental zones. Thus, I demonstrated that developmental control of vacuolar Pi sequestration is a major determinant of the steady-state Pi distribution pattern in root cytosol. Additionally, I measured relative ATP levels and dynamics in different root developmental zones, which confirmed a correlation between cytosolic Pi and ATP levels. I also analyzed cytosolic Pi dynamics in root hairs, which revealed that Pi gradients exist in root hairs with highest Pi levels at the tip. I

showed that this gradient is established through high Pi uptake and low vacuolar sequestration at the hair tip.

DEDICATION

To my family and friends who made this possible

ACKNOWLEDGEMENTS

I would like to thank my advisor Dr. Wayne Versaw for giving me an opportunity to pursue my PhD research in his lab. He has been an incredible mentor and this would not have been possible without his constant guidance and support. I would also like to thank my committee members Dr. Rene Garcia, Dr. Thomas McKnight, and Dr. Brian Shaw for their suggestions, guidance and encouragement.

I would like to thank my lab members Dr. Swayoma Banerjee and Dr. Jing Shi for being extremely patient with me in my first year in the lab and teaching me lab techniques and imaging. I would also like to thank Dr. Swayoma Banerjee for being a great friend. Thanks to Aditi S. Raju for her help and cooperation. I also extend my thanks to members of the Plant Biology Journal Club for their valuable feedback on my research.

Thanks to my graduate advisors Dr. Arne Lekven and Dr. Rene Garcia for their support. I am also thankful to our graduate coordinator, Ms. Jennifer Bradford, for being the extremely caring and affectionate person that she is. Graduate school can be tough for various reasons but she made a lot of things much easier and simpler.

I am thankful to my parents without whose support I would not have been able to get through this. Thanks to my Dida and Mama for their continuous encouragement. I would like to specially mention my friend Satwik for being a fabulous companion and also guiding me in doing statistical analyses of my experiments. Finally, I thank my friends in College Station who made my days at Texas A&M fun and memorable.

CONTRIBUTORS AND FUNDING SOURCES

Contributors

This work was supervised by a dissertation committee consisting of Dr. Wayne K Versaw [advisor], Dr. L. Rene Garcia and Dr. Thomas D. McKnight of Department of Biology, and Dr. Brian Shaw of Department of Plant Pathology.

Experiments for figures 6, 7, 8, 9 and 10 described in Chapter 2 were performed by Dr. Swayoma Banerjee. These figures are adapted from her doctoral dissertation (1) with her permission.

All other work conducted for the dissertation was completed by the student independently.

Funding Sources

This work was supported by the Department of Energy (DE-SC0014037). Its contents are solely the responsibility of the authors and do not necessarily represent the official views of the Department of Energy.

TABLE OF CONTENTS

LIST OF FIGURES

LIST OF TABLES

Page

CHAPTER I

INTRODUCTION AND REVIEW OF LITERATURE

1.1 Role of inorganic phosphate (Pi) in plant growth and metabolism

Inorganic phosphate (Pi) is an essential macronutrient that constitutes 0.2% of plant dry weight, and it is a component of nucleic acids, phospholipids and ATP (2). Pi is therefore crucial for cell division, membrane synthesis, redox reactions, enzyme regulation, and cell signaling (2). It is also essential for regulating photosynthesis and carbon metabolism. During the light reactions of photosynthesis, ADP and Pi are combined via photophosphorylation to form ATP, which is used to fuel CO_2 assimilation and the Calvin-Benson cycle. Ultimately, these processes produce reduced carbon molecules that can be transported to other organs, broken down to release energy, or stored as starch for later use. Thus, plants need a continuous supply of Pi to maintain carbon fixation and myriad other cellular metabolic processes. However, 80% of phosphorus exists in soil in the form of insoluble inorganic salts like $AlPO_4$ and $FePO_4$, and organic compounds like phytate and lecithin, rendering it inaccessible to plants (3). Hence, Pi concentrations available to plants are very low (< 10 μM) in most arable land (3). Moreover, Pi has a low diffusion coefficient in soil (10^{-12} to 10^{-15} m^2 s^{-1}) (2). As a result, an unequal balance between high Pi uptake rates and low diffusion rates of Pi in soil creates a zone of depletion in the rhizosphere. This depletion may be circumvented through the application of Pi fertilizers. However, these fertilizers are derived from rock phosphate, which is a finite and non-renewable resource. It is predicted that a peak in global phosphorus production will be reached by 2033 after which it will sharply decline (4). Also, leaching of excess Pi causes eutrophication in aquatic ecosystems (4). Therefore, it is important to gain a comprehensive understanding of how

plants acquire and use Pi so that we can then develop economically and environmentally sustainable strategies to generate crops with high Pi use efficiency.

1.2 Route of Pi from soil to cells

Pi is acquired from soil via a family of Pi transporters located on the plasma membrane of root epidermal cells (5-8). It is then rapidly assimilated into ATP by oxidative and substrate-level phosphorylation (9). ATP hydrolysis is then used to energize biosynthetic reactions for production of other macromolecules and metabolites. Pi is recycled from these metabolites at varied rates and magnitudes. Pi is also stored in vacuoles and remobilized during Pi starvation to buffer cytosolic Pi (10). Thus, Pi uptake, recycling, and organellar sequestration must be integrated to maintain homeostasis and thereby sustain cellular activities.

1.2.1 Pi acquisition from soil

Pi can exist in multiple ionic forms, $H_2PO_4^-$, HPO_4^{2-}, and PO_4^{3-}, depending on pH. At pH 5-6, which is typical of most soils (11), Pi exists predominantly as $H_2PO_4^-$, and this is the ionic form that plants transport across the plasma membrane (2, 12, 13). $H_2PO_4^-$ partially dissociates in the cytosol (pH 7.3) to yield nearly equal amounts of $H_2PO_4^-$ and HPO_4^{2-} given that the relevant pKa is ~7. Cellular Pi concentrations range from 5-20 mM, while its concentration in soil solution is typically just 2 -10 μM (3). Consequently, Pi must be transported across the plasma membrane against a steep concentration gradient. This is achieved by co-transport of Pi with H^+, referred to as symport, where the proton electrochemical gradient provides the energy to drive the thermodynamically-unfavorable uptake of Pi (11). This Pi uptake is mediated by members of the PHT1 family of transporters located at the root-soil interface.

In *Arabidopsis thaliana*, the PHT1 transporter family consists of 9 members, PHT1;1 through PHT1;9. Although some PHT1 proteins can be detected in aerials organs, e.g., leaves

and flowers, *in situ* hybridization and immunoblot analyses indicate that most are present in the root epidermis, root cap, tips of lateral roots, and root hairs (8, 14-16). Translational fusions of PHT1 proteins with GFP are located in the plasma membrane (17-19) where they mediate Pi/H^+ co-transport with the stoichiometry of 2-4 H^+ per Pi ion (12, 20, 21). PHT1 proteins contain 12 membrane-spanning domains that can be subdivided into two groups of 6, linked by a hydrophilic loop (22). These transporters are regulated both transcriptionally and post-transcriptionally. Pi-deficiency increases transcription of PHT1 transporter genes, whereas they are expressed at basal levels in Pi-replete conditions (15, 16, 23). Functional analyses of mutants *pht1;1* and *pht1;4* using radioactivity assays showed reduced rates of Pi uptake under both high- and low-Pi regimes suggesting that the effected transporters are vital for Pi uptake (5, 15). Similar results were observed in triple, quadruple and quintuple *pht1* mutants combined with RNAi or mutations (*phf1*) that prevent targeting of PHT1 proteins to the plasma membrane (6). PHF1 is an endoplasmic reticulum (ER)-localized protein that is necessary for intracellular trafficking of PHT1 proteins (17). Impaired Pi uptake in *phf1* mutants highlights post-translational regulation of PHT1 proteins (17, 18). This mutant has also been used to study the role of the root cap in Pi uptake by merging radioactivity assays with light transmission micrographs (24), which demonstrated that the root cap provides a large fraction of total Pi uptake in Arabidopsis roots.

1.2.2 Fate of Pi after uptake

1.2.2.1 Cytosolic Pi

Cytosol serves as the nexus for both intercellular and intracellular transport activities. Therefore, cytosolic Pi levels have to be maintained within a relatively narrow range. Pi concentration in the cytosol of plants grown under Pi-replete conditions is estimated to be 1-10

mM based on ^{31}P-NMR and Pi biosensors (25, 26). However, it declines during Pi-starvation, especially when the large vacuolar pool is exhausted (26). Following its uptake from the external environment, Pi is rapidly assimilated into ATP to sustain a wide range of biochemical reactions (9). It is also transported to subcellular organelles, e.g., plastids, mitochondria, and vacuoles. Each of these organelles are equipped with unique sets of transporters that import/export Pi.

1.2.2.2 Intracellular transport

After Pi enters a cell, it is transported to each organelle to serve as substrate or effector for compartmentalized biochemical reactions. Therefore, Pi concentration has to be tightly regulated within these cell compartments. Specific Pi transporter families are responsible for the movement of Pi between each organelle and the cytosol. These include PHT2, PHT4 and pPT in non-photosynthetic plastids and chloroplasts, PHT3 in mitochondria, PHT4;6 in Golgi (27-39), and PHT5 and VPE in vacuoles (14, 40-42).

1.2.2.2.1 Pi transport in chloroplasts

Chloroplasts are double membrane-bound photosynthetic organelles that are capable of converting solar energy into chemical energy. Porins present in the outer membrane allow free diffusion of ions and metabolites. However, the inner membrane is not freely permeable; therefore, specific transporters are required for passage of ions and metabolites between the cytosol and the plastid fluid matrix, which is called stroma. Chloroplasts also contain stacks of thylakoid that harbor the light harvesting complex for photosynthesis (**Figure 1**). Photosystems located on the thylakoid membrane capture light energy (photons) and reduce water to H^+ and O_2. A high energy electron released during water oxidation is sequentially passed down an electron transport chain to energize ATP synthesis. Photostimulated electrons are also used to reduce NADP to NADPH. ATP and NADPH produced in the light reactions are used to fuel the

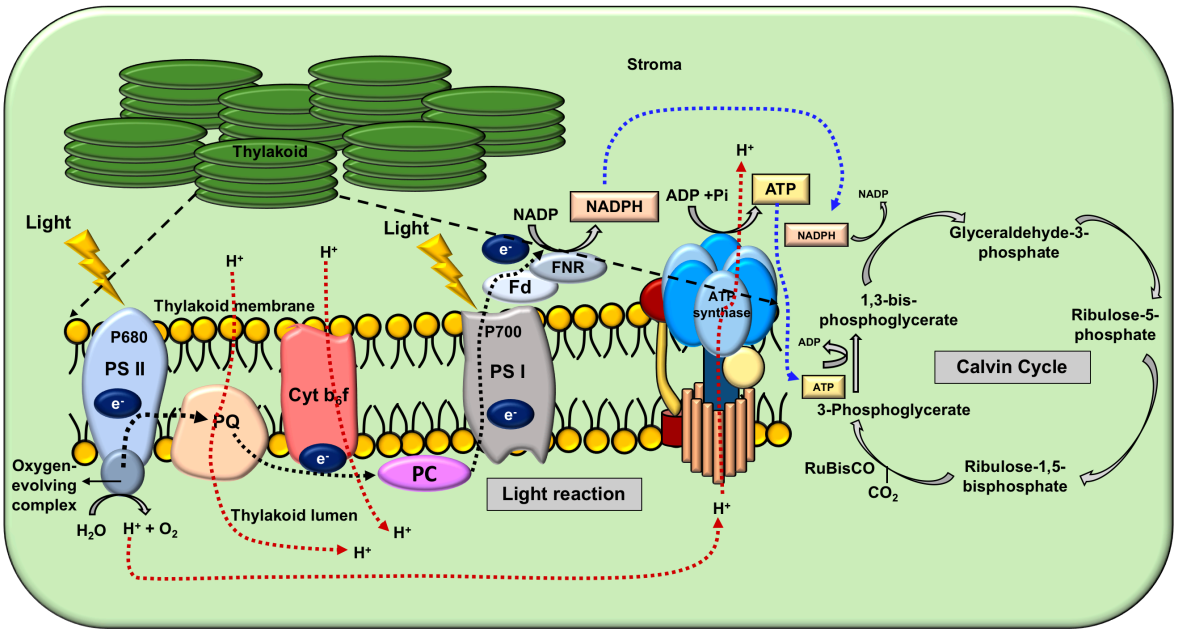

Figure 1: Schematic representation of light and dark (Calvin Cycle) reactions of photosynthesis in chloroplasts. Light reactions occur in the thylakoid membrane. Photons absorbed by pigments in Photosystem II (PSII) cause excitation of electrons (e^-) in chlorophyll. Electrons are transferred along the electron transport chain and accepted by Photosystem I (PSI). The electrons are ultimately used in NADPH formation. As electrons move through the series of electron carrier proteins, H^+ accumulate in the thylakoid lumen. The flow of H^+ ions through ATP synthase provides the energy for ATP synthesis. NADPH and ATP are used to fuel the Calvin cycle in the stroma. CO_2 is fixed and sugar molecules are produced during this phase.

Calvin-Benson cycle in the stroma. CO_2 is fixed during this phase to form reduced carbon molecules that are either used for transitory starch synthesis within the stroma or exported to the cytosol for plant-wide distribution of carbon as sucrose.

Because Pi is required during photophosphorylation of ADP to form ATP, if stromal Pi concentration is too low, ATP synthesis will be limited (43). In contrast, high stromal Pi levels inhibit synthesis of transitory starch (44). Therefore, it is important to regulate Pi concentration in the stroma within a narrow range to sustain photosynthesis and carbon partitioning. The triose-phosphate/Pi translocator (TPT) was the first chloroplast Pi transporter to be characterized (27).

TPT mediates transport of triose phosphates (glyceraldehyde 3-phosphate and dihydroxyacetone phosphate) and 3-phosphoglycerate from the chloroplast stroma to the cytosol in stoichiometric exchange for cytosolic Pi (28) (**Figure 2**). These metabolites are then used for sucrose synthesis in the cytosol, releasing Pi for delivery back to chloroplasts to continue ATP synthesis (28). Localization of another Pi transporter, PHT2;1, to the chloroplast inner membrane (**Figure 2**) was revealed by PHT2;1-GFP fusion constructs introduced into Arabidopsis and tobacco leaves by particle bombardment (31, 33). Functional analyses in yeast suggest that PHT2;1 is a low affinity Pi/H^+ symporter. An Arabidopsis *pht2;1-1* null mutant showed impaired Pi allocation at the whole plant level, including remobilization of Pi from older to younger leaves (33). Similarly, knockdown of the homolog in wheat, *TaPHT2;1*, showed reduced Pi accumulation in chloroplasts and decreased photosynthetic performance (31). Another family of Pi transporters, PHT4, consists of six members, of which PHT4;1 and PHT4;4 are located in chloroplasts (29). Heterologous ^{32}Pi uptake assays in yeast suggest that these proteins transport Pi coupled with either H^+ or Na^+ (30, 45). PHT4;4 also catalyzes ascorbate transport based on assays using proteoliposomes (32). Two knockout lines, *pht4;4-1* and *pht4;4-2,* contain less ascorbate in leaves than wildtype, which further supports this claim (32). The *pht4;1* mutant has small rosettes and reduced biomass (46). There are conflicting reports regarding the localization of PHT4;1, which indicate localization to the thylakoid membrane or to the inner envelope (45, 47-49) (**Figure 2**). Chloroplast-localized Pi transporters are ideally positioned to regulate Pi levels in the chloroplast stroma. Expression of *TPT*, *PHT2;1* and *PHT4;4* is induced by light (30, 33, 50), whereas *PHT4;1* expression is circadian (51). How these transporters collectively regulate Pi levels in the chloroplast stroma, and in turn, photosynthesis and carbon fixation, remains unclear.

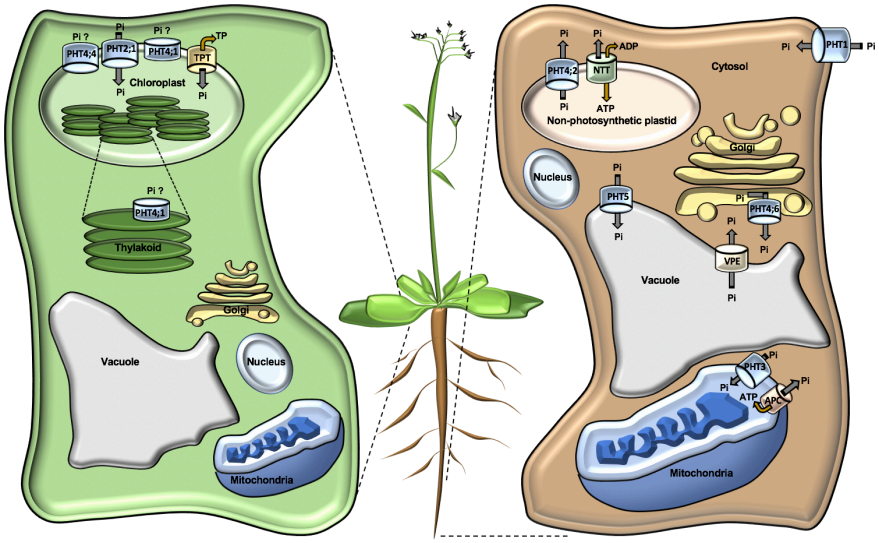

Figure 2: Intracellular Pi transport in leaf (left) and root (right) cells. Pi transporters responsible for Pi import and export in different organelles are depicted. Direction of transport is currently unknown for PHT4;1 (thylakoid membrane or chloroplast inner membrane) and PHT4;4 (chloroplast inner membrane).

1.2.2.2.2 Pi transport in non-photosynthetic plastids

Non-photosynthetic plastids are responsible for various biosynthetic activities, including the synthesis of starch (amyloplast), fatty acids (elaioplast), and amino acids (52). ATP is required for these processes but non-photosynthetic plastids are not capable of ATP synthesis. Therefore, ATP is imported from the cytosol by nucleotide transporters (NTTs) in exchange for stromal ADP (53) (**Figure 2**). Excess Pi that would accumulate in the stroma due to the unequal exchange of phosphate moieties during this transport process must be exported from plastids to prevent deleterious effects. For example, Pi allosterically inhibits ADP-glucose pyrophosphoylase (AGPase), an enzyme that is essential for starch synthesis. Pi export from root plastids in Arabidopsis is catalyzed by PHT4;2 (34) (**Figure 2**). A *pht4;2* null mutant is defective in Pi export, and the resulting hyper-accumulation of Pi was confirmed using a FRET-based Pi

biosensor localized to plastids (26). As expected, starch accumulation is also reduced in *pht4;2* roots (34).

1.2.2.2.3 Pi transport in mitochondria

Pi is a substrate for ATP synthesis via oxidative phosphorylation in mitochondria, which requires the transport of Pi from cytosol to the mitochondrial matrix. This transport activity is catalyzed by members of the PHT3 family, which is also referred to as Mitochondrial Phosphate Transport (MPT) and Mitochondrial Proton/Phosphate symporter (P_iC) (38). Swelling of yeast mitochondria suspended in a phosphate salt solution is indicative of mitochondrial Pi import, and this heterologous assay was used to characterize several PHT3 transporters (54). There are three PHT3/MPT proteins in Arabidopsis (55) (**Figure 2**). Overexpression of *AtMPT3* results in a dwarf phenotype, curly leaves, and reduced reproductive ability (55). Notably, these plants also accumulate more ATP than wild-type plants suggesting that Pi is a limiting factor for ATP synthesis in mitochondria. Pi export from mitochondria to cytosol is mediated by ATP-Pi carrier (APC) proteins in exchange for cytosolic ATP, which may be important when roots are subjected to hypoxic conditions (56) (**Figure 2**). Voltage dependent anion channel (VDAC) proteins catalyze mitochondrial Pi transport in animal cells, and homologs have been identified in Arabidopsis. VDAC1 and VDAC3, which possess a 23-aa mitochondrial porin signature (MPS) sequence at the C-terminus, were localized to mitochondria, but no transport activities were reported (57).

1.2.2.2.4 Pi transport in Golgi

Golgi bodies play an important role in intracellular trafficking, protein and lipid modification, and polysaccharide synthesis for cell wall formation. Golgi bodies harbor nucleoside diphosphatase, which catalyzes breakdown of nucleoside diphosphate to nucleoside

monophosphate and Pi (35). Excess Pi generated as a by-product in the Golgi lumen can have inhibitory effects on enzymes like glucan synthase, thus limiting glycosylation (58). Therefore, Pi is maintained at a low concentration in the Golgi. The PHT4;6 transporter is localized to the Golgi membrane (59) **(Figure 2)** as inferred from transgenic Arabidopsis lines expressing PHT4;6-GFP (35). Heterologous ^{33}Pi radioactivity assays using isolated yeast vacuoles suggest that Pi accumulation is reduced in vacuoles expressing PHT4;6. Also, PHT4;6-containing vacuoles loaded with ^{33}Pi showed faster Pi export than controls when transferred to Pi-free media (35). These results support the idea that PHT4;6 is responsible for Pi export from Golgi bodies. Disruption of the *PHT4;6* gene leads to a dwarf phenotype in Arabidopsis (37). These knock-out mutants also have altered cell wall composition and defects in other Golgi-related processes, including abundance of N-glycosylated proteins, sensitivity to Golgi alpha-mannosidase, and accelerated senescence in response to darkness (36, 37).

1.2.2.2.5 Pi storage and remobilization

Vacuoles are the major storage sites for Pi with up to 95% of the total intracellular Pi (60). Pi release from vacuoles is crucial for maintaining cytosolic Pi in starved plants. Also, Pi is sequestered in vacuoles when starved plants are replenished with Pi to avoid Pi toxicity. Therefore, vacuolar Pi transporters are important for regulating cytosolic Pi levels.

Vacuolar Pi import is mediated by members of the PHT5 transporter family (**Figure 2**), which consists of three members, PHT5;1, PHT5;2 and PHT5;3 in Arabidopsis (14). *PHT5;1* is expressed ubiquitously in leaves and roots, *PHT5;2* in vascular tissue, pollen, and guard cells, and *PHT5;3* in root stele (14). Based on ^{31}P-NMR spectroscopy, the loss-of-function mutant *pht5;1-2* has a lower vacuolar:cytoplasmic Pi ratio than wildtype (14). It should be noted that NMR-based methods cannot readily distinguish cytosolic Pi from that in organelles other than

the vacuole so results are reported as cytoplasmic. Patch-clamp assays revealed that Pi influx currents in vacuoles isolated from *pht5;1* are lower than those of wildtype, and thus further support its role in vacuolar Pi import (42, 61). The importance of vacuolar Pi import to overall plant growth and Pi accumulation is apparent from reduced growth of single, double, and triple mutants of these transporters (14, 42). Similarly, *PHT5;1* overexpression lines that show reduced growth due to excessive Pi loading into vacuoles and presumably reduced cytosolic Pi levels (14). Downregulation of Pi-starvation induced (PSI) genes like *PHT1;1*, *PHT1;4*, and *RNS1* were observed in *pht5* mutants when grown in Pi-replete medium (14). However, during Pi deficiency, acid phosphatase secretion, another PSI marker, was elevated. When starved plants were replenished with Pi, both single and double *pht5* mutants had lower mass and shorter roots (42) due to hyperaccumulation of Pi in the cytosol. Collectively, these observations suggest that PHT5 transporters play a crucial role in plant adaptation to fluctuating levels of Pi in the environment.

When plants are Pi-starved, vacuolar Pi is gradually released to the cytosol to sustain cellular activities. Pi export from vacuoles is catalyzed by members of the VPE family (**Figure 2**), which were identified in rice (40). These transporters localize to the tonoplast (vacuolar membrane) in cells of the root cap, mature root, leaf mesophyll, and vascular bundle. ^{31}P-NMR spectroscopy showed Pi hyperaccumulation in *vpe1* and *vpe2* loss-of-function mutants, whereas vacuolar Pi was reduced in over-expression lines (40). These results indicate that VPE1 and VPE2 facilitate Pi export from vacuoles. These transporters are transcriptionally induced during Pi-starvation to release vacuolar Pi into cytosol (40). Therefore, mutants that are defective in Pi export from vacuoles are hypersensitive to Pi-starvation, which is evident from the retarded

growth of single and double mutants of *vpe1* and *vpe2* (40). Thus, vacuolar Pi import and export both contribute to cytosolic Pi homeostasis and influence plant growth.

1.2.2.3 Intercellular transport

Following uptake from soil, Pi flows radially through the root epidermis, cortex, and endodermis. This can occur either via apoplastic or symplastic (through plasmodesmata) transport mechanisms (62). However, the presence of the lignin-containing Casparian strip in the endodermal layer prevents apoplastic movement of ions into the vasculature. Therefore, Pi movement from endodermis to stele occurs via specialized Pi transporters (63). Pi loading into xylem vessels is mediated by members of the PHO1 family of transporters (64). The most extensively characterized member of this family, *PHO1,* is expressed predominantly in mature roots (65, 66), which supports its role in xylem loading. PHO1 localizes to the Golgi/trans-Golgi network, although some of the protein was also detected in the plasma membrane (67). PHO1 contains an EXS domain, which is essential for Pi transport and proper localization to the Golgi network (68). EXS is named after ERD1/XPR1/SYG1 proteins. It includes portions of SYG1 (Suppressor of Yeast Gpa1) signal transduction protein, XPR1 (Xenotropic and Polytropic Retrovirus Receptor 1) and ERD1 (ER retention defective) yeast proteins. Pi uptake from the environment and movement of Pi through xylem are not altered in the *pho1* mutant. However, Pi transfer from roots to shoots is impaired and results in low Pi content shoots (64). The *pho1* mutation severely affects plant growth and leads to a dwarf phenotype, anthocyanin accumulation, delayed flowering, and a very low seed-set with low germination (64, 69). These phenotypes highlight the importance of intercellular and inter-organ Pi transport for plant development.

1.2.3 Signaling networks in plants for Pi sensing

Plant growth is modulated by Pi availability in the environment as well as internal Pi content. Local Pi sensing is responsible for modifications of the root system architecture (RSA), whereas systemic signaling is involved in Pi uptake and homeostasis. These signaling pathways must be tightly integrated to support the growth of both roots and shoots.

1.2.3.1 Local Pi sensing: Modifications of root system architecture

When plants are subjected to Pi deficiency, their root systems undergo morphological changes to facilitate higher Pi uptake from the environment. This includes an increase in lateral root growth and increased density and length of root hairs (70). With decreasing Pi availability, root mass increases with a concomitant decrease in shoot mass (71). That is, root:shoot ratio increases in Pi-starved plants.

Low Pi availability can be sensed by the root tip and results in the attenuation of primary root growth by inhibiting cell elongation (72). Several genes related to primary root growth inhibition in low Pi have been identified. *Low Phosphate Root1* (*LPR1*) and its paralog, *LPR2* encode multicopper oxidases that are essential for this phenomenon (73) as evident from the longer roots of *lpr1-1*, *lpr2-1,* and *lpr1-1 lpr2-1* mutants than wildtype when grown in Pi-deficient conditions. This phenotype is not apparent under Pi-replete conditions, suggesting that LPR1 and LPR2 are specific for low Pi-induced growth inhibition (73). A compartmented root growth experiment revealed that primary root growth is arrested when roots are in contact with low Pi even when leaves are maintained in high Pi (73). This supports the idea that local Pi sensing by the root tip is independent of internal Pi concentrations. ER-localized Phosphate Deficiency Response2 (PDR2), a P_5-type ATPase, is also involved in primary root growth (74). Its expression is restricted to root meristem and the transition zone (74). This is consistent with

inhibition of cell division in *pdr2* mutants during Pi-starvation resulting in a conditional short-root phenotype. This phenotype can be rescued by application of phosphite, a Pi analog that cannot be metabolized by plants, suggesting that Pi acts as a signal in this response (75). There is evidence of genetic interaction between PDR2 and LPR1/LPR2 and PDR2 probably acts upstream of LPR1/LPR2 because the long root phenotype of a *pdr2 lpr1 lpr2* triple mutant is similar to that of a *lpr1 lpr2* double mutant (74). PDR2 is also required for Scarecrow (SCR) activity in stem cell maintenance and radial cell patterning (74). Another gene involved in primary root inhibition in low Pi is *Low Phosphorus Insensitive* (*LPI*). Two *lpi* mutants, *lpi1* and *lpi2,* are insensitive to Pi deprivation; they do not show any signs of Pi stress like short primary root, increased root hair growth, increased lateral roots, or induction of PSI genes (76). Similarly, *phosphorus starvation insensitive* (*psi*) mutants are also unresponsive to Pi deficiency and produce long primary roots under Pi-deficient conditions (77). *psi* is an allele of *lpr1* (77). Thus, these genes collectively contribute to primary root growth in response to Pi availability.

Pi deprivation also triggers root hair production to increase Pi capture from soil (78, 79). Growth rate of root hairs and their duration of growth is higher in plants growing in low Pi conditions (78). Pi availability also regulates root hair density. With decreasing Pi concentrations, root hair density increases progressively (79). Root hair development and related genetic studies will be discussed in Section 1.2.5 of this chapter.

1.2.3.2 Systemic Pi signaling

Systemic or long-distance Pi signaling involves communication between roots and shoots to regulate Pi status at the whole-plant level to sustain metabolic activities under varying environmental conditions. Signaling molecules that participate in this process include Pi, microRNA, PHO2, a family of non-coding RNAs, and IPS/At4-like genes.

1.2.3.2.1 Role of Pi as a signaling molecule

Application of phosphite (Phi), a non-metabolizable analogue of Pi, results in suppression of Pi starvation responses (PSRs) (80). Phi enters the cells through Pi transporters but it cannot be further oxidized or assimilated (81). This suggests that Pi acts as a signaling molecule. That is, because signaling machinery within the cell cannot distinguish between Pi and Phi due to their structural similarity, PSR genes are repressed when plants are fed with Phi, even during Pi starvation (80, 82). For example, growth of root hairs is attenuated, induction of nucleolytic enzymes is disrupted, and chlorophyll content is decreased (82).

Expression of the Pi transporter MtPT4 is downregulated when half of the roots were supplied with sufficient Pi and the other half was held without Pi, as shown by split root experiments (83). This indicates that Pi transporters are regulated systemically based on the internal Pi content of the plant.

1.2.3.2.2 Role of microRNA399 and PHO2

The Arabidopsis *pho2* mutant was identified from an ethyl methanesulfonate (EMS) screen based on its high accumulation of Pi in leaves (84). *PHO2* encodes the ubiquitin-conjugating E2 enzyme UBC24 and is expressed in vascular tissue of cotyledons, leaves, and roots (85). Pi uptake assays indicated higher Pi uptake in *pho2* and that the high Pi accumulation in *pho2* shoots was due to greater translocation from roots to shoots (86). However, Pi uptake was similar to wildtype when shoots of *pho2* were removed, indicating that *pho2* has a higher capacity for storing Pi in the shoot (86). *PHO2* expression is regulated by microRNA399 (miRNA399), which is one of the conserved microRNAs in plants (87). Binding of miR399 to the 5'-UTR of *PHO2/UBC24* results in a truncated transcript and loss of ubiquitin conjugation function (85, 88). During Pi-deprivation, miR399 is upregulated by 1000 to 10,000-fold (88, 89),

and *PHO2* transcripts are therefore strongly reduced (89). It was also observed that miR399 overexpression plants hyperaccumulated Pi in leaves and developed leaf necrosis due to Pi toxicity, similar to *pho2* mutants (85, 88). In rapeseed and pumpkin, miRNA399 is specifically induced by Pi limitation in the phloem sap (90). Grafting experiments with chimeric plants that had wild-type roots and overexpressed miRNA399 in shoots showed massive miR399 accumulation in roots, indicating translocation of miR399 from shoots to roots where it exerts its effect on its target gene, *PHO2* (90). Co-localization of miR399 and PHO2 in the root vasculature supports their *in vivo* interaction (85). Collectively, these results suggest that miR399 serves as a systemic signal for Pi homeostasis by regulating PHO2 levels in the root depending on the Pi status of the shoot.

1.2.3.2.3 Role of non-coding RNAs

Pi-starvation induced transcripts that do not code for long open reading frames include *At4*, *AtIPS1,* and two *At4*-like genes *At4.1* and *At4.2*. These genes have a conserved 23-nt motif that is partially complementary to miR399 except at the region required for miR399-guided cleavage of mRNA targets (91). Expression of *At4* and its *Medicago truncatula* homolog, *Mt4,* is induced in roots by Pi deficiency (83). An *at4* mutant allocates more Pi to shoots and has a higher shoot:root Pi ratio than wildtype, whereas overexpression of *At4* results in decreased Pi in shoots (91), indicating its involvement in PHO2-miR399 circuitry (92). Another member of this gene family, *AtIPS1,* suppresses the effect of miR399 on *PHO2* mRNA. Therefore, overexpression of *IPS1* leads to accumulation of *PHO2* mRNA and lower shoot Pi (91). This strategy of miR399 inhibition by *At4/IPS1* as riboregulators is referred to as target mimicry.

1.2.4 Root development

In most plants, the root tip is protected by a layer of parenchyma cells that form the root cap (RC). It consists of initial cells, lateral root cap (LRC), and columella. The LRC consists of border cells that accumulate on the RC periphery and eventually slough off. Mucilage secreted by RC cells reduces friction as the root grows through the soil. It also contains polysaccharides that serve as nutrients for soil microorganisms. Some of the mucilage is broken down by microbes to forms that can be utilized by plants (93).

The tip of the root apical meristem contains a group of slowly-dividing cells called the quiescent center (QC) that maintain a population of stem cells. These stem cells undergo post-embryonic divisions to generate the cells that eventually undergo morphological and functional changes as they pass through development. Arabidopsis roots consist of five developmental zones that are distinguished by morphologies and cellular activities. From the tip upwards, these are meristematic zone (MZ), transition zone (TZ), elongation zone (EZ), differentiation zone (DZ) and mature root (MR).

The MZ consists of actively dividing cells that encompass the first 250 microns of the root tip (94). A mitotic marker, cyclin, serves as an excellent reporter for actively dividing cells. *cyc1At* transcripts accumulate in G2-phase nuclei and decline when the cell cycle is blocked (95). Fusion of the *cyc1At* promoter with the GUS reporter revealed that *cyc1At* is expressed in all dividing cells of the root meristem (96, 97). The rate of cell division in this zone is one of the factors that regulate root growth. However, these cells lack the necessary cytoarchitecture for cell elongation as present in the EZ so first move into an intermediate phase of development called the transition zone (TZ).

The TZ is characterized by slow cell growth with cells that are isodiametric in shape at the distal (toward the root tip) end (98). As cells approach the EZ, their length increases. Cells at the distal end of the TZ are competent for cell division based on the presence of CDC2, whereas cells at the proximal end are at the onset of fast elongation, indicating that the TZ is developmentally plastic (99). During normal root growth, cells in the TZ undergo cytoskeletal remodeling, vacuolar rearrangements, and cell wall restructuring in preparation for their transition to the EZ. For cytoskeletal remodeling, F-actin undergoes massive changes in its arrangement to drive anisotropic growth (100). Cortical microtubules also align in transverse arrays parallel to the root axis, which is required for expansion of vacuoles (101). A central vacuole starts to develop in cells at the proximal end of the TZ, which coincides with increased expression of γ-TIP tonoplast aquaporin (102). Extensive changes also occur in the cell wall of cells in the TZ to facilitate cell expansion. Increased xyloglucan endotransglucosylase (XET) activity has been observed in the proximal TZ cells (103). XET is responsible for cleaving and re-joining xyloglucan, a structural polysaccharide of plant cell walls (104). Cross-linking of xyloglucan with cellulose microfibrils restrains cell expansion. Therefore, XET-mediated cleavage of xyloglucan causes cellulose microfibrils to move apart and loosen the cell wall to allow in cell growth. Cell wall loosening is also aided by expression of expansins, which is restricted to proximal TZ and EZ cells (105, 106). The pectic polymer (1-4)-β-D-galactan has also been reported as a marker of cell elongation (107). Proximal TZ cells also contain *COBRA (COB)* mRNA and proteins that are involved in establishing cell polarity. *COBRA* encodes a GPI-anchored protein that localizes to the plasma membrane and is involved in cellulose deposition. *cob* mutants fail to establish cell polarity and display radial growth of cells, suggesting that COBRA proteins are required for the longitudinal expansion of cells (108). These

processes collectively act as a switch from isodiametric growth at the distal TZ to strictly polarized rapid cell elongation in the EZ.

The second phase of cell expansion begins in the EZ where radial expansion ceases and longitudinal expansion continues. In Arabidopsis, the EZ encompasses a region 500-850 microns from the root tip (99). This is a zone of rapid elongation; cells increase in length from 35 microns to 135 microns in a span of 2 hours (99). Cells are gradually filled with a central vacuole and the nucleus is appressed against the cell wall (109). Arabinogalactan-proteins (AGPs), especially fucosylated-AGPs, are required for cell elongation in this zone (110). This is supported by the *mur1* mutant, which is defective in L-fucose biosynthesis and shows 50% decrease in cell elongation (111). F-actin is also required for cell elongation given that treatment with latrunculin B, which disrupts actin polymerization, causes a dwarf phenotype (112). Another characteristic feature of EZ cells is the parallel orientation of cellulose fibrils, transverse to the root axis (113). When the orientation changes from transverse to longitudinal, cell elongation ceases. Beyond this zone, cells become symplastically isolated (114) and root hairs develop from specialized epidermal cells.

The differentiation zone (DZ) in Arabidopsis spans a region 850 -1000 microns from the root tip. This zone can be easily distinguished by the presence of root hairs, although not at all epidermal cells can form root hairs (described in the following sections). Cell elongation is much slower in the DZ with only small changes in length until cells become a part of the mature root and have reached their final size.

1.2.5 Root hairs

Root hairs (RHs) are epidermal outgrowths that help plants acquire water and nutrients from soil, anchor the root to soil, and interact with soil microbes. Root hairs increase the area of

contact of roots with the soil, thereby increasing absorptive capacity, which is especially important during drought and nutrient deprivation.

1.2.5.1 Root hair development

Root hairs (RHs) form from specific epidermal cells called trichoblasts. These are interspersed with non-hair forming epidermal cells called atrichoblasts. Following epidermal cell patterning, a bulge forms on the surface of trichoblasts, the RH tube initiates, and then tip growth occurs. An increase in the number and length of root hairs is a hallmark of Pi deficiency. Stages of RH development will be discussed in detail in the following sections.

1.2.5.1.1 Epidermal cell patterning

The positions of trichoblasts and atrichoblasts in a root transverse cross-section are indicated in **Figure 3**. Trichoblasts (H-cell position) are located between two underlying cortical cells, whereas atrichoblasts (N-cell position) are located directly above its underlying cortical cell.

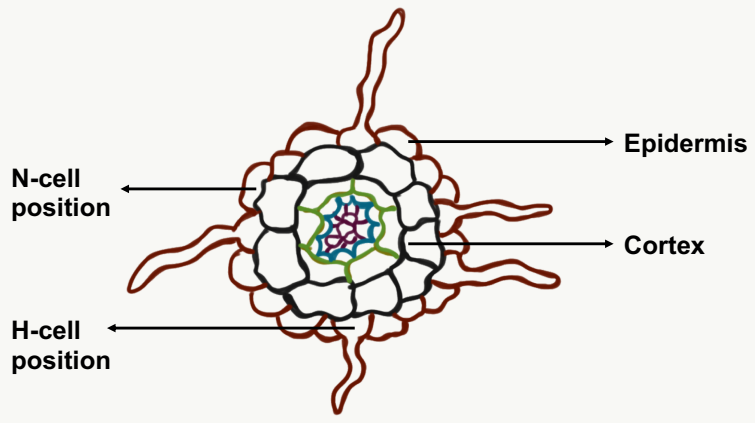

Figure 3. Schematic representation of an Arabidopsis root transverse section showing the positions of hair cells (trichoblasts, H-position) and non-hair cells (atrichoblasts, N-position).

1.2.5.1.2 Bulge formation

Root hair formation is initiated by a bulge in the cell wall. Analyses of root hairless (*rth*) mutants, specifically *rth3,* revealed that these plants are defective in RH formation (115); they form root hair primordia but do not elongate further. *RTH3* has significant similarities to members of the *COBRA* gene family and encodes a GPI anchor protein (116). *In situ* hybridization showed that *RTH3* transcripts are present in elongating, root-hair forming cells. Other genes involved in RH initiation encode peroxidase, xyloglucan endotransglycosylase, extensin, arabinogalactan protein, leucine-rich-repeat protein, phosphatidylinositol phosphatidylcholine transfer protein (117). These are required for cell wall modifications essential for bulge formation. In addition, trichoblasts accumulate high amounts of ROS. Expression of peroxidase genes *HvPRX45* and *HvPRX2* is significantly reduced in the hairless mutant *rh1.a* (118). Arabinogalactan proteins (AGPs) are also essential for RH development (119). They are abundant in the cell wall of root hairs and trichoblasts. Treatment with β-D-glucosyl residues (βGlcY) precipitates AGPs and inhibits the formation of RH tube (119).

1.2.5.1.3 Root hair tube elongation

RH elongation requires cytoskeletal remodeling, vesicular transport of cell wall components to the tip, and cell wall synthesis. UDP-glucose (UDP-Glc) forms the building blocks of cell wall polysaccharides like cellulose. Glucose is phosphorylated by hexokinase and the resulting hexose phosphates are converted to UDP-Glc by UDP-Glc pyrophosphorylase (UGP) (120). UDP-Glc is a substrate for cellulose synthase in the formation of cellulose microfibrils (121). *OsCSLD1*, which encodes cellulose synthase-like D1 protein in rice, is one of the first genes identified as essential for RH elongation. Mutants that have non-functional *OsCSLD1* grow shorter root hairs, whereas its overexpression results in root hairs that are twice

as long as in wild-type plants (122). Bulge formation occurs normally in a loss-of-function mutant for *OsCSLD1*, *rth2,* but fail to elongate further (123). A mutant for the *AtCSLD3* gene in Arabidopsis has a similar root hair growth phenotype. In addition, most RHs in this mutant leak cytoplasm from their tip, indicating reduced tensile strength of cell walls (124). Similar observations were recorded in *srh2* mutants, which are deficient in xyloglucan 6-xylosyltransferase (*OsXXT1*) (125). These data collectively show that disruption of cell wall synthesis inhibits RH elongation.

Another group of proteins required for cell wall modifications and tip growth are expansins. This is consistent with the phenotype of the root-hairless mutant *rhl1.a*. Expression of *HvEXPB1*, which encodes β-expansin, is disrupted in this mutant (126). The *HvEXPB1* promoter is active specifically in RH cells (127). Another gene, *OsEXPA17*, was identified in a rice mutant with short root hairs (128). Expression of this gene was observed in RH-forming cells in the DZ and it is upregulated by Pi-starvation (129). Cell wall loosening by expansins, thus, plays an important role in RH development.

Cell wall components are transported to the RH tip by vesicles. The *roothairless1*(*RTH1*) gene, which is a homolog of exocyst complex component *SEC3*, is involved in RH elongation (130). A *rth1* mutant has a short RH phenotype, while pollen tube growth is not affected in these plants, indicating a RH-specific function. Formins are also essential for RH elongation. This was demonstrated by reduced RH elongation in rice mutants defective in *Formin homology 1* (*OsFH1*) (131). Formins play a central role in actin polymerization and microtubule dynamics (132-134), and also in cell division and cell expansion (133). Phosphorylation is important for interaction of cellulose synthase complex with microtubules. Movement of Cellulose Synthase A (CESA) complex along microtubule tracks was affected in lines that are mutated in specific

phosphorylation sites (135). This affects the structure of cellulose microfibrils, thus leading to a defect in cell expansion. Collectively, RH elongation requires multiple proteins to facilitate cell wall synthesis, cytoskeletal rearrangement, and tip growth.

1.2.5.2. Genetic control of root hair development

Genes that are involved in different stages of RH development have been identified. They regulate root hair growth rate, length, and density. This influences Pi uptake capacities of plants in low-Pi environments (136). Therefore, mutants for these genes are ideal tools for studying the roles of root hairs in Pi nutrition.

1.2.5.2.1 Genes regulating epidermal cell specification

Transparent Testa Glabra (*TTG*) was one of the first genes identified based on its involvement in epidermal cell fate specification (137). A loss-of-function *ttg1* mutant grows root hairs from all epidermal cells irrespective of their position, suggesting a role for TTG1 in either specification of H-cells or suppression of N-cell specification. *TTG* encodes a WD40 repeat protein (138), and this class of proteins function in signaling, RNA processing, vesicular trafficking, cell cycle regulation and transcriptional repression. Therefore, TTG may be a signaling factor that specifies fate of root epidermal cells. The increased RH density phenotype of the *ttg* mutant can be complemented by Maize *R*-cDNA, which encodes a protein with a basic-helix-loop-helix domain (137). In addition, hairless cells do not show any sign of RH initiation. Similar to *ttg*, mutants of *Glabra2* (*GL2*) also show RH growth from all epidermal cells (139). They alter epidermal cell identity by causing hairless cells to develop root hairs. However, unlike *ttg*, these abnormal hair cells are similar to atrichoblasts in terms of cytoplasmic density and timing of vacuolation. This indicates that *GL2* affects only a part of position-dependent patterning. Expression studies of *GL2* by *in situ* hybridization and GUS fusion suggest that *GL2*

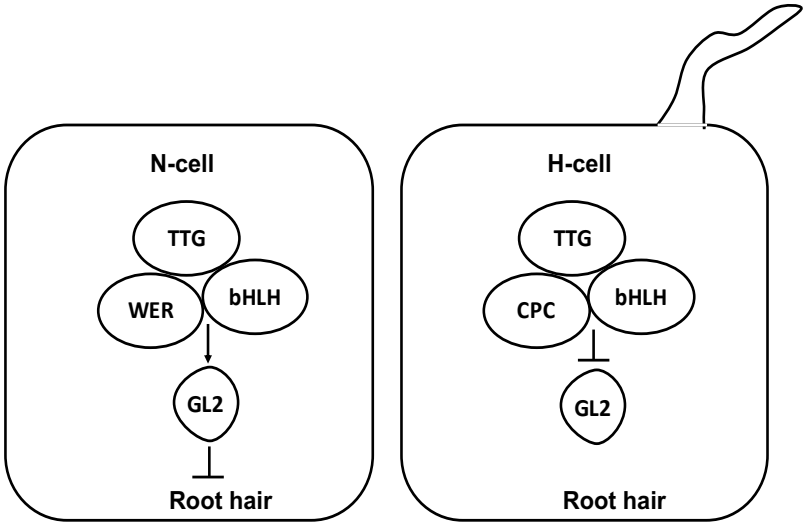

Figure 4. Proposed model for epidermal cell patterning in Arabidopsis root epidermis. The WER-bHLH-TTG complex activates *GL2,* which then inhibits root hair formation in cells in the N-cell position. CPC-bHLH-TTG inhibits *GL2* transcription thereby allowing root hair growth in cells in the H-cell position.

is expressed in the differentiating hairless cells (139). *GL2* encodes a DNA-binding HD-Zip protein (140, 141). *GL2* promoter activity is reduced in *ttg* mutants suggesting that *TTG* is required for maximal GL2 activity (142). Together, these studies suggest that TTG and GL2 are negative regulators of root hair cell differentiation. TTG activates an R-like bHLH transcription factor that is a positive regulator of *GL2* and specifies non-hair fate of N-cells (**Figure 4**). *Caprice* (*CPC*) also positively regulates hair-cell specification (143). This was demonstrated by the reduced number of root hairs phenotype of a *cpc* mutant. Notably, the number of root hairs in a *cpc gl2* double mutant is almost the same as *gl2,* whereas *cpc ttg* has same number of root hairs as *cpc* but less than *ttg*. This suggests that *CPC* is epistatic to *GL2* and that *TTG* and *CPC* function together upstream of *GL2* (**Figure 4**). This suggests that CPC is a transcriptional repressor of *GL2* in H-cells. Another gene involved in epidermal patterning is *WER,* which encodes a MYB-type transcription factor with two MYB domains in its N-terminus and is

preferentially expressed in epidermal cells in the N-position. Homozygous *wer* mutants show ectopic hair production resulting in a hairy root phenotype (144), indicating that *WER* is required for non-hair cell specification. Reduced expression of *GL2* in *wer* mutants suggests that *WER* acts upstream of *GL2* and is required for *GL2* transcription. WER interacts with bHLH proteins as demonstrated by yeast two-hybrid assay, which may be responsible for transcriptional regulation of *GL2*. A *wer-1 cpc* double mutant produces an intermediate number of hair and non-hair cells compared to either of the single mutants. *GL2* expression was also intermediate in the double mutant. Together, these observations suggest that WER and CPC work in an opposite manner in cell patterning (144).

1.2.5.2.2 Genes regulating root hair morphogenesis

Root hair growth begins with an outgrowth on an epidermal cell followed by bulge formation. Epidermal patterning is normal in mutants defective in RH initiation; however, the number of RHs are reduced. Hormones like auxin and ethylene are essential for RH initiation. For example, roots of the auxin-resistant mutant *axr2* completely lack root hairs (145). However, they develop root hairs upon external application of auxin, which suggests that RH initiation depends on auxin sensitivity. Ethylene also acts as a positive regulator of RH development. Blocking ethylene synthesis results in reduction of root hair density, but when plants are supplied with excess exogenous ethylene, root hairs also develop from N-cells (146). One of the genes involved in RH initiation is *Root Hair Defective6* (*RHD6*). Mutants for this gene show no sign of RH initiation in most H-cells thereby reducing RH density (147). However, a few root hairs can emerge, but they undergo a shift in their site of emergence; most arise from the basal end of the cell rather than the apical end as in wildtype. These *rhd6* phenotypes can be rescued by supplemental auxin or ethylene. The next step of RH morphogenesis is bulge formation. *RHD1* is

required for proper initiation of root hairs (148). *rhd1* mutants show a bulbous region at the base of root hairs, larger than in wildtype. However, root hair length is not affected by this mutation. Another gene required for normal RH initiation is *TIP1*. Plants with defects in this gene not only show a larger bulge than usual but also form branched root hairs (149). Length of these root hairs is also much shorter, approximately 10-fold less than wildtype. Continuation of RH growth beyond this stage depends on the process of tip growth. *RHD2* is essential for initiation of tip growth. Inactivation of this gene inhibits RH elongation producing stubby hairs (148). Other *RHD* mutants, *rhd3* and *rhd4*, have wavy and occasionally branched root hairs implying their role in tip growth (148). These *RHD* mutants have been extensively studied to understand Pi uptake efficiency under different growth conditions (115, 136). *Can Of Worms1* (*COW1*) is another gene involved in RH morphogenesis. Root hairs of *cow1* mutants have a slower elongation rate (150). Thus, these genes participate in different stages of RH morphogenesis and play an important role in RH development.

1.2.5.3 Role of root hairs in Pi nutrition

The primary function of root hairs is nutrient absorption from soil. The earliest evidence for Pi uptake via root hairs was presented by Gahoonia et al. (151). In this study, rye plants were grown such that only the root hairs grew through a nylon mesh into radioactively labelled soil. After 2 and 4 days of growth, radioactivity was detected in shoots, which suggests that root hairs absorbed ^{32}P from soil. Radiolabeling in shoots correlated with the number of root hairs. In this set-up, root hairs contributed 63% of total Pi uptake by the root system. Root hairs are especially important in low-Pi environments because they increase the absorptive surface and thus access to a larger volume of soil. On examining the Pi depletion profile surrounding roots with and without root hairs, the width of the Pi depletion zone increased by 70% when root hairs were

present compared to roots without hairs (152). Simulation modeling indicated that Pi uptake is 10-fold greater in roots with hairs (152). The main reason for the high Pi uptake efficiency of root hairs is their small radius; each unit of absorbing surface samples a greater volume of nutrients so total Pi influx occurs at a higher rate (152). *In situ* hybridization and immunolocalization studies showed that Pi transporters are present in root hairs of different species. For example, *LePT1* transcripts are most abundant in root hairs of tomato seedlings (8). Similar observations were made for MtPT1 in *Medicago truncatula* (7). In Arabidopsis, the PHT1 family of Pi transporters consists of nine members, PHT1;1 through PHT1;9. Of these, strongest signals for GUS or GFP expression driven by *PHT1;1* and *PHT1;2* promoters were observed in Pi-starved root hairs (23, 153). Expression of *StPT2* in potato is also restricted to DZ cells and root hairs (154). Apart from its effect on transcript levels, low Pi also induces changes in RH morphology, including increased length and growth rate (78). RH mutants *rhd2* and *rhd6*, which are defective in RH initiation and RH development, respectively, were used to evaluate Pi uptake (136). Pi absorption is higher in wild-type plants than RH mutants in low Pi, although this was not observed when plants were grown in high Pi. Plant growth in terms of biomass and seed yield are also reduced in the root hairless mutant *rhd2* (155).

1.2.6 *In vivo* measurement of Pi

Pi concentrations are expected to vary between cellular and subcellular compartments of plants depending on rates of Pi transport, recycling, and sequestration. Analytical tools with subcellular spatial resolution are therefore needed to study *in vivo* Pi dynamics. Commonly used methods include Nuclear Magnetic Resonance (NMR), ^{32}P radioisotope imaging, synchrotron X-ray fluorescence, and imaging of genetically encoded biosensors.

NMR spectroscopy exploits the magnetic nature of an atomic nucleus. When an external magnetic field is applied, there is shift in energy from the base to a higher level. When a sample is irradiated with electromagnetic radiation, a magnetic field is generated in the same or opposite direction of the nuclear spin based on the energy level. This can be detected spectroscopically in magnetic elements. Phosphorus is a magnetic element; therefore, it can be detected by ^{31}P NMR. NMR signal can be detected from a wide range of phosphorylated metabolites, Pi, and NTPs. This is a non-destructive method that can be adapted in an imaging mode so samples can be analyzed over time to study metabolite dynamics. Cytoplasmic and vacuolar P contents were quantified in mature root tips of maize using ^{31}P NMR. Total-P contents declined when external supply of the nutrient was disrupted. Because ^{31}P NMR signals respond to pH, it is possible to distinguish vacuolar Pi (pH 5.5) from cytoplasmic Pi (pH ~7.5) (156). This feature confirmed that the vacuolar P pool was exhausted upon P-starvation before the cytoplasmic pool was reduced (157, 158). However, given its limited spatial resolution, NMR can only report Pi from the whole plant or organ, not from individual cells. Also, some NMR signals may be undetectable due to overlap with other signals, precipitation, or binding with other molecules rendering it immobile (159).

Radioisotope imaging has also been used for real-time tracking of P in plants. When plants are fed with radioisotopic Pi, it is absorbed and transferred within the plant. ^{32}P and ^{33}P emit β-rays that can be converted to visible light by a scintillator plate and the resulting image can then be captured with a CCD camera (160). Quantitative data can be acquired by this approach based on radioactivity counts. It has a higher spatial resolution than traditional NMR; it can distinguish P located in the root tip from that in root hairs and primary root (24, 160).

However, a major drawback of this method is that it cannot distinguish between organic P and inorganic Pi.

Another rapidly evolving technique for *in vivo* metabolite analyses is synchrotron-based X-ray fluorescence. A synchrotron is a source of X-rays that are focused with bending magnets and insertion devices. X-rays are focused as thin beams that scan a sample in a raster pattern and X-ray fluorescence is emitted with wavelengths that are element specific (161). This method has been used to study distribution patterns of several elements in cellular and subcellular compartments *in vivo* (162). However, this procedure is highly destructive so is limited to static measurements.

Genetically encoded FRET-based biosensors are highly effective tools for live monitoring of ions and metabolites in plants. Imaging of these biosensors is non-invasive, non-destructive, and provides high spatial and temporal resolution. In 1962, a green fluorescent protein (GFP) was isolated from jellyfish *Aequorea victoria* (163). Since then, many GFP spectral variants have been isolated and these fluorescent proteins were used to construct fluorescence and FRET-based biosensors. FRET or Forster Resonance Energy Transfer is based on radiation-less transfer of energy between two fluorophores. The 'donor' fluorophore transfers its excitation energy to the 'acceptor' fluorophore through a long-range dipole-dipole interaction. FRET efficiency is inversely proportional to the distance between the fluorophores. Therefore, the fluorophore pair should be within a very short distance from each other, i.e., 4 to 6 nm or less. FRET is also dependent on the orientation angle between the two fluorophores with highest efficiency when the fluorophores are aligned parallel to each other. Another important requirement for FRET is that the fluorophores have spectral overlap. Apart from this, high

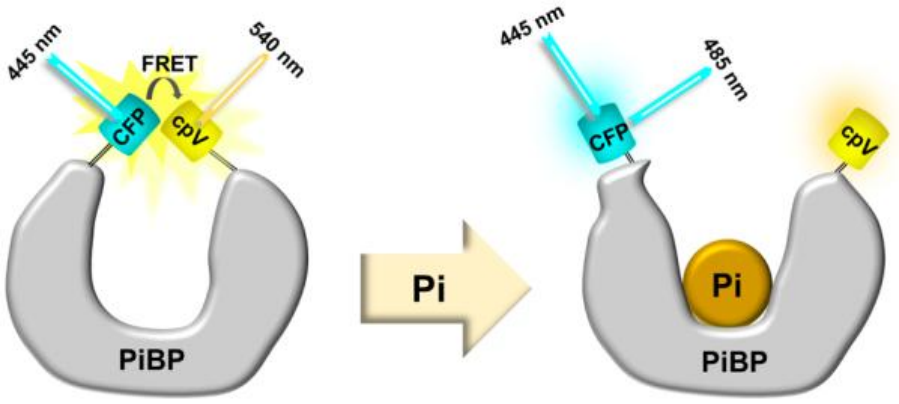

Figure 5: Schematic representation of Pi biosensor cpFLIPPi-5.3m. The Pi binding domain, PiBP, is translationally fused between CFP (donor) and cpVenus (acceptor). Conformational change induced by ligand binding results in loss of FRET.

quantum yield of donor and high extinction coefficient of acceptor are ideal. CFP and YFP meet these criteria and have been used in many biosensors.

A FRET-based biosensor for Pi was developed by translational fusion of a phosphate binding protein (PiBP) from *Synechococcus* with eCFP as donor and Venus, a YFP variant, as acceptor (164). This sensor was called Fluorescent Indicator Protein for Inorganic Phosphate (FLIPPi). When Pi binds with the sensor, it undergoes conformational change resulting in a change in FRET. A FLIPPi sensor was capable of detecting changes in Pi concentrations in cultured animal cells (164). However, this sensor was not suitable for studies in plants due to its small dynamic range. Therefore, the sensor was modified and optimized to predict Pi changes in live plants (165). The resulting sensors were named cpFLIPPi (**Figure 5**) based on the substitution of the acceptor fluorophore YFP with cpVenus, a circularly permuted version of Venus. This substitution increased the dynamic range of the FRET response. In addition, a targeted mutagenesis was used to generate a series of sensors with binding affinities ranging from 80 μM to 11 mM, which encompasses the predicted range of physiological Pi

concentrations. *In vitro* experiments showed that FRET ratios of these sensors decrease with increasing Pi concentrations (165). On subsequent testing in plants, changes in Pi-dependent FRET ratio using cpFLIPPi-5.3m were detected in seedlings grown in Pi-replete and Pi-starvation conditions. *In vivo* functionality of this sensor was further validated by reversal of FRET ratio changes when Pi-starved plants were replenished with Pi (165). This sensor was also targeted to plastids to examine the Pi-accumulation phenotype of *pht4;2*, a mutant with a defect in a plastid-localized Pi transporter. Relative FRET ratios showed hyper-accumulation of Pi in *pht4;2*, indicating that PHT4;2 catalyzes Pi export from root plastids (165). Hence, these results suggest that cpFLIPPi-5.3m can be useful for *in planta* analyses.

Quantitative analysis of FRET ratios using confocal microscopy requires multiple controls (166). These include spectral correction for CFP bleed-through and cpVenus cross-excitation. Bleed-through refers to CFP emission that is detected in the FRET emission channel, whereas cross-excitation is when cpVenus is inadvertently excited by the CFP excitation laser. These signals are subtracted from raw FRET signals to obtain sensitized FRET. In my experiments, sensitized FRET ratios were calculated for all experiments using the same image acquisition parameters for the sensor, CFP, and cpVenus. However, FRET ratio is a relative measure and Pi quantification cannot be determined from *in vitro* calibrations due to differences in absolute FRET ratios observed *in vitro* and *in vivo*. Therefore, an *in vivo* calibration was generated by microinjecting defined Pi concentrations into the cytosol of root cells (1). I used this calibration to convert sensitized FRET ratios to absolute measures of Pi concentration. To eliminate the possibility of detecting non-specific changes, I employed a Pi-insensitive sensor, cpFLIPPi-null (166), in my studies.

1.2.7 Role of ATP in plant growth and metabolism

All anabolic reactions require energy. Adenosine triphosphate (ATP) serves as the primary source of energy for these reactions. Hydrolysis of ATP yields a large amount of free energy that can be used to drive energetically unfavorable cellular reactions. In heterotrophic or non-photosynthetic organs, ATP is generated in the cytosol via glycolysis and in mitochondria via oxidative phosphorylation, whereas in autotrophic organs like leaves, ATP is also synthesized in chloroplasts via photo-oxidative phosphorylation. ATP is essential for nutrient uptake, gene expression, protein synthesis, and many other biochemical reactions, including respiration and photosynthesis. For many of these processes, ATP must be transported from its site of synthesis to another subcellular compartment.

1.2.7.1 ATP transport in mitochondria

Current studies suggest that mitochondria are the main source of cytosolic ATP in both the light and dark (167, 168). ATP transport from mitochondria to cytosol occurs through antiport with exchange for ADP catalyzed by ADP/ATP carriers (AAC) (169). The Arabidopsis genome encodes three AACs (170). These were functionally characterized by heterologous expression in *E. coli* where ATP uptake activity was confirmed using radiolabeled adenylates (171).

1.2.7.2 ATP transport in plastids

Autotrophic plastids, i.e., chloroplasts, are capable of generating ATP via photosynthesis. However, non-photosynthetic plastids like amylopasts, leucoplasts, chromoplasts, and etioplasts cannot synthesize ATP. Therefore, ATP must be imported from the cytosol in these plastids. Arabidopsis contains two plastidic ATP/ADP transporters, AtNTT1 and AtNTT2 (172, 173). Spatial and temporal differences in promoter activities were observed during initial stages of

development (174). Highest activity of the *AtNTT2* promoter is detected in the root tip, root hairs, cotyledons, and mature leaves. In contrast, *AtNTT1* is only detected in vascular bundles of leaves after 5 days of growth. Mutations of *AtNTT2* impaired primary root growth, chlorophyll content, thylakoid structures, and reduced rosette size during short day conditions (174). Thus, this study emphasizes the importance of ATP import into plastids to sustain root and leaf development. For example, fatty acid biosynthesis in root plastids rely on ATP import from cytosol (175). Therefore, reduced synthesis of fatty acids may be responsible for impaired root growth.

1.2.7.3 ATP in cytosol

In photosynthetic cells, ATP is required in the cytosol for various biosynthetic processes, including sucrose synthesis. The demand for ATP may exceed that supplied by glycolysis. In the light, both chloroplasts and mitochondria can generate ATP by photophosphorylation and oxidative phosphorylation, respectively. However, there is no evidence of ATP export from chloroplasts to cytosol (168). Therefore, mitochondria are the primary contributors of ATP to the cytosol. This was demonstrated by the decrease in cytosolic ATP levels after suppression of the mitochondrial respiratory chain, whereas photosynthetic inhibitors did not affect cytosolic ATP levels (168). ATP transport from mitochondria to cytosol occurs via AACs, as discussed previously. Cytosolic ATP is also imported into non-photosynthetic plastids like amyloplasts (176). ATP required to drive high-energy processes like protein transport, protein folding, and phosphorylation and glycosylation of proteins and lipids in the endoplasmic reticulum (ER) lumen is transported from the cytosol via ER-ANT1 transporters (177). Therefore, cells require constant transport of ATP between the cytosol and multiple organelles, which creates a highly dynamic environment. A better understanding of ATP dynamics in some of these compartments

has been accomplished through development of imaging tools discussed in Chapter IV of this dissertation.

1.2.8 Key questions addressed in the following chapters

Although substantial research has been conducted on Pi and ATP transport in plant cells, there are still many unanswered questions. These include: i. Is cytosolic Pi uniformly distributed in Arabidopsis roots or are there distinct spatial differences? ii. Do cells of all developmental zones participate in Pi uptake equally? iii. Is there any spatial difference in metabolic recycling, Pi uptake, and vacuolar sequestration between zones? These questions are addressed in Chapter II of this dissertation.

In Chapter III, I describe spatial analysis of Pi distribution in Arabidopsis root hairs. This project answers the following questions: i. Does cytosolic Pi concentration in root hairs correlate with hair length? ii. Is Pi uniformly distributed in a root hair? iii. Is there any spatial difference in Pi uptake activity and vacuolar sequestration within a root hair? iv. Are cytosolic Pi concentrations in root hairs the same as those in primary root cells?

Chapter IV of this dissertation addresses the following questions: i. What are the appropriate imaging controls for quantitative ratiometric analysis of FRET-based ATP sensors in plant cells? ii. How do cytosolic ATP levels vary between different developmental zones of Arabidopsis root?

CHAPTER II

CONTRIBUTIONS OF PHOSPHATE UPTAKE, RECYCLING, AND VACUOLAR SEQUESTRATION IN DEVELOPMENTAL CONTROL OF CYTOSOLIC PHOSPHATE IN ARABIDOPSIS ROOTS *

2.1 Introduction

Phosphorus is an essential nutrient that plants acquire, assimilate, and distribute to cellular and subcellular organelles as inorganic phosphate (Pi). Although substantial amounts of Pi are needed for optimal plant growth and productivity, much of the Pi in soil is unavailable because it exists as sparingly soluble complexes or in organic forms that are not directly accessible to plants (2). To cope with low Pi conditions, plants activate a complex array of adaptive responses to enhance Pi acquisition and to recycle and reallocate internal stores. These Pi starvation responses (PSRs) include growth of lateral roots and root hairs to increase the range and capacity for nutrient scavenging (78, 178), which are extended in many species through the formation of mycorrhizal symbiosis (179); secretion of organic acids and phosphatases to increase the concentration of available Pi in soil solution (180); increased production of Pi transporters at the root-soil interface (11); modification of metabolic pathways to conserve cellular Pi (181); and redistribution of Pi between organs and subcellular compartments (22, 182, 183). Signaling mechanisms governing PSRs include responses to external Pi concentrations to modify the root system architecture (71, 73, 74, 184, 185) and responses to internal Pi concentrations to maintain Pi homeostasis (186-191). How these signaling mechanisms are coordinated is unclear, but Pi itself is regarded as a primary signal (82, 187, 192, 193). For

* Part of the data reported in this chapter is reprinted with permission from "Live Cell Imaging of Inorganic Phosphate Distribution in Multicellular Organisms Using a FRET Based Biosensor" by Dr. Swayoma Banerjee. Doctoral Dissertation, Texas A&M University. Copyright 2017 Swayoma Banerjee.

metabolites such as diphosphoinositol phosphates (PP-InsPs) promote interaction between SYG1/Pho81/XPR (SPX)-domain containing proteins and Phosphate Starvation Response (PHR) transcription factors to modulate the activation of many PSR genes (187, 190, 193, 195, 196). Together, these observations suggest that the concentration of Pi in the cytosol elicits appropriate responses to changes in Pi availability.

Because the cytosol is the nexus for both intracellular and intercellular Pi distribution, multiple processes must be coordinated to maintain cytosolic Pi concentrations within a relatively narrow, but dynamic range. Initially, Pi uptake is mediated under both Pi-replete and Pi-deficient conditions by members of the PHT1 family of Pi transporters located in the plasma membrane of root epidermal and cortical cells as well as the root cap (6, 24). Mutants with defects in PHT1 transporters or their trafficking to the plasma membrane exhibit reduced Pi uptake and diminished overall plant growth and development (6, 17, 18, 24, 92). An innovative ^{33}P imaging technique demonstrated that PHT1 transporters in the root cap contribute a substantial portion of total root Pi acquisition (24). However, the impact of this uptake activity on cytosolic Pi concentrations in the root cap and other parts of the root is unknown because this imaging approach does not distinguish subcellular locations or inorganic from organic forms of Pi.

Pi acquired by the root is rapidly assimilated to form ATP via oxidative and substrate-level phosphorylation (9) and then incorporated into macromolecules and metabolites from which Pi is subsequently recycled with varied rates and magnitudes (181). Much of the assimilation and metabolic recycling of Pi occurs in organelles, and intracellular Pi transporters are therefore required to direct Pi between the cytosol and each cell compartment (182). Notably, Pi transport into the vacuole, the largest reservoir of Pi in the cell, is catalyzed by members of the

PHT5 (also named VPT) transporter family (14, 40, 61), whereas its export from the vacuolar lumen is mediated by members of the VPE transporter family (40). Mutants with defects in these transporters exhibit altered patterns of vacuolar Pi accumulation consistent with their roles in either import or export, as well as altered expression of PSR genes and reduced overall plant growth, suggesting that these defects also affect cytosolic Pi concentrations (14, 40, 61). Although the vacuolar Pi pool can help buffer the cytosol against concentration changes (183, 197), this buffering can be exhausted or outpaced by chronic or acute Pi deprivation, respectively, resulting in altered cytosolic Pi concentrations (165, 197, 198).

Pi is mobile in plants and its distribution between cells in the root, as well as its movement to shoots via xylem and its redistribution back to roots via phloem, could also influence cytosolic Pi concentrations within individual root cells. Mechanisms of intercellular movement of Pi within the root vary with development. Cell-to-cell diffusion through plasmodesmata (symplastic transport) is possible in apical parts of the root spanning from the meristematic zone to the first root hair-containing region of the differentiation zone (199, 200). However, symplastic connectivity is blocked in the differentiation and mature root zones, including root hairs, necessitating transmembrane transport processes to cross the plasma membrane. The transfer of Pi from root to shoot requires export of cytosolic Pi to the xylem apoplastic space, which is mediated by PHO1 transporters in cooperation with a subset of PHT1 transporters (64, 66, 201, 202). Mutations of *PHO1* cause reduced Pi content in shoots, stunted growth, and strong expression of PSR genes (64, 66). It is currently unclear which transporters are responsible for the redistribution of Pi from shoot to root, but transcript localization data suggest that members of the PHT1 family may be involved (201).

The relative contributions of the different processes that influence cytosolic Pi homeostasis and any spatiotemporal variations in these processes within roots are largely unknown. This is primarily due to the difficulty of distinguishing cytosolic Pi from other cellular pools in live plants (203). We previously reported that ratiometric imaging of a genetically encoded FRET-based Pi sensor stably expressed in Arabidopsis could be used to monitor relative changes in cytosolic Pi concentrations in epidermal cells within the differentiation or mature zones of the root (165, 166). Here, we have extended and calibrated this live imaging approach to systematically evaluate absolute, rather than relative, cytosolic Pi concentrations in different tissues and developmental zones of the root under Pi-replete and Pi-deficient growth conditions. We show that cytosolic Pi concentrations differ between developmental zones with highest levels in the transition zone, and that this distribution pattern is independent of Pi supply. We also distinguish the contributions of Pi uptake and metabolic recycling to cytosolic Pi levels by blocking Pi assimilation with cyanide. Similar experiments conducted with a vacuolar Pi uptake mutant, *pht5;1-2* (14), suggest that developmental differences in vacuolar sequestration are responsible for the observed pattern of Pi distribution in the root.

2.2 Results

2.2.1 Spatial Analysis of Cytosolic Pi Concentrations in the Root Under Pi-replete Growth Conditions

We hypothesized that cytosolic Pi concentration is not uniform in the root due to spatial differences in Pi uptake activities (24) and metabolic demands for Pi, e.g., cell division in the root apical meristem (204). To explore this possibility, we first examined relative cytosolic Pi levels in epidermal cells throughout the developing and mature root of seedlings grown under Pi-replete (0.25 mM) conditions. Seedlings that constitutively express a Pi sensor (cpFLIPPi-5.3m) were grown for 6 days, which surpassed the time after germination needed to establish root

meristem size (205). We then imaged roots to determine Pi-dependent FRET ratios (FRET/eCFP) as a readout of relative Pi concentration (166). Images were captured of cells in each of the developmental zones starting from the root tip, namely the meristematic zone (MZ), transition zone (TZ), elongation zone (EZ), differentiation zone (DZ), and mature root zone (MR) (99, 109, 206). Representative images shown in **Figure 6** (1) revealed that Pi-dependent FRET ratios varied between root zones with a consistent pattern in which cells in the TZ had the highest relative Pi levels. We attributed differences in FRET ratio to Pi concentrations rather than nonspecific effects of cellular environments or to imaging artifacts because no spatial variation in FRET ratio was detected for a Pi-insensitive control sensor (cpFLIPPi-Null) (166) (**Figure 6**) (1). Although these results supported our initial hypothesis of non-uniform Pi distribution in the root, the developmental pattern was surprising because cells in the MZ, TZ, and EZ are symplastically connected (199, 200).

To determine absolute, rather than relative, cytosolic Pi concentrations in the root we needed to calibrate Pi sensor FRET ratios. *In situ* calibration has been used for other FRET-based ion sensors (207, 208), but we were unable to use this approach because no suitable ionophore and membrane-permeable chelator for Pi was available. We found that *in vitro* calibration was also unsuitable because FRET ratios measured in roots were consistently outside the saturation limit measured *in vitro* despite the use of identical imaging conditions and regardless of assay buffer composition (165), suggesting that the cell wall or other cell materials may unequally influence, e.g., quench, emission from the two fluorescent protein components of the sensor. We therefore employed a microinjection strategy to directly manipulate cytosolic Pi concentration and then measure FRET ratio within the injected cell (1).

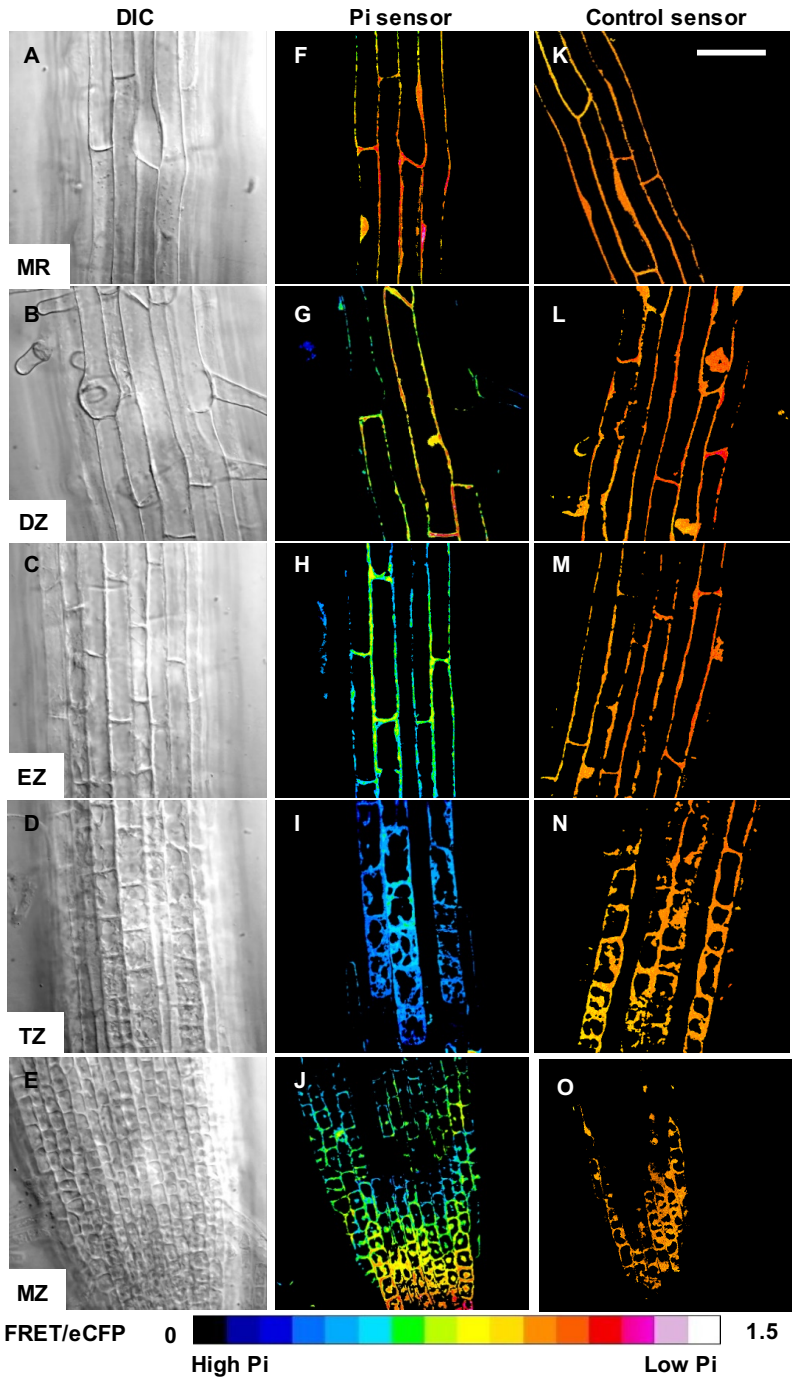

Figure 6: Ratiometric imaging of cytosolic Pi levels in Arabidopsis roots. DIC (A-E) and FRET/eCFP ratio micrographs (F-O) of five developmental zones: MZ, meristematic zone; TZ, transition zone; EZ, elongation zone; DZ, differentiation zone; MR, mature root. Panels F-J show representative FRET ratio images of a Pi sensor and panels K-O show representative FRET ratio images of a control sensor that is unresponsive to Pi. Scale bar is 50 microns. *This figure is adapted from Swayoma Banerjee, Doctoral dissertation, Texas A&M University (1).*

Epidermal cells located in the TZ were injected with solutions buffered at cytosolic pH (7.3) (208) that contained defined Pi concentrations, potassium gluconate as needed to maintain constant potassium ion concentration, and the fluorescent protein mRuby2 as a marker (**Figure 7A**) (1). To ensure that cytosolic Pi concentrations closely matched injected concentrations, including those below endogenous levels, 6 to 8-fold greater volumes than the average cytosolic volume of these cells (**Table 1**) were injected. As shown in **Figure 7B** (1), the mRuby2 marker

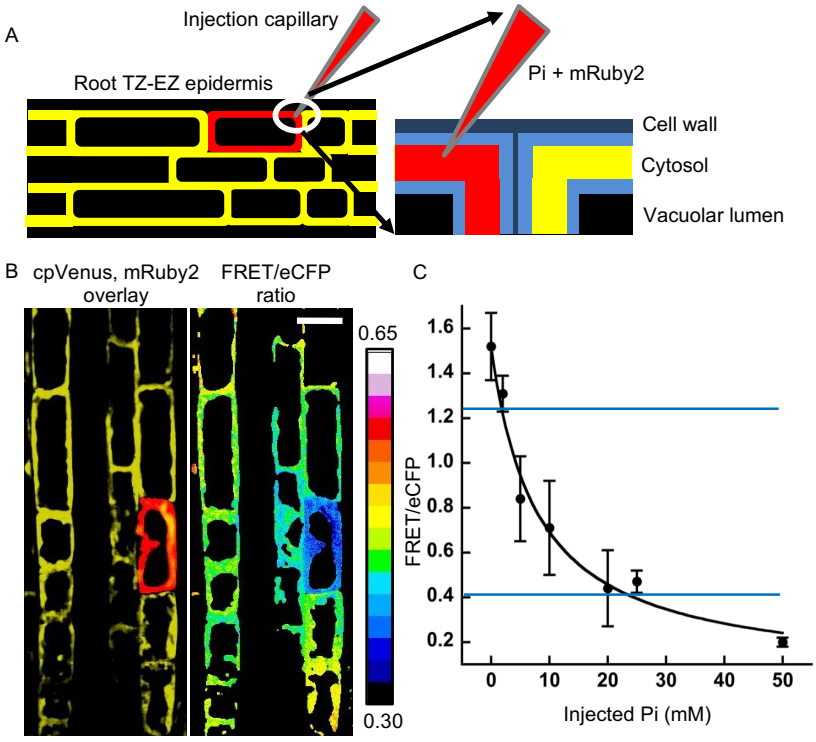

Figure 7. *In vivo* calibration of Pi sensor FRET ratios. (A) Schematic representation for microinjection of an epidermal cell in the TZ located near the EZ junction. Red color (mRuby2) demarcates the spread of injection solution within the cell. Inset shows the capillary tip positioned in the cytosol and injection of Pi and mRuby2 marker. (B) Fluorescent micrographs indicating cpVenus emission merged with mRuby2 emission and FRET/eCFP ratio image of the root after Pi injection. The color scale represents FRET/eCFP ratios. Scale bar is 20 micron. (C) *In vivo* calibation curve for Pi sensor FRET/eCFP ratio. Plotted values are mean FRET/eCFP ratios ± SD obtained from 6-8 individual cells. *This figure is adapted from Swayoma Banerjee, Doctoral dissertation, Texas A&M University* (1).

	Growth condition	
	Pi-replete	Pi-starved
Location	Volume (pL)	Volume (pL)
MR	17.3 ± 6.2	13.7 ± 7.1
DZ	15.9 ± 2.6	8.6 ± 4.4
EZ	14.1 ± 5.2	4.5 ± 0.9
TZ	2.8 ± 1.3	2.1 ± 0.3
MZ	1.5 ± 0.4	1.4 ± 0.6
LRC	5.9 ± 2.4	3.5 ± 0.6

Table 1: Volume of cytosol in root epidermal cells. Mean ± SD volumes were determined from voxel counts in image Z-stacks of 3-22 cells in 4-5 independent plants.

remained confined within the cytosol of the injected cell; however, altered FRET ratios in adjacent cells suggested that Pi in the excess volume of injection buffer flowed into these cells via plasmodesmata (199, 200). Cells were not visibly damaged by injection, and FRET ratios returned to the pre-injection value within 5 min. To minimize variation in Pi concentrations as the cells reset, cells were imaged within 1.5 s after injection. The resulting data were fit to a single-site binding isotherm to generate an *in vivo* calibration curve (**Figure 7C**) (1) that encompassed all endogenous cytosolic Pi FRET ratio values measured in this study. Moreover, the dissociation constant (K_d) of 7.4 ± 1.7 mM was the same as that measured *in vitro* (7.4 ± 0.5 mM), suggesting that the sensor was unaffected by the cellular environment.

We used *in vivo* calibration of the Pi sensor to systematically quantify cytosolic Pi concentrations in different tissues and developmental zones of the root. Optical sections were captured in 50 μm increments from the root tip to the MR at multiple depths to distinguish Pi concentrations in the epidermis, cortex, and endodermis. As shown in **Figure 8** (1), independent plants exhibited a highly consistent distribution pattern with highest cytosolic Pi concentrations in the TZ (~10 mM), and lowest concentrations in the MZ and MR (3.5 to 4 mM). Pi

concentrations were the same in each tissue within a given developmental zone. However, we were unable to measure cytosolic Pi in the endodermis in the youngest portion of the root because we could not detect fluorescence from the sensor in this region regardless of whether the sensor was expressed from the Arabidopsis *UBQ10* or *CaMV35S* promoters.

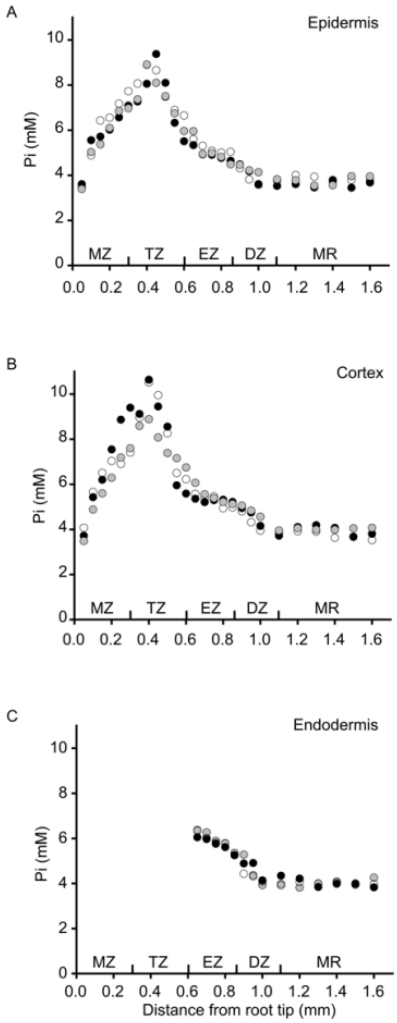

Figure 8: Quantification of cytosolic Pi concentrations in root tissues and developmental zones. Cytosolic Pi concentrations were measured at 50 micron increments from root tip to the beginning of the MR in (A) epidermal, (B) cortical, and (C) endodermal cells of three independent plants. *This figure is adapted from Swayoma Banerjee, Doctoral dissertation, Texas A&M University* (1).

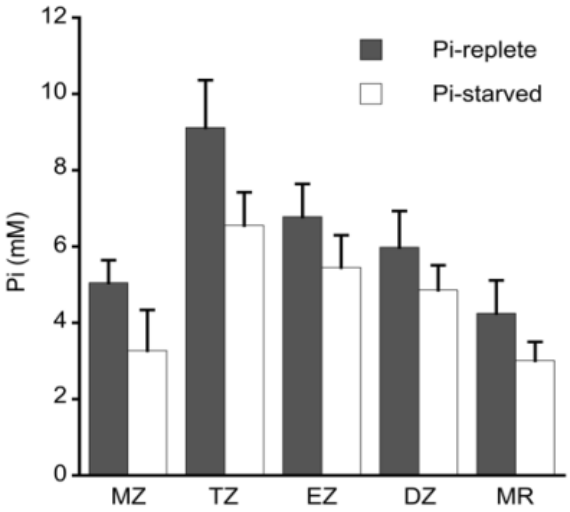

Figure 9. Effect of Pi deprivation on cytosolic Pi concentrations. Seedlings were grown in Pi-replete conditions for 6 d then transferred to the same medium or to medium lacking Pi (Pi-starved) for an additional 2 d. Pi concentrations (mean ± SD) were measured in epidermal cells of 5-7 independent plants. Pi concentrations in all developmental zones of Pi-starved plants are significantly less than those in plants held in Pi-replete conditions ($p<0.05$, Student's t-test). *This figure is adapted from Swayoma Banerjee, Doctoral dissertation, Texas A&M University* (1).

2.2.2 Effect of Pi Availability on Cytosolic Pi Concentrations in the Root.

We observed previously that relative cytosolic Pi levels in the DZ and MR decreased when plants were starved for Pi (165, 166). We therefore sought to determine the magnitude of these changes in absolute Pi concentration and to test if this response to Pi deprivation also occurs in other parts of the root. Seedlings were grown for 6 d in Pi-replete medium and then transferred to either fresh replete medium or to medium lacking Pi (Pi-starved) for an additional 48 h. Previous experiments demonstrated that this starvation regime is sufficient to induce other PSRs but does not initiate cell death, which is observed when deprivation is prolonged (165). Cytosolic Pi concentrations were measured in epidermal cells within each root developmental zone. As shown in **Figure 9** (1), Pi concentrations were reduced in all developmental zones by the starvation treatment. The reduction was greatest in the TZ (2.6 mM) and least in the DZ (1.1

mM). However, these changes, and those in all other developmental zones, were proportional to the respective initial concentrations. As a result, the distribution pattern with peak concentrations in the TZ was maintained.

Given the magnitudes of spatial differences in cytosolic Pi concentrations in the root under both Pi-replete and Pi-starved growth conditions, we next asked if there are also temporal differences in responses to Pi starvation and to subsequent replenishment. Seedlings were grown and then starved for Pi for 48 h as described above and then returned to Pi-replete medium for an additional 60 h. Cytosolic Pi concentrations were measured every 12 h and compared to those in plants that were held in Pi-replete medium (**Figure 10**) (1). Cells in the MZ and MR were the first to respond to Pi starvation with a reduction in cytosolic Pi concentration detected in 12 h that continued to steadily decrease throughout the treatment, suggesting that cells in these developmental zones are most sensitive to Pi deprivation. In contrast, Pi levels in the EZ and the DZ showed the highest resistance to Pi deprivation with cytosolic Pi levels remaining constant for 36 h and a decline detected only after 48 h. Surprisingly, cytosolic Pi levels in cells within the TZ fluctuated during the starvation treatment with low concentrations at both 24 h and 48 h.

Although cells in the EZ and DZ appeared to be the most resistant to Pi deprivation, these cells showed the fastest response to Pi replenishment with hyperaccumulation of Pi beyond pre-deprivation levels within 12 h. Pi levels in the EZ declined slowly over the next 48 h, whereas Pi levels in the DZ returned to baseline within an additional 12 h. Hyperaccumulation of cytosolic Pi also occurred in cells within the MZ and TZ, but unlike cells in the EZ and DZ, it took 24 h to reach peak values. High Pi concentrations persisted in the MZ throughout the remainder of the

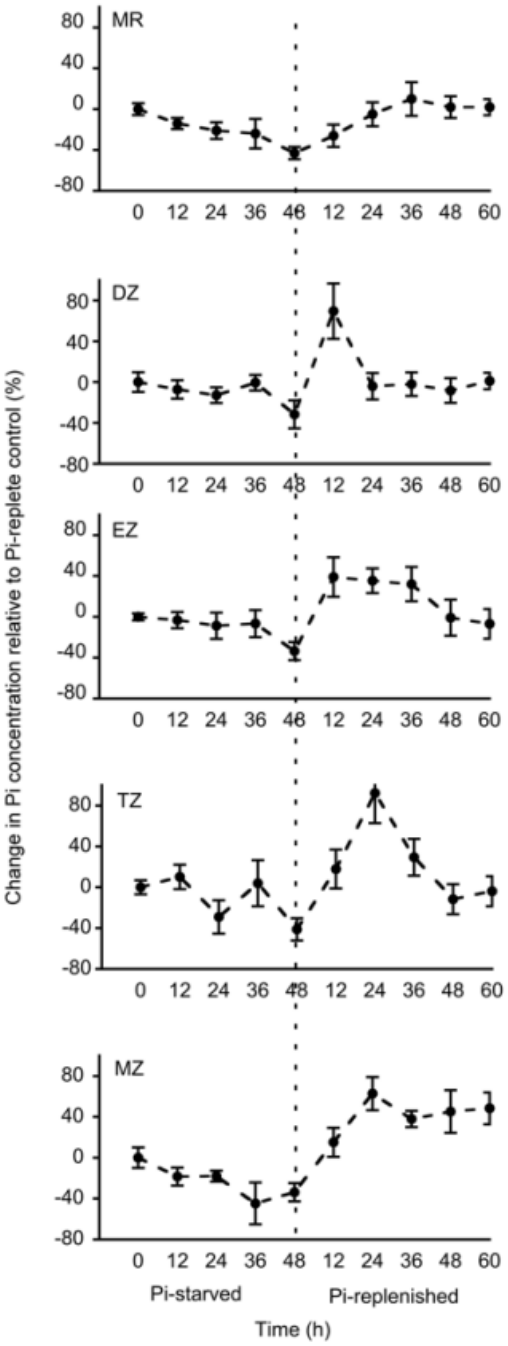

Figure 10. **Spatiotemporal dynamics of cytosolic Pi concentrations during changes in Pi supply.** Seedlings were grown in Pi-replete medium for 6 d then transferred to medium lacking Pi (Pi-starved) for 48 h and then transferred back to Pi-replete medium (Pi-replenished) for 60 h. Epidermal root cells were imaged every 12 h. A control group of plants were maintained in Pi-replete medium. Plotted values are mean ±SD percent change in Pi concentration relative to the control plants with 6-8 independent plants in each group. The dashed vertical line indicates the transition point from Pi-starved to Pi-replenished. *This figure is adapted from Swayoma Banerjee, Doctoral dissertation, Texas A&M University* (1).

experiment, whereas Pi levels in the TZ returned to baseline within an additional 24h. Cells in the MR were the slowest to respond to replenishment and reattained baseline concentrations after 24 h. These varied spatiotemporal responses to Pi deprivation and replenishment suggest specialization of mechanisms controlling cytosolic Pi concentration in each developmental zone of the root.

2.2.3 Spatial Analysis of Pi Recycling and Uptake in the Root

Because cellular Pi is rapidly assimilated to ATP and subsequently recycled from ATP and other organic-P molecules at unknown rates (9, 181), it has not been possible to resolve the individual contributions of uptake, assimilation, and metabolic recycling toward cytosolic Pi concentration. Moreover, the effects of any spatial variations in these processes within the root would be diluted, if not fully masked, in steady-state conditions due to symplastic and vascular transport. However, I reasoned that I could distinguish the initial contributions of Pi uptake and recycling, and also identify potential spatial differences in these processes, through a novel application of our Pi imaging approach. Specifically, if I used cyanide (CN) to rapidly inhibit the assimilation of Pi to ATP (209) then I expected to see increased cytosolic Pi levels in the absence of external Pi due primarily to metabolic recycling (hydrolysis of Pi from organic-P molecules). Similarly, if Pi was supplied to a CN-treated root then I predicted that cytosolic Pi concentrations would increase further due to uptake, and I could determine the contribution of this process by difference. To test this strategy, I grew plants grown under our standard Pi-starvation regime to maximize uptake activities while maintaining the spatial pattern of cytosolic Pi concentrations. Preliminary experiments indicated that 10 mM CN was sufficient to induce a maximum change in cytosolic Pi concentration (**Figure 11**) with no nonspecific effects detected with the Pi-

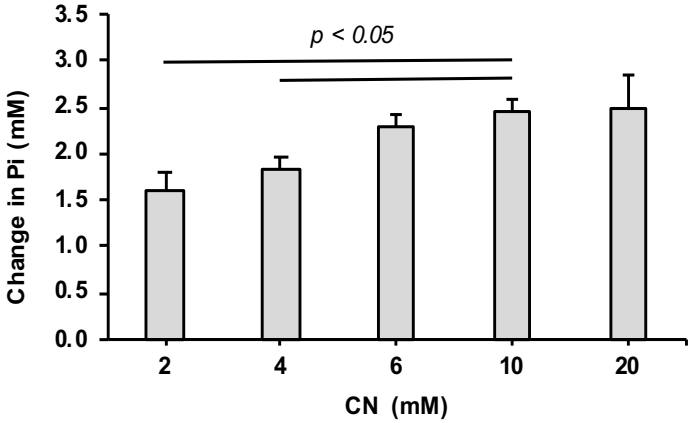

Figure 11. Change in cytosolic Pi in response to increasing concentrations of cyanide. Seedlings were grown in Pi-replete medium for 6 d then transferred to medium lacking Pi for 48 h. Change in cytosolic Pi was calculated in epidermal MZ cells after seedlings were treated with different concentrations of cyanide. Plotted values are mean ± SD change in Pi concentration after 5-11s of cyanide treatment in 3-4 independent seedlings. There is a statistically significant difference between indicated groups ($p<0.05$, Student's t-test).

insensitive sensor, and that cell viability, as assessed by SYTOX orange was unaffected even if the treatment was continued for 2 min (**Figure 12**).

As shown in **Figure 13A**, CN treatment in the absence of external Pi induced a rapid increase in cytosolic Pi levels that I attribute to recycling. Pi concentrations consistently reached a maximum within 8 to 10 s, which presumably reflects the time needed to exhaust the Pi recycling capacity of the cell and/or the existing ATP pool. To compare Pi recycling activities in different parts of the root I measured the maximum CN-induced changes in cytosolic Pi concentrations in the lateral root cap (LRC) and in epidermal cells within each developmental zone (**Figure 13B**). I found that Pi recycling occurs at a low level in the LRC, MZ, and TZ, and a higher level in the EZ, DZ, and MR. However, these activities did not correlate with the respective cytosolic Pi concentrations (**Figure 9)** (1) indicating that recycling is not a major determinant of the developmental pattern of Pi distribution.

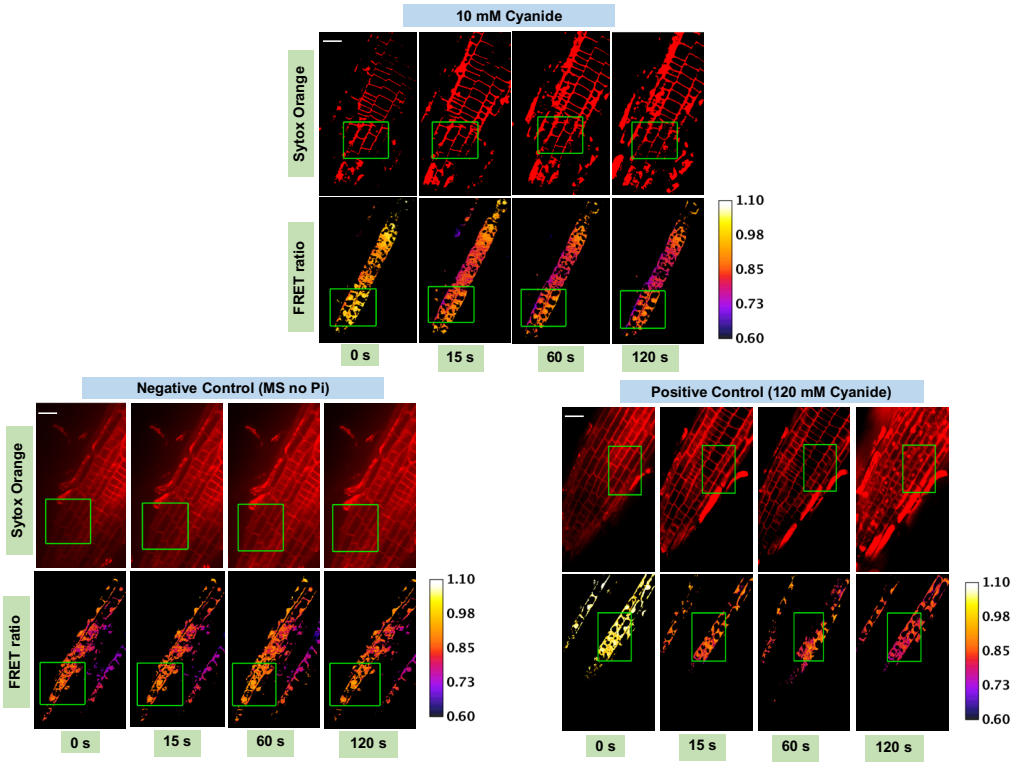

Figure 12. Testing cell viability after cyanide treatment using SYTOX Orange. Seedlings were grown in Pi-replete medium for 6 d then transferred to medium lacking Pi for 48 h. Plants were incubated in 250 nM SYTOX Orange for 10 min before imaging and then subjected to CN (10 mM or 120 mM) or MS medium (negative control). No cell death was observed in plants treated with 10 mM CN or the negative control. Nuclear staining was observed in seedlings treated with 120 mM CN (positive control) indicating cell death. Size bar, 50 μm.

To distinguish the contribution of uptake to cytosolic Pi levels I treated seedlings with CN as described above but also included external Pi (0.5 mM). As shown in **Figure 13A** , the combination of CN plus Pi resulted in higher cytosolic Pi concentrations than with CN alone, as I predicted, and the difference in Pi concentrations for these two treatments reflects newly acquired Pi. The differences in Pi levels were equivalent regardless of whether CN and Pi were added together or sequentially, indicating that CN had no measurable effect on uptake during the timespan of the assay (**Figure 14**).

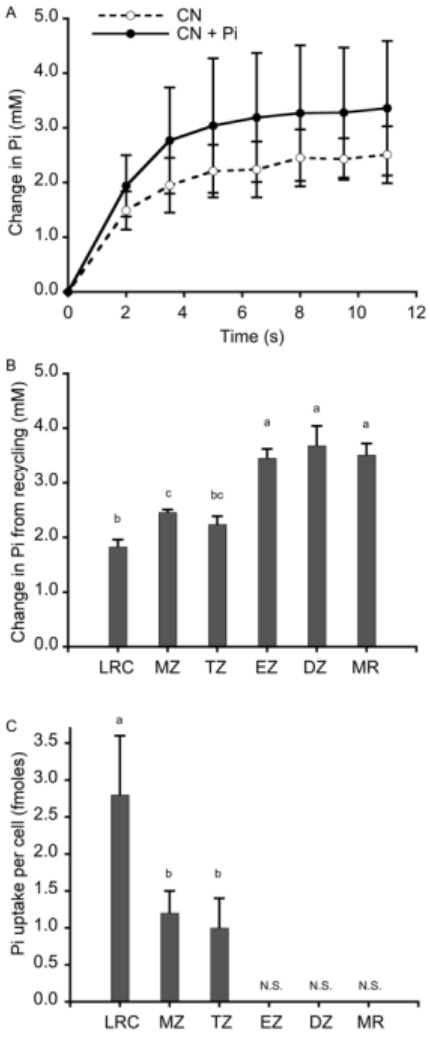

Figure 13: Spatial analysis of Pi recycling and uptake in roots. Seedlings were grown in Pi-replete medium for 6 d then transferred to medium lacking Pi (Pi-starved) for 48 h. (A) Change in cytosolic Pi concentrations in epidermal MZ cells when treated with CN and CN plus Pi, which reflect recycling and recycling plus uptake, respectively. Plotted values are mean ± SD change in Pi concentration (mM) at each time point for 6 independent plants. (B) Change in cytosolic Pi concentration from metabolic recycling. Plotted values are mean ± SD change in Pi concentration (mM) after CN treatment in 6-8 independent plants. There is a statistically significant difference between group means as determined by ANOVA ($p< 0.05$). A post hoc Tukey test showed that Pi recycling in TZ is significantly less than in EZ, DZ and MR but not significantly different from LRC and MZ. (C) Pi uptake calculated from differences in Pi concentrations when treated with CN with and without external Pi, and corrected for differences in cytosolic volumes. Plotted values are mean ± SD Pi uptake (fmoles) per cell during the 10 s assay period. Data were collected from 3-7 independent plants. There are statistically significant differences ($p< 0.05$) between group means as determined by ANOVA and Tukey HSD test. No significant uptake (N.S.) was detected in the EZ, DZ, and MR.

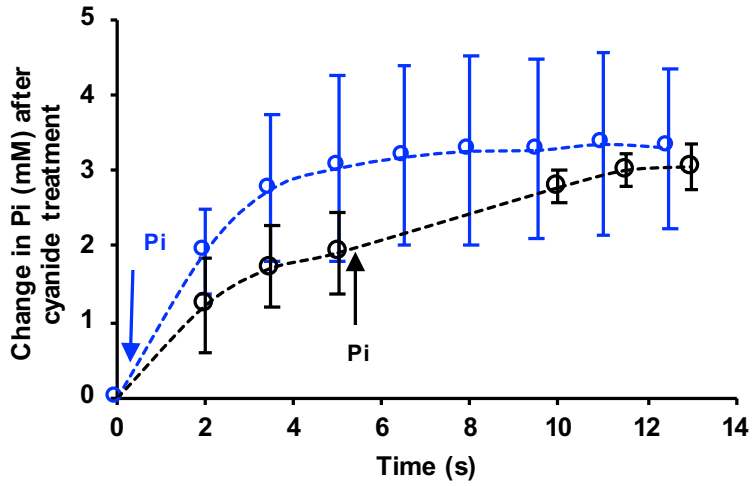

Figure 14. Effect of cyanide on Pi transport competency. 6 d old WT seedlings grown in 0.5X MS were Pi-starved for 48 hr. Blue markers represent seedlings treated with CN + Pi and change in Pi (mM) was measured for 12.5 s. Black markers represent change in Pi (mM) in seedlings that were first treated with CN for 5 s, then Pi was added. Mean Pi (mM) ± SD from 5- 6 individual seedlings are plotted.

To compare Pi uptake activities in different parts of the root, I measured maximum CN-induced changes in cytosolic Pi concentrations in the presence and absence of external Pi then calculated the differences. I detected equivalent changes in Pi concentrations indicative of Pi uptake in the LRC and MZ (0.78 ± 0.07 and 0.84 ± 0.02 mM, respectively), a lower activity in the TZ (0.47 ± 0.07 mM), and no significant changes in the EZ, DZ, and MR. The failure to detect Pi uptake in basal portions of the root is inconsistent with previous findings from radioisotopic Pi uptake experiments (24, 210). However, our assay did not account for differences in cytosolic volume. As a result, larger cells with more cytosol would require greater uptake to induce an equivalent change in Pi concentration. Because accounting for cytosolic volumes in cells that exhibited a change in Pi concentration (LRC, MZ, and TZ) would provide a more accurate comparison of uptake activities, I measured cytosolic volumes of epidermal cells in each location from voxel counts in image Z-stacks (**Table 1**) then calculated uptake as the

amount of Pi acquired during the 8 s needed to achieve the maximum change in concentration. As shown in **Figure 13C**, Pi uptake was greatest in the LRC (2.8 ± 0.8 fmoles), and less active in the MZ and TZ (1.2 ± 0.3 and 1.0 ± 0.4 fmoles, respectively). If Pi uptake occurred in the EZ, DZ, and MR at a rate equal to that in the TZ then the corresponding change in Pi concentration would have been at or below the limit of detection given the larger cytosolic volumes in these zones. Therefore, I can only conclude that Pi uptake in these regions occurs at a rate that is equal to or less than that in the TZ. Regardless, uptake activities measured in the LRC, MZ, and TZ did not correlate with the respective cytosolic Pi concentrations (**Figure 9**) (1), indicating that spatial differences in Pi uptake are not directly responsible for the observed developmental pattern of cytosolic Pi concentrations in the root.

2.2.4 Effect of Vacuolar Sequestration on Cytosolic Pi Concentrations in the Root

Given that vacuoles can store upto 90% of intracellular Pi in plants (10, 183), I hypothesized that spatial differences in cytosolic Pi concentrations in the root are the result of developmental differences in its vacuolar sequestration. That is, regions with less vacuolar Pi sequestration would exhibit higher cytosolic Pi concentrations. To test this idea, I compared cytosolic Pi concentrations in each developmental zone of the root in wild-type (WT) plants; a vacuolar Pi import-defective mutant, *pht5;1-2*; and a transgenic line in which the PHT5;1 transporter is overexpressed (*35S:PHT5;1*) (14). Although Arabidopsis encodes three PHT5 transporters, PHT5;1 is the primary source of vacuolar Pi sequestration (14, 42). All plants were grown under Pi-replete conditions for 6 d then imaged to determine steady-state cytosolic Pi concentrations. As shown in **Figure 15**, Pi accumulated to higher cytosolic concentrations in *pht5;1* than in WT in all developmental zones, although the difference was not significant in the TZ. In contrast, Pi concentrations in the *35S::PHT5;1* line were significantly lower than WT in

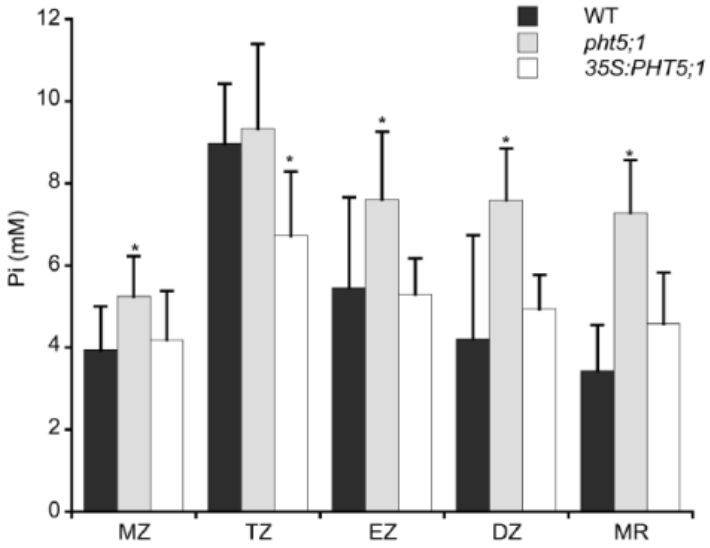

Figure 15. Effects of vacuolar sequestration on cytosolic Pi concentrations in the root. Seedlings were grown in Pi-replete medium for 6 d then imaged. Cytosolic Pi concentrations in *pht5;1-2* plants were significantly greater than WT in all zones except the TZ ($p < 0.05$, Student's t-test), whereas in *35S:PHT5;1* plants, cytosolic Pi levels were significantly less than WT ($p < 0.05$) only in the TZ. Plotted values are mean ± SD cytosolic Pi concentration from 5-16 independent plants.

the TZ, but similar in all other zones. These results suggest that in WT plants, less vacuolar Pi sequestration occurs in the TZ than in other developmental zones.

To more directly estimate spatial differences in vacuolar Pi sequestration I focused on cells in the MZ and TZ because these zones showed significant differences in Pi sequestration (**Figure 15**) but similar levels of recycling and uptake (**Figure 13B,C**). WT and *pht5;1-2* seedlings were grown with our standard Pi-starvation regime then treated with CN in the absence of external Pi. I monitored the increase in cytosolic Pi concentration until it reached saturation, which yielded changes in Pi concentration due to recycling as in **Figure 13B**. I then added CN + 0.5 mM Pi to the same seedlings and again monitored the increase in cytosolic Pi concentration until it reached saturation. The difference in Pi concentrations for these treatments indicated the combined activites of uptake and vacuolar sequestration (**Figure 16**). The contribution of

vacuolar sequestration could then be estimated by comparing the changes in cytosolic Pi concentration in WT to those in the *pht5;1* mutant. For cells in the MZ, changes in Pi concentration due to vacuolar sequestration and to uptake were nearly equal, indicating that a substantial fraction of newly acquired Pi is shuttled into vacuoles with a rate that is comparable to that of cellular uptake. This difference was much smaller for cells in the TZ, which is in agreement with results from steady-state measurements (**Figure 15**) indicating that significantly less vacuolar Pi sequestration occurs in this zone despite uniform expression of *PHT5;1* throughout the developing root (211). I also evaluated vacuolar Pi sequestration in *35S::PHT5;1* plants, but I detected no effect of *PHT5;1* overexpression on cytosolic Pi levels in either the MZ or TZ (**Figure 16**). It is possible that overexpression of *PHT5;1* augments vacuolar Pi sequestration at rate that is below the limit of detection for the short-term assay.

It was formally possible that the changes in cytosolic Pi concentrations in the *pht5;1* mutant that I attributed to a loss of vacuolar sequestration were instead due to greater Pi uptake in this mutant background. To test this possibility I grew plants under the same conditions, but transferred them to Pi-replete medium and measured the depletion of Pi from the medium as a readout of uptake (**Figure 17**). Pi concentrations in the media decreased with equal rates and magnitudes for WT and *pht5;1* indicating that Pi uptake was unaffected by the *pht5;1* mutation. These results suggest a developmental difference in vacuolar Pi sequestration with less activity in cells within the TZ, resulting in greater cytosolic Pi concentrations in this zone.

2.3 Discussion

The availability of Pi in most soils is suboptimal for crop growth and productivity, and this has led to the widespread use of Pi-containing fertilizers. However, this practice is not economically or environmentally sustainable (4). A comprehensive understanding of how plants

acquire and use Pi is therefore needed to optimize agricultural practices and to develop cultivars that are less reliant on Pi fertilizers to obtain high yields. Toward this goal, I developed a dynamic, high-resolution map of cytosolic Pi concentrations in the root, as well as the means to distinguish the contributions of distinct processes that influence cytosolic Pi homeostasis, i.e., uptake, metabolic recycling, and vacuolar sequestration.

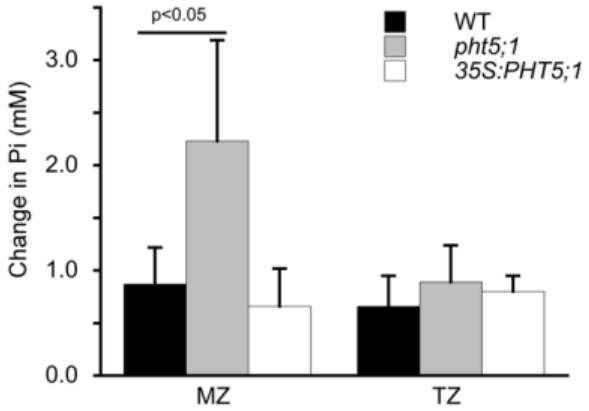

Figure 16. Contributions of vacuolar sequestration in cytosolic Pi of MZ and TZ. WT and *pht5;1-2* seedlings were grown in Pi-replete medium for 6 d then transferred to medium without Pi (Pi starved) for 48 h. Seedlings were sequentially treated with CN and then CN+Pi and the changes in cytosolic Pi concentrations after each treatment were measured. Differences in Pi concentrations (mean ± SD for 5-10 independent plants) between these treatments reflect the combined activities of Pi uptake and vacuolar Pi sequestration. The difference between WT and pht5;1 in the MZ was significant ($p<0.05$, Student's t-test).

Ratiometric imaging of a genetically encoded FRET-based Pi sensor that was constitutively expressed in Arabidopsis revealed that cytosolic Pi concentrations are not uniform in the primary root (**Figure 6**) (1). However, as with other sensors that report ratiometric or normalized fluorescence values, this approach yielded relative rather than absolute measures of Pi concentration, so I could not define the magnitudes of the observed differences. Estimates of Pi concentrations based on an *in vitro* calibration were unreliable because FRET ratio values

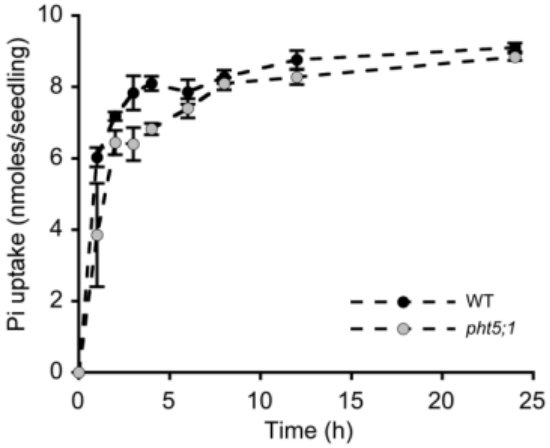

Figure 17. Uptake of external Pi by entire root. WT and *pht5;1* seedlings were grown for 6 d in Pi replete medium then transferred to medium without Pi (Pi-starved) for 48 h. Seedlings of each genotype were then transferred in groups of 12 to single wells of a 12-well plate containing Pi-replete medium and then aliquots were withdrawn over time for Pi measurement. Pi uptake was calculated from the depletion of Pi in the medium. Plotted values are mean ± SD nmoles Pi/seedling from four independent groups of each genotype. There is no significant difference in Pi uptake activities for these genotypes.

measured in plants were outside the calibration limits. This incongruity was eliminated, however, when I used *in vivo* calibration (1). This suggests that the cell wall or other cell components unequally affect, e.g., quench, fluorescence emission from the two fluorescent protein portions of the sensor. Caution is therefore warranted when making estimates of *in vivo* concentrations of analytes from *in vitro* calibrations of fluorescence-based sensors, especially those that contain the same or closely related fluorescence protein variants of CFP and YFP as those present in the Pi sensor (165).

In vivo calibration of Pi sensor FRET ratios relied on microinjection to dilute and displace endogenous cytosolic Pi with buffers containing defined Pi concentrations and rapid imaging to minimize the effects of compensatory processes. I used the resulting calibration curve to estimate endogenous cytosolic Pi levels throughout the root and found that these ranged from a low of 3 mM in the MZ and MR under Pi-starved conditions to a maximum of 12 mM in the

TZ under Pi-replete conditions. These concentrations agree with estimates derived from enzyme kinetic studies in which Pi is a substrate or effector (212-214), as well as studies using ^{31}P NMR spectroscopy with plant cell suspensions (215), although values as low as 60 μM have been reported (197). Lower Pi levels can be attained with prolonged Pi starvation, but I observed previously that this also led to substantial cell death under our growth conditions (165). Microinjection is technically challenging and requires specialized equipment, both of which limit the utility of this approach for others. However, because there is little variation in Pi concentration profiles between plants (**Figure 8**) (1), I suggest that Pi sensor-expressing plants grown under the same conditions described here can be used as references for other imaging systems. Moreover, because Pi concentrations were the same across tissue layers within a given zone, confocal capabilities may not be necessary.

Although cytosolic Pi concentrations diminished in all developmental zones of the root when plants were starved for Pi, reductions after two days were proportional so the overall pattern with highest concentrations in the TZ was maintained. However, when temporal changes in cytosolic Pi concentrations during Pi deprivation and subsequent resupply were examined, we found that responses differed between zones (1). For example, cells in the EZ and DZ had the slowest response to Pi starvation, suggesting that they are relatively insensitive to Pi deprivation, but these cells also exhibited the fastest recovery with transient hyperaccumulation when Pi was replenished. Distinct spatiotemporal responses to Pi availability suggest differences in one or more of the mechanisms that control cytosolic Pi homeostasis. These include uptake from the environment, assimilation to organic forms, metabolic recycling from assimilated forms, sequestration in organelles, and intercellular movement. Although most of these processes are likely to occur simultaneously in a given cell, I was able to distinguish individual contributions

of some processes by inhibiting Pi assimilation in the presence and absence of external Pi in combination with short assay times that minimized the effect of its intercellular movement.

When Pi assimilation was blocked in the absence of external Pi (no uptake) I detected rapid increases in cytosolic Pi levels that I attributed to metabolic recycling. Recycling activities consistently reached maximum levels within 10 seconds suggesting that additional effects of intercellular movement in this timespan would be negligible. However, because re-assimilation of Pi liberated from organic forms during this time would also be inhibited, my measures of Pi recycling must be viewed as under-estimates. Nevertheless, Pi recycling activity was not uniform in the root. Pi recycling was greater in the basal portion of the root with equivalent activities in the EZ, DZ, and MR, while less recycling occurred in the apical part of the root with equivalent activities in the LRC, MZ, and TZ (**Figure 18**). The basis for this spatial difference in metabolic recycling is unclear because there was no correlation with cell size or with processes associated with specific developmental zones, e.g., cell division in the MZ and cell elongation in the EZ. It is therefore likely that the two levels of Pi recycling we observed reflect distinct combinations of metabolic activities.

Adding Pi to roots while also inhibiting its assimilation led to increases in cytosolic Pi concentrations beyond those due to metabolic recycling alone. I attributed these additional gains in Pi concentration to uptake, which I detected in cells within the LRC, MZ, and TZ, but not the EZ, DZ, and MR. However, because this measure of Pi uptake is dependent on changes in its concentration, its magnitude is also a function of cytosolic volume. I therefore accounted for differences in cytosolic volumes to evaluate uptake as the amount of newly acquired Pi per cell. On this basis, uptake in the larger cells within the EZ, DZ, and MR may occur at rates equal to or

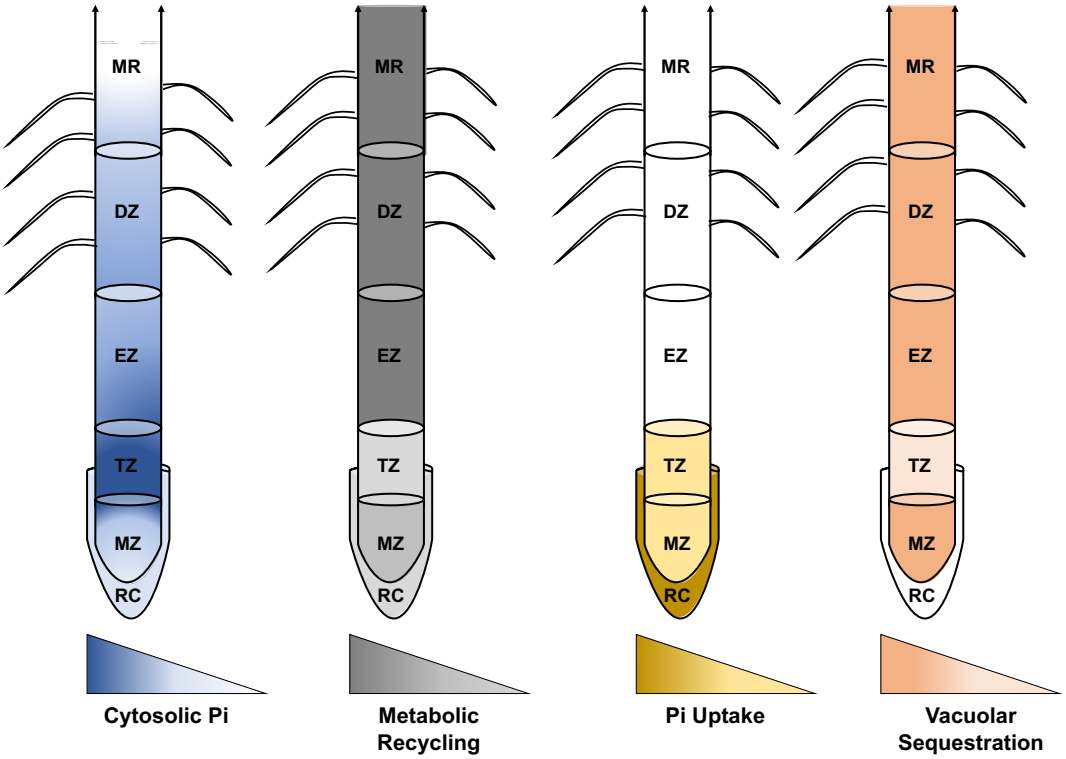

Figure 18: Schematic representation of spatial profiles for cytosolic Pi accumulation, metabolic recycling, uptake, and vacuolar sequestration in the root. Relative levels of each process are represented by color gradients. Missing information for uptake is represented by white. The pattern for vacuolar sequestration correlates with Pi distribution in the root.

less than those in the smaller, more apical cells. I found that Pi uptake was greatest in the LRC, which is consistent with localization of PHT1-type Pi transporters and the accumulation of total P after exposing roots to ^{33}Pi (24). Substantial Pi uptake was also detected with nearly equal activities in the MZ and TZ (**Figure 18**) suggesting that one or more PHT1-type transporters are also active in these zones. Future efforts to extend the live imaging approaches described here to Pi transport mutants may discern cell- or developmental zone-specific contributions of individual transporters.

Although I observed distinct spatial patterns in the root for both uptake and metabolic recycling of Pi, neither of these patterns correlated with cytosolic Pi concentrations. In contrast, the spatial pattern of vacuolar Pi sequestration suggested that this activity is a major determinant of the cytosolic Pi concentration profile in the root (**Figure 18**). Under Pi-replete growth conditions, the *pht5;1* mutant, which has a defect in loading Pi into vacuoles (14), showed hypera-accumulation of Pi in the cytosol throughout the root with the exception of the TZ. This implies that in WT plants, PHT5;1 is developmentally regulated for low activity in the TZ. As a result, cytosolic Pi concentrations are maintained at higher levels in the TZ than in the adjacent developmental zones. The mechanism by which PHT5;1 transport activity is regulated is unknown, but *PHT5;1* transcript abundance does not vary between developmental zones of the root (211). Interestingly, overexpression of *PHT5;1* reduced cytosolic Pi levels in the TZ but had no significant effect in the rest of the root. This difference may reflect a thermodynamic limitation for augmenting transport of Pi into vacuoles that already contain high concentrations of Pi.

The TZ precedes the elongating (EZ) cells where cellular architecture is reorganized to enable rapid cell elongation (216). It is possible that elevated Pi levels in the TZ are simply a consequence of concomitant vacuolar reorganization. Alternatively, I speculate that TZ-specific vacuolar control of cytosolic Pi levels may influence aspects of Pi signaling to affect cell elongation and cell division in neighboring root regions. Although cells in the TZ have the highest cytosolic Pi concentrations in the root, they also exhibit the greatest concentration change in response to Pi deprivation, ideally positioning these cells to sense fluctuations in Pi availability. My idea is based on recent findings supporting that the TZ integrates environmental cues, including low-Pi stress, with hormone signals to control cell fate and root growth (205,

217, 218). For example, when the root apex encounters low external Pi, cell elongation is rapidly inhibited through apoplastic malate, Fe, and peroxidase-dependent stiffening of the cell wall (184, 219). These processes are regulated through activities of three molecules: the transcription factor Sensitive To Proton Rhizotoxicity (STOP1), which is recruited to the nucleus under low Pi conditions via an unknown mechanism (184), Low Phosphate Root 1 (LPR1), which mediates ferroxidase activity in the cell wall (184, 219, 220); and Clavata3/Endosperm Surrounding Region 14 (CLE14) peptide, which is coupled with Fe and callose deposition in the MZ to trigger terminal differentiation and arrest of mitotic activity (184, 219-221). I speculate that low cytosolic Pi levels in the TZ promote nuclear recruitment of STOP1 and thereby modulate subsequent cellular responses to changes in Pi availability. A downstream response to Pi deprivation is the elevated synthesis of the PHR1-regulated VTC4 ascorbate synthase (184, 219, 220, 222). Ascorbate efflux, facilitated by VTC4, could couple with LPR1 ferroxidase activity to complete an Fe redox cycle to produce ROS that promote callose deposition in the EZ and MZ (219). In contrast, high Pi concentrations in the TZ would suppress PHR1/SPX1-mediated Pi signaling either directly through binding SPX1 or indirectly by affecting the concentration of PP-InsP isoforms, which are high-affinity ligands for SPX1(193, 196). Differential control of PHR1/SPX1-mediated Pi signaling in the TZ may tune spatial and/or temporal responses to Pi availability in the EZ and MZ, and would provide a link between systemic and local Pi signaling pathways. It will be interesting to test the effects of vacuolar Pi sequestration and cytosolic Pi levels in the TZ, as well as vacuolar development on these complex aspects of Pi signaling in roots.

2.4 Materials and Methods

2.4.1 Plant growth

Arabidopsis seeds from plants expressing the cpFLIPPi-5.3m Pi sensor (165) or a control sensor, cpFLIPPi-null, that is insensitive to Pi (166, 223) were germinated and grown in 96-well microplates containing 0.5x Murashige and Skoog (MS) medium (223) with 0.25% (w/v) sucrose and, unless indicated otherwise, 0.25 mM Pi (Pi-replete). All plants carry the *suppressor of gene silencing3-13* (*sgs3-13*) mutation to improve sensor signal intensity and stability (165, 224). *pht5;1* and *pht1;1* transgenic lines were obtained from Tzyy-Jen Chiou. Plates were incubated in a growth chamber (60% relative humidity, 21°C, and 110 μmol/m^2/s light intensity for a 16 h photoperiod). After 6 days the seedlings were imaged or transferred to fresh medium as indicated with replacement of the medium every 24 h. For longer-term growth, plants were grown on 23 x 23 cm square plates containing agar-solidified (0.7% w/v) Pi-replete medium.

2.4.2 Live Pi imaging

Seedlings were mounted on a coverslip in the same medium used for growth. A smaller coverslip was placed on top of the root as a weight to keep it flat during imaging. Roots were imaged using an inverted Olympus IX81 microscope with a Yokogawa CSU-X1 Spinning Disk confocal unit, an iXon3 897 EMCCD camera (Andor Technology, Concord, MA, USA), and a 40x (numerical aperture 1.3) oil immersion objective. A 445 nm laser was used to excite the eCFP component of the sensors. The eCFP emission was detected with a 483/32 nm filter, and FRET-derived cpVenus emission was detected with a 542/27 nm filter. The cpVenus component of the sensor was excited by a 515 nm laser. Cell viability was confirmed using SYTOX orange as described previously (165, 225). Image acquisition parameters such as laser power, electron multiplier gain, and camera sensitivity were the same for all experiments. Images were analyzed

using ImageJ. Background fluorescence values (mean fluorescent intensities) for each channel were determined by imaging root cells of untransformed plants. In order to eliminate background noise, the mean background values were subtracted from the images of transgenic plants before further processing. Sensitized FRET ratios were calculated after correcting for donor spectral bleedthrough and acceptor cross excitation as described previously (166). FRET/eCFP ratios were calculated by dividing the mean sensitized FRET intensity values by mean eCFP emission intensity values.

2.4.3 *In vivo* calibration of Pi sensor ratios

Cytosolic Pi concentrations in individual cells were manipulated via microinjection (1). Borosilicate microinjection capillaries (1 mm outer diameter, 0.58 mm inner diameter) containing a filament were pulled then filled with injection buffer: 50 mM MOPS-KOH (pH 7.3), 0.5 mM $MgCl_2$, and varied concentrations of potassium phosphate buffer (pH 7.3) and potassium gluconate. Potassium gluconate was included as needed to maintain the total potassium ion concentration at 75 mM. Injection buffer also included 1 μM mRuby2 protein (226) to demarcate the injected cell and to monitor dispersion of injection buffer. The mRuby2 protein was expressed in bacteria and purified as described (165). Filled microinjection needles were fit onto a micromanipulator and connected to an Eppendorf FemtoJet pump. Seedlings grown for 6 d in liquid medium were placed on a coverslip and most of the root was covered with wet filter paper then fixed to the coverslip with adhesive tape (227). Epidermal cells located in the transition zone of the root were impaled and then 20 to 25 pL injection buffer was delivered into the cytosol. The total injection time was 5 s, and cells were imaged within an additional 1.5 s. Six to eight independent cells were injected for each Pi concentration. Injection volume was estimated from mock experiments in which injection buffer was delivered into a

puddle of halocarbon oil for the same injection time and then the diameter of the spherical droplets was used to calculate volume. To generate a calibration curve, sensitized FRET/eCFP values were plotted versus injected Pi concentrations then data were fit to a single-site binding isotherm: $S=(R-R_0)/(R_{sat}-R_0)=[L]/K_d+[L])$, where S is saturation, R is the FRET/eCFP ratio, R_0 is the ratio in the absence of ligand, R_{sat} is the ratio at saturation, L is ligand (Pi) concentration, and K_d is the dissociation constant (164).

2.4.4 Pi recycling, uptake, and vacuolar sequestration

Seedlings were mounted on a cover slip in 0.5x MS medium without Pi. A smaller cover slip was placed on top of the root to keep it flat against the larger cover slip and to limit its movement during imaging. Initial images were captured then the medium was replaced with 30 µl of medium containing 10 mM NaCN (with or without Pi) and the same cells were imaged. For Pi uptake experiments, the Kolmogorov-Smirnov test (228) was used to evaluate significance of differences in Pi concentrations observed for CN versus CN plus Pi treatments. ANOVA and Tukey HSD analysis were used to evaluate differences between root developmental zones (Fig. 7B, C). For some studies of vacuolar Pi sequestration (Fig. 16), CN and Pi treatments were conducted sequentially, and results were evaluated with Student's t-test.

2.4.5 Estimation of cytosolic volume

Seedlings that express the cytosolic Pi sensor were mounted in 20 µl of 0.5x MS medium without Pi and Z-stacks were acquired using a 40x silicone oil objective (numerical aperture 1.25) and a step size of 0.5 µm to yield a voxel size of 0.06 μm^3. A 515 nm laser was used for excitation of cpVenus and a 542/27nm filter was used to detect its emission. For image analysis, background fluorescence was subtracted in batch from the entire stack. A threshold was set for each slice separately and regions of interest (ROIs) were drawn to distinguish individual cells.

The Voxel Counter ImageJ plugin was used to determine total voxels per cell then these were converted to picoliters.

2.4.6 Pi uptake assay for whole roots

Wild-type and *pht5;1-2* plants expressing cpFLIPPi-5.3m were grown in Pi-replete medium for 6 days then transferred to 0.5x MS medium without Pi for 48 h, with replacement of medium every 24 h. Seedlings were then transferred to 0.5 ml of Pi-replete medium in a 12-well plate (12 seedlings per well) and placed in the growth chamber. Aliquots of 15 µl medium were withdrawn from each well at the indicated time points then Pi in these samples was measured based on Pi-dependent FRET using the high-affinity Pi sensor cpFLIPPi-80u (165). Each aliquot was mixed with 15 µl assay buffer (50 mM MOPS-KOH (pH 7.3), 50 mM KCl, 0.5 mM $MgCL_2$, 1 mg/ml BSA, and 1 µM cpFLIPPi-80u) in a well of a black 384-well plate. The plate was incubated at room temperature for 10 min then fluorescence was measured using a microplate reader (Synergy HT) using excitation at 420/27 nm and emission at 485/20 nm and 540/25 nm. Direct cpVenus excitation was set at 500/20 nm with emission at 540/25 nm. FRET ratios were converted to Pi concentrations based on an *in vitro* calibration of cpFLIPPi-80u prepared with known Pi concentrations (165). Pi uptake was calculated from the depletion of Pi in the medium and expressed as nmoles Pi/seedling.

CHAPTER III

SPATIOTEMPORAL ANALYSIS OF CYTOSOLIC Pi IN ARABIDOPSIS ROOT HAIRS

3.1 Introduction

Plants are exposed to continuous fluctuations in nutrient availability, water content, and salinity. The development of root hairs is one of the primary adaptive responses to these environmental stresses. Root hairs are epidermal cell extensions that emerge in the differentiation zone of the primary root. They help in soil anchorage (229, 230), soil penetration (231), water absorption (232-234), and also act as adherence sites for soil microbes (235). Root hairs enhance nutrient acquisition by increasing the surface area of the root to maximize root-soil contact (236). As discussed in Chapter I and Chapter II, low Pi availability is a major constraint for crop productivity worldwide. In Pi-limited growth conditions, root architecture is altered, and growth of root hairs is triggered (22). Root hairs increase the plant's ability to scavenge scarce amounts of Pi from soil. Therefore, root hairs serve as a model to study Pi uptake and P use efficiency, which has significant implications for sustainable agriculture.

Movement of Pi through soil occurs by diffusion (236, 237). Due to high uptake rates of relatively immobile nutrients like Pi, a zone of depletion is created around the primary root. Under such conditions, root hairs help scavenge the low amounts of Pi within the depletion zone and to forage beyond it. Since soil Pi concentration is low, flux per unit area of absorbing surface is limited. The axial growth of root hairs increases the effective absorptive surface of the root during Pi starvation (236, 238).

There are several direct and indirect lines of evidence for Pi acquisition by root hairs. Rapid depletion of ^{32}P around root hairs within the first few days of their appearance was one of the first (237, 239). Later, Gahoonia and Nielsen (151) demonstrated that root hairs are

responsible for nearly 63% of P uptake in a plant, which is in close agreement with mathematical modeling studies (152, 240). Comparisons of WT and mutants (*rhd2* and *rhd6*) that are defective in root hair development indicate that Pi absorption is lower in mutants in Pi-limited conditions (136). Localization of Pi transporters to root hairs further strengthens the claim that root hairs are principle sites of Pi uptake (5, 7, 8, 11, 15, 17, 18, 23, 241). Gene expression studies revealed that transcript levels of these transporter genes increase during Pi-starvation in root hairs similar to the primary root (5, 7, 8). Pi starvation also induces an increase in length and density of root hairs (5, 78, 79, 242-244). Root hair lengths can vary between species (245, 246) and plants with longer root hairs have higher Pi uptake (243, 247, 248) and larger depletion zones around the root (237, 239). Increased Pi acquisition promoted by root hairs has a significant impact on grain yield of plants grown in low Pi (249). Thus, root hairs provide a competitive advantage to plants during Pi limitation (155).

Development of root hairs from bulge formation to maturity requires extensive cytoskeletal organization (250-253), vesicular trafficking (254-257) and cell wall synthesis (258, 259) to support polar cell expansion or tip growth. Actin and microtubules help traffic secretory vesicles towards the hair apex where cell wall materials are deposited by exocytosis. Actin is indispensable for tip growth of root hairs (250, 260, 261), whereas disruption of microtubules results in wavy, branched hairs suggesting that microtubules are essential for maintaining both morphology and directionality of hair cells (250, 251). ATP hydrolysis during actin polymerization liberates Pi. Similarly, motor protein movement along microtubules also involves ATP hydrolysis and release of Pi.

Tip growth of root hairs requires deposition of cell wall materials at the hair apex. Cellulose is a major component of the cell wall, and Pi is produced during its synthesis from

glucose. Cellulose chains are extruded into the apoplast as the cellulose synthase complex moves along the microtubules. Phosphorylation of specific sites in cellulose synthase is necessary to maintain its mobility on microtubules (135, 262).

Phospholipid signaling plays an important role in cytoskeletal remodeling and membrane trafficking (263). Pi is required for phosphorylation of phosphatidylinositol-4-phosphate (PtdIns-4-P) to phosphatidylinositol 4,5- bisphosphate (PtdIns(4,5)P_2) by PIP5K3 (phosphatidylinositol phosphate 5-kinase 3). PIP5K3 is preferentially expressed in growing hair cells and localization of PtdIns(4,5)P_2 to hair tips suggests its involvement in tip growth (264). Thus, metabolic reactions involving cytoskeletal organization, vesicular trafficking, and cellulose synthesis either require Pi as substrate or generate Pi as a product. Therefore, a combination of these activities plus Pi uptake from external sources contribute to the control of steady-state cytosolic Pi levels in root hairs.

Although the importance of root hairs for Pi acquisition has been established, the fate of Pi after its uptake, including any potential spatial restrictions for its distribution and absolute concentration within the cell, is unknown. In this work, I used the Pi sensor cpFLIPPi-5.3m (165) to study cytosolic Pi dynamics in root hairs. I show that cytosolic Pi concentration in the root hair is higher than in its originating cell body (trichoblasts) and adjacent epidermal cells (atrichoblasts) in the primary root. I also show the correlation between cytosolic Pi concentration and length of root hairs as well as a gradient for Pi concentration spanning from the hair tip to the base. Using a combination of mutants and Pi uptake assays, I found that higher Pi uptake and lower vacuolar sequestration at the tip contribute to this Pi gradient.

3.2 Results

3.2.1 Cytosolic Pi Quantification in Root Hairs

Because root hairs are extensions of epidermal cells, I expected that cytosolic Pi concentrations would be equivalent in the cell body and hair. To test this hypothesis, I measured FRET ratios for the Pi sensor (cpFLIPPi-5.3m) expressed in root hairs and in epidermal cell bodies located within the differentiation zone (DZ) of the primary root. To compare results with those using the control sensor (cpFLIPPi-null, see below), I did not convert FRET ratios to absolute Pi concentrations as in Chapter 2. Contrary to my hypothesis, I found that mean FRET ratio was significantly lower for root hairs than epidermal cells (**Figure 19**), indicating higher Pi concentrations in root hairs. These results also suggested that Pi concentrations vary more widely in root hairs as indicated by the larger relative standard deviation (RSD, **Figure 19**). RSD is the standard deviation (SD) divided by the mean, and therefore accounts for differences in means. I

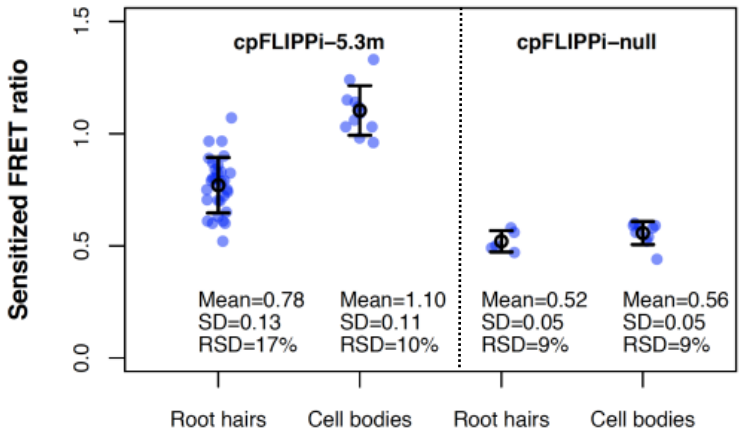

Figure 19. Sensitized FRET ratios in root hairs and epidermal cells. Root hairs and epidermal cell bodies in the DZ of 6 d old Arabidopsis seedlings expressing either cpFLIPPi-5.3m or cpFLIPPi-null were imaged. FRET ratios (mean ± SD) from 5-31 cells are plotted. RSD, relative standard deviation.

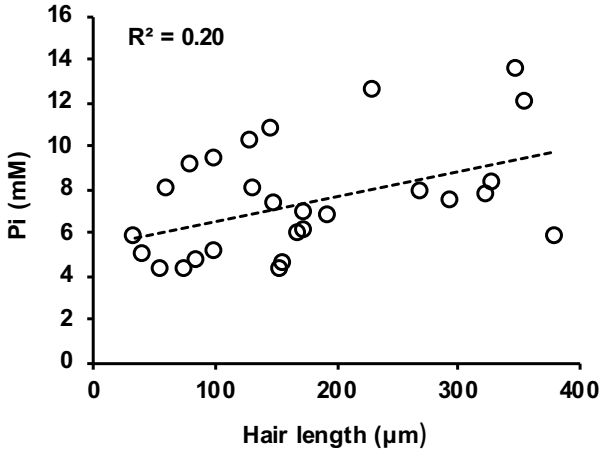

Figure 20. Correlation of cytosolic Pi concentration with root hair length. Root hairs of 6 d old Arabidopsis seedlings expressing cpFLIPPi 5.3m were imaged. Data were collected from 27 individual root hairs from 5 independent seedlings.

attribute this greater variation in FRET ratio to differences in Pi concentrations rather than imaging artifacts because RSD was similar for cpFLIPPi-null FRET ratios measured in root hairs and epidermal cells (**Figure 19**).

My initial analysis of Pi levels in root hairs (**Figure 19**) was conducted with a random population of root hairs. However, because root hair growth requires vesicular transport and cell wall deposition at the tip (254, 256-259), it was possible that cytosolic Pi concentration varies with hair cell length and that this was the source of variation in the population. To test this idea, I imaged root hairs with lengths ranging from 30 to 400 microns. Root hairs that did not fit in a single field of view were imaged in multiple fields. Because FRET ratios for cpFLIPPi-null were equivalent in root hairs and epidermal cells (**Figure 19**), FRET ratios for the Pi sensor could be converted to absolute Pi concentration using the *in vivo* calibration described in Chapter 2. I observed a weak correlation between cytosolic Pi concentration and hair length (**Figure 20**). The regression coefficient, R^2, for this correlation was low, but a Pearson correlation test (265) confirmed correlation with a P-value of 0.018 indicating statistical significance. Nevertheless,

the effect of length did not fully account for the variation observed in the random population, indicating the presence of additional contributing factors.

It was possible that Pi concentration also varied spatially within individual root hairs. I therefore measured Pi concentrations at the tip, center, and base of each root hair as shown in **Figure 21**. The junction of the root hair and its cell body was defined as the base, and the midpoint between the base and tip was defined as the center. This analysis was restricted to hair cells with uniformly distributed sensor protein. Nevertheless, since different regions of a single cell were analyzed, the same number of pixels in each region of interest (ROI) were used to avoid potential bias. These localized Pi measurements revealed distinct patterns of cytosolic Pi distribution (**Figure 22**), which I categorized as tip-high, center-high, and base-high based on the location of maximum Pi concentration, or uniform if the difference in Pi concentration between each region was less than 1 mM.

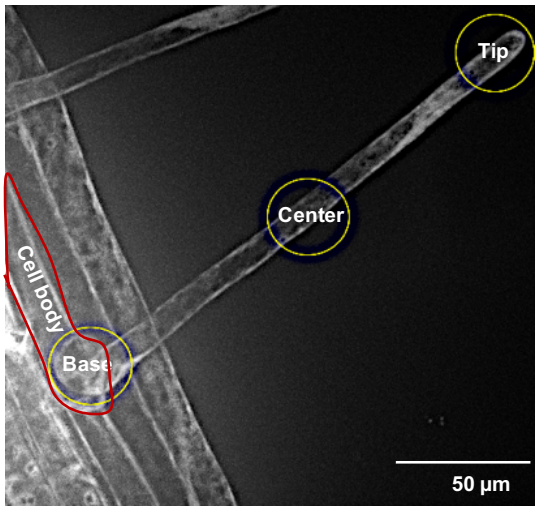

Figure 21. Representative image of a root hair extending from its cell body. ROIs with fixed area were drawn at the tip, center and base of the hair. ROIs, regions of interest. The red border demarcates the cell body of the trichoblast.

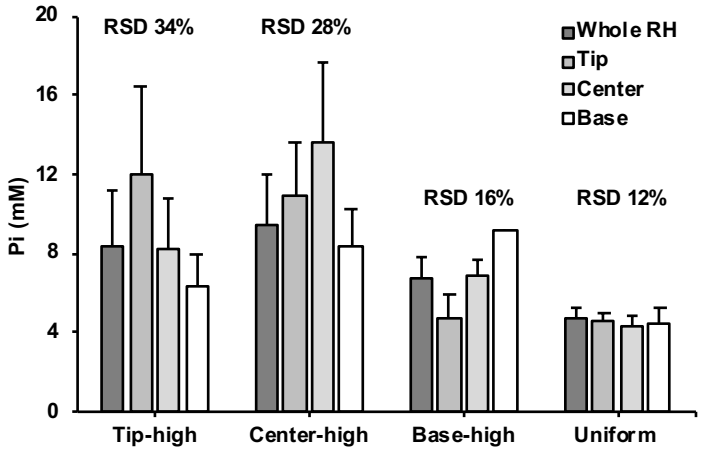

Figure 22. Cytosolic Pi distribution within root hairs. ROIs were drawn at the tip, center, and base of each hair. Pi was measured in these regions and root hairs were categorized based on the location of maximum Pi concentration. RSD of whole root hairs is reported for each group to compare variation. N= 28 hair cells from 5 independent seedlings. RSD, relative standard deviation.

Interestingly, RSD values were higher in root hairs with a non-uniform distribution of Pi, especially those with highest Pi concentrations at the tip, whereas RSD values for root hairs with

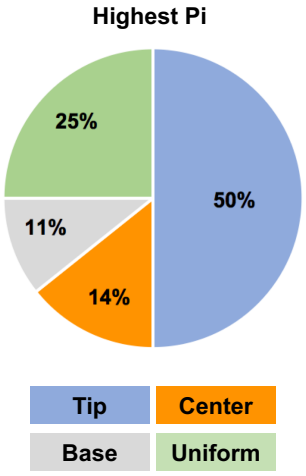

Figure 23. Pi distribution categories for root hairs in plants grown in Pi-replete conditions. Plot represents percentage of root hairs in each category (a) tip-high (blue) (b) center-high (orange) (c) base-high (grey) (d) uniform (green). N = 28 hairs from 5 independent seedlings.

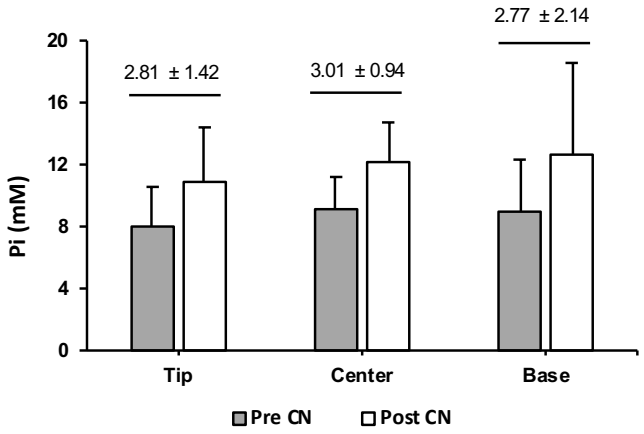

Figure 24. Spatial analysis of metabolic recycling in root hairs. Cytosolic Pi concentrations at the tip, center, and base of root hairs before and after cyanide treatment are plotted. Values are mean ± SD Pi concentration for 5 independent root hair cells. Numbers above each group represent mean ± SD change in Pi (mM) after cyanide treatment. A post-hoc Tukey test showed no significant differences between root hair locations.

uniformly distributed Pi were similar to those in primary root epidermal cells (**Figure 22**). Moreover, as shown in **Figure 23**, these Pi distribution categories were not equally represented in the population. The most prevalent category was tip-high, which constituted 50% of all root hairs.

3.2.2 Spatial Analysis of Metabolic Recycling, Uptake, and Vacuolar Sequestration of Pi in Root Hairs

Since most root hairs have highest Pi concentration at the tip, I hypothesized that this reflects high levels of its metabolic recycling from organic-P at the tip. Pi is rapidly assimilated to ATP and then liberated from ATP and other organic-P molecules during recycling (9). I used cyanide to block Pi assimilation (209) and then measured the increase in cytosolic Pi concentration resulting from its metabolic recycling. Root hairs grown in Pi-replete medium were imaged to define pre-treatment Pi concentrations then treated with 10 mM cyanide. As expected, I detected rapid increases in cytosolic Pi levels after the cyanide treatment (**Figure 24**)

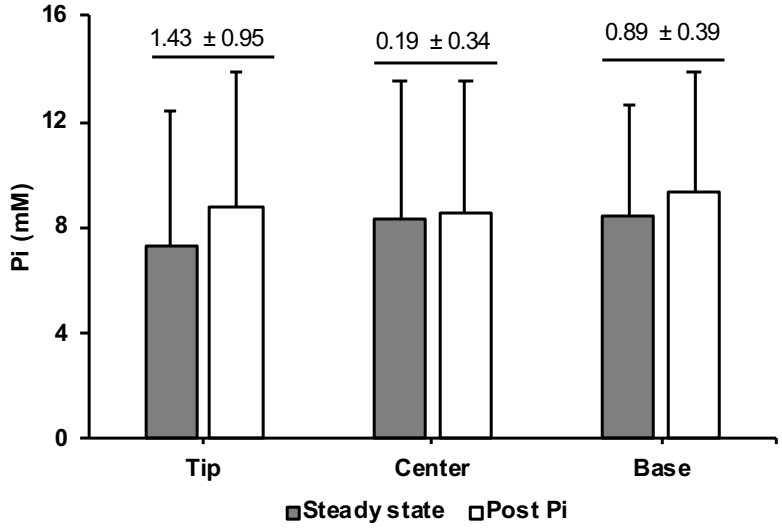

Figure 25. Spatial analysis of Pi uptake in root hairs. 6 d old Arabidopsis seedlings were transferred to medium without Pi for 48 h before imaging. Cytosolic Pi at the tip, center and base of root hairs was measured, then hairs were treated with 500 μM Pi. Plotted values are mean ± SD cytosolic Pi (mM) in 4 independent root hair cells. Numbers above each group represent mean change in Pi (mM) ± SD after addition of external Pi.

that reached maximum levels after 30 to 35 s. However, there were no significant differences between locations within root hairs suggesting that metabolic recycling occurs uniformly throughout the root hair and thus cannot be responsible for Pi accumulation at the tip.

I then hypothesized that greater Pi uptake at the tip was responsible for tip-high Pi concentrations. Members of the PHT1 class of Pi transporters localize to root hairs (5, 7, 8), and in *Medicago truncatula*, immunolocalization for MtPT1 showed highest accumulation of the protein at root hair tips (7). To test if Pi transport activity is highest at the tips, I treated Pi-starved root hairs with 500 μM Pi and monitored the change in cytosolic Pi concentration at each location in the root hair. Pi-starved seedings were used in this experiment because PHT1 transporter abundance increases in response to starvation (5-7) and therefore maximizes uptake activities. Consistent with my hypothesis, the largest change in cytosolic Pi concentration

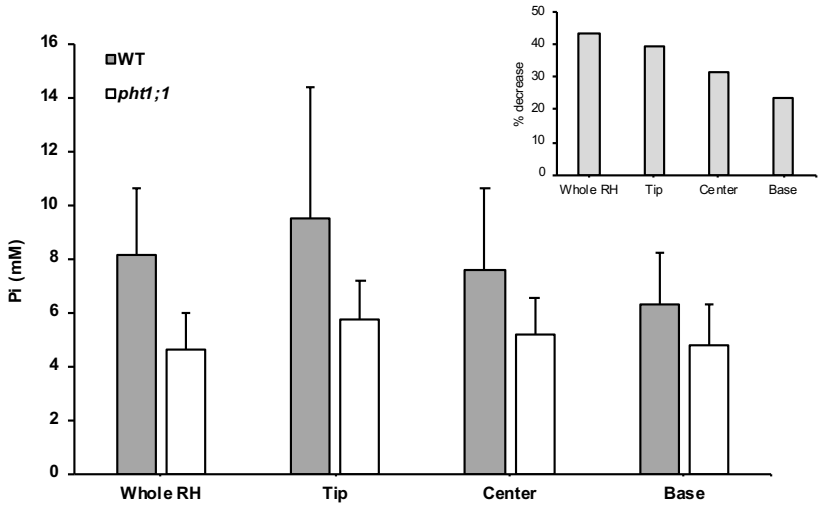

Figure 26. Quantification of cytosolic Pi in root hairs of WT and *pht1;1* root hairs. Arabidopsis seedlings were grown in Pi-replete medium for 6 d. Cytosolic Pi was measured in the whole root hairs and also in the tip, center and base of these hairs. Plotted values are mean ± SD cytosolic Pi (mM) in 26-28 root hairs from 5 independent seedlings. Inset plot shows percent decrease in cytosolic Pi concentration in *pht1;1* relative to WT.

occurred at the tips (**Figure 25**). To explore the basis for tip-localized Pi uptake, I compared cytosolic Pi concentrations in root hairs of wild-type plants to those in a Pi transporter mutant, *pht1;1-2*, which shows reduced Pi uptake in whole-root assays (5). I found that under steady-state growth conditions, the *pht1;1* mutation reduced cytosolic Pi levels throughout the root hair (**Figure 26**), but the largest difference was at the tip (**Figure 26 inset**). This strongly indicates that PHT1;1 activity is greatest at the root hair tip and that this contributes to the accumulation of Pi at the tip.

Vacuoles are the major Pi reservoir in plant cells (10, 183), and developmental control of vacuolar Pi sequestration plays an important role in regulating cytosolic Pi levels in the primary root (**Figure 15**). I therefore sought to determine if vacuolar Pi sequestration is also spatially controlled in root hairs. I hypothesized that lower vacuolar sequestration at the hair tip helps

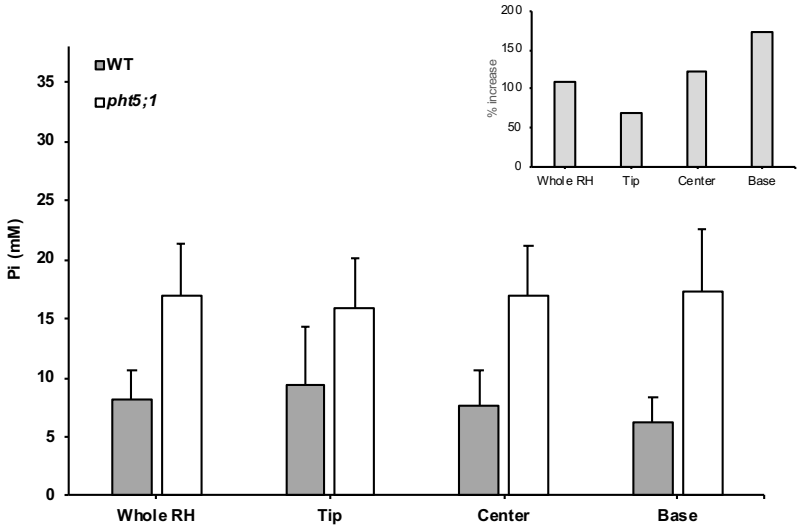

Figure 27. Quantification of cytosolic Pi concentration in WT and *pht5;1* root hairs. Seedlings were grown in Pi-replete medium for 6 d. Cytosolic Pi concentration was measured in whole root hairs and also in the tip, center, and base. Plotted values are mean ± SD cytosolic Pi (mM) in 17-26 root hairs from 4-5 independent seedlings. Inset plot shows percent increase in cytosolic Pi concentration in *pht5;1* root hairs relative to WT.

maintain high cytosolic Pi concentrations. To test this, I compared cytosolic Pi levels in root hairs of wild-type plants to those in the vacuolar Pi transport mutant *pht5;1-2*. PHT5;1 is responsible for most vacuolar Pi loading in Arabidopsis (14, 61). Cytosolic Pi levels were elevated in *pht5;1-2*, indicating that substantial vacuolar Pi sequestration occurs in root hairs (**Figure 27**), but the effect was lowest at the tip (**Figure 27 inset**). These results indicate that PHT5;1-mediated vacuolar Pi sequestration is lower at the root hair tip. Consequently, high cytosolic Pi concentrations at the root hair tip are achieved through a combination of high Pi uptake and low vacuolar Pi sequestration.

3.2.3 Flow of Pi from Root Hairs to the Primary Root

Pi acquired by root hairs eventually moves to the primary root and then to the plant shoot (24, 151). As shown previously (**Figure 19**), I detected higher Pi concentrations in root hairs

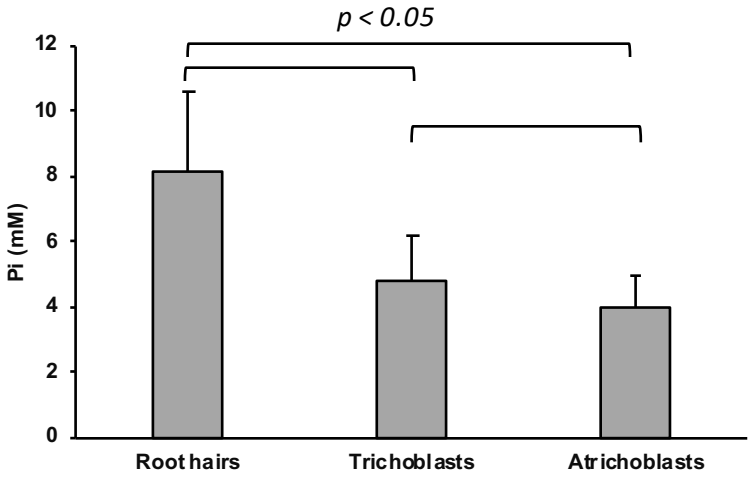

Figure 28. Comparison of cytosolic Pi concentrations in root hairs and epidermal cell bodies. Arabidopsis seedlings were grown in Pi-replete medium for 6 d. Cytosolic Pi concentration was measured in root hairs, and the cell bodies of trichoblasts and atrichoblasts. Plotted values are mean ± SD cytosolic Pi (mM) in 17-24 cells from 5 independent seedlings. Pi is higher in root hairs than trichoblasts and atrichoblasts ($p<0.05$, Student's t-test) and also higher in trichoblasts than atrichoblasts ($p<0.05$, Student's t-test).

than epidermal cells suggesting a limit on the rate of movement from hair to cell body. However, epidermal cells include both trichoblasts and atrichoblasts so it was unclear if this limit applies solely to trichoblasts. I found that Pi concentrations in cell bodies of both trichoblasts and atrichoblasts were lower than root hairs, and atrichoblasts lower than trichoblasts (**Figure 28**). Because trichoblasts and atrichoblasts are symplastically isolated (266), these results are consistent with the ideas that atrichoblasts have lower Pi uptake activity than trichoblasts, and that the rate of Pi movement from a root hair into its cell body is slower than export from the cell body to load xylem vessels. To test the effect of altered xylem loading on cytosolic levels, I compared cytosolic Pi concentrations in epidermal cell bodies and root hairs in wild-type plants with those in the *pho1* mutant. PHO1 is responsible for loading Pi into xylem (64-66). While the *pho1* mutation does not alter Pi uptake, translocation of Pi from roots to shoots is severely reduced (64). Therefore, I expected an increase in Pi concentrations in root tissues, thus reducing

the difference between epidermal cells and root hairs. Consistent with my hypothesis, Pi concentrations in cell bodies of trichoblasts and atrichoblasts were significantly higher in *pho1* (**Figure 29**), but was not significantly different in root hairs. This further supports the idea that loading Pi into xylem is faster than the movement of Pi from root hairs into epidermal cell bodies. However, as in wild type, Pi concentrations remain higher in root hairs than in epidermal cells in *pho1*.

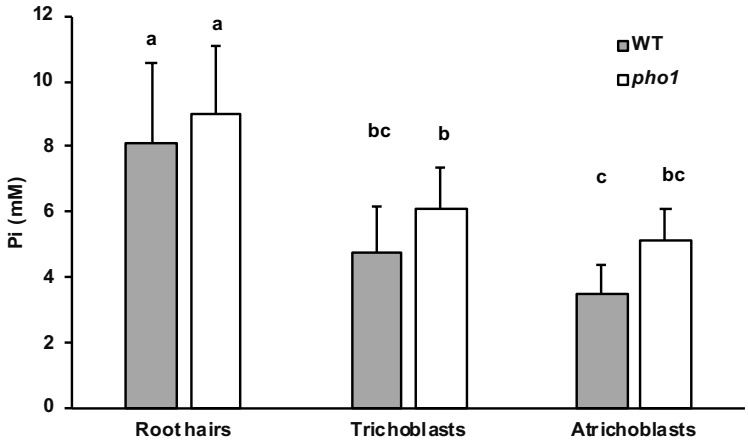

Figure 29: Comparison of cytosolic Pi in root hairs and DZ cells of WT and *pho1*. Arabidopsis seedlings were grown in Pi-replete medium for 6 d. Cytosolic Pi was measured in root hairs, trichoblasts and atrichoblasts. Plotted values are mean ± SD cytosolic Pi (mM) in 17-30 cells from 5-7 independent seedlings. There is a statistically significant difference between group means, as determined by ANOVA. A post-hoc Tukey test showed than Pi concentrations are elevated significantly in *pho1* trichoblasts and atrichoblasts, but not in root hairs.

3.3 Discussion

Pi availability limits agricultural productivity worldwide. Although phosphate-rich fertilizers can ameliorate this deficiency, they pose both environmental and economic hazards (4). One approach to reduce dependency on Pi fertilizers and thereby minimize their associated

hazards is to breed or engineer plants for greater Pi uptake capability. Root hairs are ideal targets for such efforts because plants induce root hair formation and growth in low-Pi environments to increase Pi uptake (22, 151, 236, 237), but the cellular and molecular mechanisms of Pi acquisition and its subsequent transfer to the primary root are not fully understood. In this study, I conducted a systematic analysis of cytosolic Pi distribution in Arabidopsis root hairs using confocal microscopy and ratiometric imaging of a FRET-based Pi biosensor (165).

Although I initially hypothesized that cytosolic Pi concentration would be the same in root hairs and their epidermal cell bodies given the contiguous cytosol, I found that Pi levels were consistently greater and also more variable in root hairs. Some of the variation correlated with root hair length, but a greater proportion was due to the unequal distribution of Pi within individual root hairs.

Half of all root hairs showed highest Pi accumulation at the tip. Tip growth is metabolically intensive with formation of cell wall and cell membrane (258, 259). However, metabolic recycling of Pi from organic-P, as was expected from cellulose and phospholipid synthesis and cytoskeletal reorganization, showed no spatial variation within root hairs. In contrast, Pi uptake activity was enriched at the root hair tip. Comparative analyses of uptake in wild-type root hairs and those of the Pi transport mutant *pht1;1* indicate that PHT1;1 is responsible for a large proportion of this localized activity. Similar experiments conducted with the vacuolar Pi sequestration mutant *pht5;1* indicate that Pi sequestration is minimal at the root hair tip. This may be due to preferential localization of PHT5 transporters to basal portions of the vacuole that fills a root hair or to the lack of fully-extended vacuoles in many hair cells. Nevertheless, the combination of greater uptake and lower sequestration accounts for high Pi concentrations at the hair tip.

Although most root hairs contain highest Pi concentration at the tip, there were some hairs that showed highest Pi levels at the center or the base. It is possible that these distribution patterns reflect measurements made at single time point. That is, Pi concentrations may change over time as Pi is mobilized from the tip to the base of a root hair and eventually into the primary root. Additional experiments are required to test this hypothesis. Some root hairs showed uniform distribution of cytosolic Pi. It is possible that these root hairs lost their capacity for Pi uptake and/or mobilization due to mechanical damage when seedlings were mounted for imaging. Again, temporal analyses are needed to determine if uniform distribution of Pi reflects a bona fide stage in Pi mobilization.

Pi concentrations in roots hairs were substantially greater in root hairs than in epidermal cells. This is due, at least in part, by a faster export of Pi from cell bodies for xylem loading than entry from root hairs. This idea is supported by elevated Pi levels in epidermal cells in the *pho1* mutant, which has reduced Pi loading into xylem (64). Although my analysis was restricted to the root epidermis, I predict that Pi concentrations will also be elevated in the cortex and endodermis of this mutant.

Interestingly, a comparison of trichoblasts and atrichoblasts revealed that atrichoblasts contain lower cytosolic Pi levels than trichoblast cell bodies in both wild-type and *pho1* roots (**Figure 29**). This difference may reflect cell-specific Pi uptake capacities. For example, PHT1 transporters localized to the cell body and root hairs would provide greater uptake capacity than atrichoblasts, which would contain PHT1 transporters only on the cell body. Pi imaging in *rhd2* and *rhd6* mutants, which are defective in root hair growth and development (136), may help explain the difference in Pi concentrations in trichoblasts and atrichoblasts. Similarly, it will be interesting to test if overexpression of PHT1 transporters in atrichoblasts could raise Pi

concentration to a level equivalent to that in trichoblasts, and if this enables plants to thrive on otherwise Pi-deficient conditions.

3.4 Materials and Methods

3.4.1 Plant growth

Transgenic Arabidopsis seeds expressing the cpFLIPPi-5.3m Pi sensor (165) or a control sensor, cpFLIPPi-null (166, 223) were germinated and grown in agar-solidified (0.7% w/v) 0.5x Hoagland's medium (267) with 0.25% (w/v) sucrose and 0.25 mM Pi (Pi-replete). Plates were incubated in a growth chamber (60% relative humidity, 21°C, and 110 μmol/m^2/s light intensity for a 16 h photoperiod). Seedlings were grown for 6 days and imaged or transferred to 3 ml Pi-free medium on 43 mm X 50 mm cover slips placed in a Petri plate for Pi starvation prior to imaging.

3.4.2 Live Pi imaging

Seedlings were mounted on a 43 mm X 50 mm coverslip in Pi-free Hoagland's medium. A smaller coverslip (22 mm X 22 mm) was placed on top of the root to keep the root hairs flat during imaging. Root hairs were imaged using an inverted Olympus IX81 microscope equipped with a Yokogawa CSU-X1 Spinning Disk confocal unit, an iXon3 897 EMCCD camera (Andor Technology, Concord, MA, USA), and a 40x (numerical aperture 1.3) oil immersion objective. A 445 nm laser was used for excitation of eCFP and its emission was detected with a 483/32 nm filter. cpVenus was excited using a 515 nm laser. Both FRET-derived cpVenus emission and direct cpVenus emission were detected with a 542/27 nm filter. Image acquisition parameters such as laser power, electron multiplier gain, and camera sensitivity were the same for all experiments: 70% laser intensity for the 445 nm laser, 10% laser intensity for the 515 nm laser, 500 ms exposure time, 20% electron multiplier gain and 2.4% pre-amplifier gain. Images were

analyzed using ImageJ. The mean background values for each emission channel, derived from untransformed plants, were subtracted from the corresponding images of transgenic plants and they were processed further, as described previously (166). Sensitized FRET values were obtained by correcting for donor bleedthrough and acceptor cross-excitation (166). Absolute fluorescence was lower in root hairs than primary root cells so the electron-multiplier gain was set at 20% to increase signal. FRET ratios obtained with this setting were equivalent to those used for the *in vivo* calibration. Therefore, ratio of mean sensitized FRET intensity values to mean eCFP emission intensity values (FRET ratio) was converted to absolute Pi concentration (mM) using the *in vivo* calibration (**Figure 7C**).

3.4.3 Pi recycling and uptake

Seedlings were mounted on a cover slip in Pi-free 0.5x Hoagland's medium. A smaller cover slip was placed on top of the root to keep the root hairs flat and to limit their movement during imaging. Initial images were captured then the root hairs were subjected to 10 mM NaCN (without Pi) and the same hairs were imaged. For Pi uptake experiments, 0.5 mM Pi was added to the root hairs and then imaged.

CHAPTER IV

SPATIAL ANALYSIS OF CYTOSOLIC ATP DYNAMICS AND ITS CORRELATION TO INORGANIC PHOSPHATE IN ARABIDOPSIS ROOTS

4.1 Introduction

ATP is the primary currency for intracellular energy transfer in every subcellular compartment. However, in plants, most ATP synthesis occurs in mitochondria and chloroplasts. Specifically, oxidative phosphorylation occurs in the mitochondrial matrix and photo-oxidative phosphorylation occurs in the chloroplast stroma. Multiple transport processes are therefore required to supply mitochondria and chloroplasts with the requisite substrates, ADP and Pi, and to facilitate movement of newly synthesized ATP to the cytosol and other organelles. Although many of the corresponding transport proteins have been identified, there is a gap in our knowledge of how these processes are integrated to control the production and distribution of ATP. A key limitation has been the inability to monitor ATP concentrations with sufficient spatial and temporal resolution in live plants.

One of the earliest methods developed for measuring ATP in live cells is based on enzyme-coupled chemiluminescence. When the oxidative enzyme luciferase converts its substrate luciferin to oxyluciferin, some of the energy released by this reaction is in the form of light, and the amount of light is proportional to free ATP in cells (268). However, this assay has several drawbacks, including low signal strength, a requirement for oxygen making it unsuitable for anaerobic systems, and a requirement for large concentrations of both substrate and enzyme at the desired cellular location. As an alternative, a fluorescent reporter was developed to measure ATP:ADP ratio in mammalian cells (269), but because it is not specific for ATP, it has been largely replaced by a related ATP-specific FRET-based biosensor called ATeam. ATeam

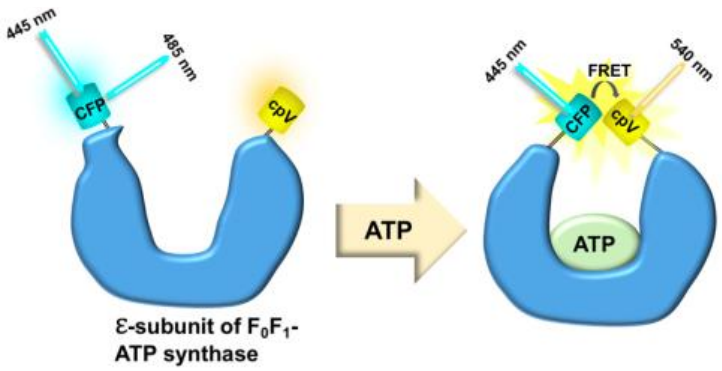

Figure 30. Schematic representation of ATP biosensor AT1.03-nD/nA. The ε- subunit of F_0F_1- ATP synthase is the ATP binding domain and it is translationally fused between CFP (donor) and cpVenus (acceptor). ATP binding to the ε- subunit induces conformational change that results in increased FRET.

contains the ε-subunit of F_0-F_1 ATP synthase translationally fused with CFP as donor and cpVenus as acceptor (270). ATP binding to the ε-subunit portion of the sensor induces a conformational change resulting in increased FRET (**Figure 30**). The dynamic range of this sensor was enhanced by replacing lysine 206 with alanine in both the donor and acceptor FP to generate AT1.03-nD/nA. These substitutions facilitate moderate dimerization of the fluorescent proteins (FPs) while maintaining the capacity for conformational change and limiting nonspecific interaction between FPs (271). Specificity of this sensor for ATP was demonstrated with *in vitro* assays; it was unresponsive to ADP, dATP, and GTP. The efficacy of these sensors *in vivo* was initially confirmed in HeLA cells (270), Drosophila larvae, and *C. elegans* (272). The utility of AT1.03-nD/nA in Arabidopsis was confirmed based on responses to hypoxia and reoxygenation (273). This sensor was also used in a recent study by Voon *et al.* to monitor ATP levels in chloroplasts, mitochondria, and cytosol (168). I validated the *in vitro* FRET response of this sensor and then established the confocal imaging conditions used in this study (168). Cytosolic ATP levels increased on illumination, but this response was prevented when mitochondrial electron transport was inhibited with rotenone, TTFA, antimycin, or oligomycin.

Photosynthetic inhibitors also reduced the light-dependent change in cytosolic ATP levels. Since there is no evidence of export of ATP from chloroplasts, these results suggest that chloroplasts export surplus reducing equivalents in the form of triose phosphates to the cytosol, which are then imported into mitochondria and utilized for ATP synthesis. ATP generated in mitochondria is then transported to the cytosol. Overall, this study highlighted an interplay of chloroplasts, mitochondria, and cytosol in the distribution and transport of ATP to fuel biosynthetic reactions. The processes governing ATP distribution and dynamics in plant roots are largely unknown, but must differ substantially from those in leaves given that root plastids are unable to synthesize ATP and consume, rather than export, carbon. I therefore explored the distribution of ATP in Arabidopsis roots. Moreover, because Pi concentrations would influence the transport and utilization of both ATP and carbon in root plastids, I also conducted a time course experiment to evaluate the inter-dependency of cytosolic Pi and ATP dynamics.

4.2 Results

4.2.1 *In vitro* characterization of ATP sensor AT1.03-nD/nA

To define confocal imaging conditions suitable for the ATP sensor AT1.03-nD/nA, hereafter AT1.03, I first evaluated the ATP-dependent changes in FRET ratio using purified sensor protein in an assay buffer adapted from Imamura *et al* (270) with slight modifications as detailed in Materials and Methods. I determined correction coefficients for CFP bleed-through and cpVenus cross-excitation using purified CFP and cpVenus as described previously (166), and these values were used to calculate sensitized FRET. As expected, AT1.03 exhibited increasing sensitized FRET/CFP ratios with increasing ATP concentrations (**Figure 31**). To estimate binding affinity (K_d), I fit FRET ratio data to the Hill equation to account for the possibility of multiple binding sites. Because FRET ratio is not zero in the absence of ligand,

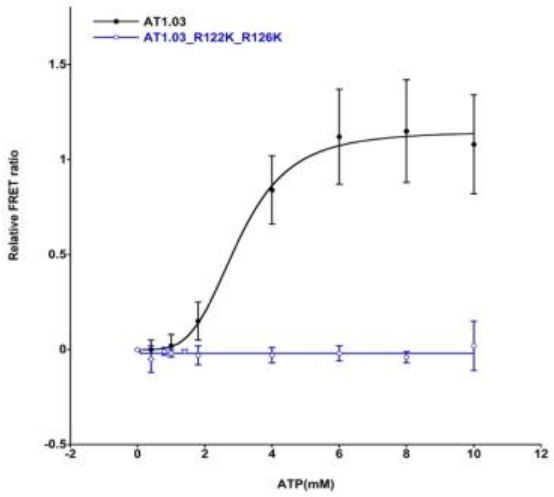

Figure 31. *In vitro* calibration of AT1.03 and AT1.03_R122K_R126K. Relative FRET ratios are plotted versus ATP concentration. FRET ratio of AT1.03 increases with increasing ATP whereas the negative control AT1.03_R122K_R126K is insensitive to ATP.

relative FRET ratios (FRET ratio - FRET ratio in absence of ATP) were plotted versus ATP concentrations. This analysis yielded a K_d of 2.8 mM, which is close to the previously reported value (3.3 mM). Saturation occurred at 6 mM ATP under these assay conditions, indicating that AT1.03 can distinguish ATP concentrations in the range of ~2-5 mM. A structural study previously reported that R122 and R126 of the ε-subunit interact with α and β phosphates of ATP (270). I therefore introduced these mutations using site-directed mutagenesis to generate a control sensor, AT1.03_R122K_R126K, that is insensitive to ATP concentration (**Figure 31**) and therefore used as a negative control in all subsequent experiments.

4.2.2 Exploring ATP dynamics in Arabidopsis roots

4.2.2.1 Validation of ligand-insensitive sensor AT1.03_R122K_R126K *in vivo*

Ligand-insensitive sensors like AT1.03_R122K_R126K allow detection and quantification of non-specific changes that may occur due to variations in cellular environment,

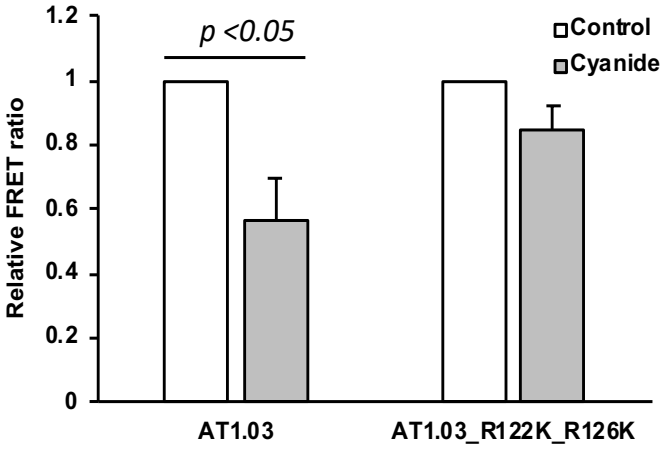

Figure 32. Effect of cyanide on ATP-dependent FRET ratio in epidermal cells. Seedlings expressing AT1.03 or AT1.03_R122K_R126K were grown in Pi-replete medium for 7 days prior to imaging. Pre-treatment ratios were used for normalization. Values shown are mean ± SD from 4 independent seedlings ($P < 0.05$, Student's t-test).

e.g., pH, ionic strength, and thereby avoid over- or under-estimates of changes reported by ligand-specific sensors. However, none of the previous studies using AT1.03 included this or an equivalent control sensor. I prepared clones for both AT1.03 and AT1.03_R122K_R126K and introduced these into Arabidopsis plants by *Agrobacterium*-mediated floral dip transformation. To validate these sensors, I subjected 6 d old seedlings to cyanide. Cyanide binds with iron in cytochrome a_3 thereby inhibiting electron transport and ultimately blocking ATP synthesis (209). However, ATP hydrolysis continues so cytosolic ATP levels should decrease. I imaged epidermal cells in the meristematic zone (MZ) of 7 d old seedlings expressing either AT1.03 or AT1.03_R122K_R126K before and after 14 s of cyanide treatment. Absolute FRET ratios differ for these sensors even when imaged in same location under same conditions due to ATP concentration as well as relative orientation of the respective fluorophore components. I therefore reported FRET ratios normalized to their pre-treatment values to allow direct

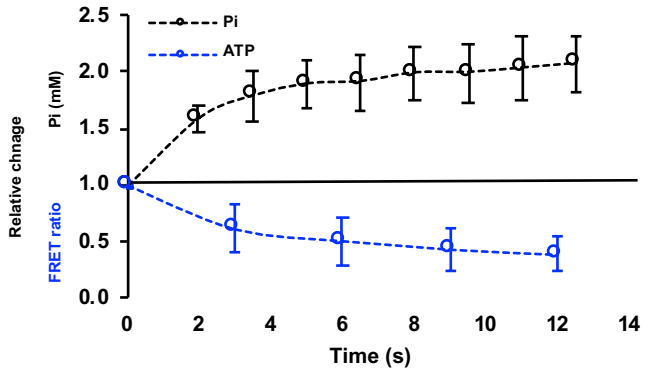

Figure 33. Comparison of Pi assimilation and ATP hydrolysis kinetics. Epidermal cells in the root MZ were imaged before and over time after treatment with cyanide. Values are normalized to pre-cyanide treatment ratios. Mean ± SD from 3-5 independent seedlings are plotted.

comparison between sensor and control. As shown in **Figure 32**, there is a significant decrease in FRET ratio for cyanide-treated plants expressing AT1.03 indicating a reduction in cytosolic ATP as expected. However, the change in FRET ratio for plants expressing AT1.03_R122K_R126K was not significant, confirming its insensitivity to ATP.

4.2.2.2 Correlation between cytosolic Pi and ATP dynamics

Pi-starvation and replenishment studies previously reported by Mukherjee et al (165) revealed that relative cytosolic Pi levels in starved plants required nearly 24 h of Pi-replenishment to return to levels equivalent to fed plants. As shown in **Figure 13A**, this slow reset time is due to rapid assimilation of Pi into ATP after its acquisition from external sources followed by a slower phase of homeostatic adjustment. To demonstrate that Pi and ATP are tightly coupled, I conducted a time-course experiment with seedlings expressing either the Pi sensor cpFLIPPi-5.3m or the ATP sensor AT1.03 in which I monitored changes in Pi and ATP levels after exposure to cyanide. Although cyanide blocks mitochondrial Pi assimilation into

ATP, ATP hydrolysis continues. Therefore, cytosolic Pi levels should increase with roughly the same kinetics as the reduction in ATP levels. As shown in **Figure 33**, the results fit this prediction. No changes were observed when the same experiment was conducted with plants expressing either of the control sensors cpFLIPPi-null and AT1.03_R122K_R126K. Thus, the interdependence of Pi and ATP can be monitored with high spatiotemporal resolution.

4.2.2.3 Spatial analysis of cytosolic ATP in developmental zones of the Arabidopsis root

As shown in **Figure 8**, cytosolic Pi concentrations vary between developmental zones of the root with highest Pi levels in the transition zone (TZ) (1). However, it was unknown if ATP concentrations also vary in the root. Given the interdependence of Pi and ATP (**Figure 33**), I hypothesized that cytosolic ATP levels vary with a pattern opposite that of Pi. To test this, I measured ATP-dependent FRET ratios in epidermal cells from each developmental zone of the root in plants grown in Pi-replete medium. These zones include the meristematic zone (MZ), transition zone (TZ), elongation zone (EZ), differentiation zone (DZ) and mature root (MR). Representative images in **Figure 34A** showed that FRET ratio was lowest in the TZ, indicating lower ATP levels in these cells. In contrast, no variation in FRET ratio was observed in plants expressing the control sensor, confirming that the pattern is ATP-specific. I also measured ATP-dependent FRET ratios from the root tip upwards in 50 μm increments. As shown in **Figure 34B**, relative ATP levels in the root follows a pattern that is opposite that for Pi.

4.3 Discussion

Multiple research groups have used fluorescent ATP sensors to monitor relative ATP levels in mammalian cells and tissues (270-272, 274), but these have been used in plants only recently. De Col *et al.,* were first to demonstrate ATP sensing in Arabidopsis seedlings using AT1.03-nD/nA (273). An ATP gradient was observed across tissues; FRET ratios were relatively

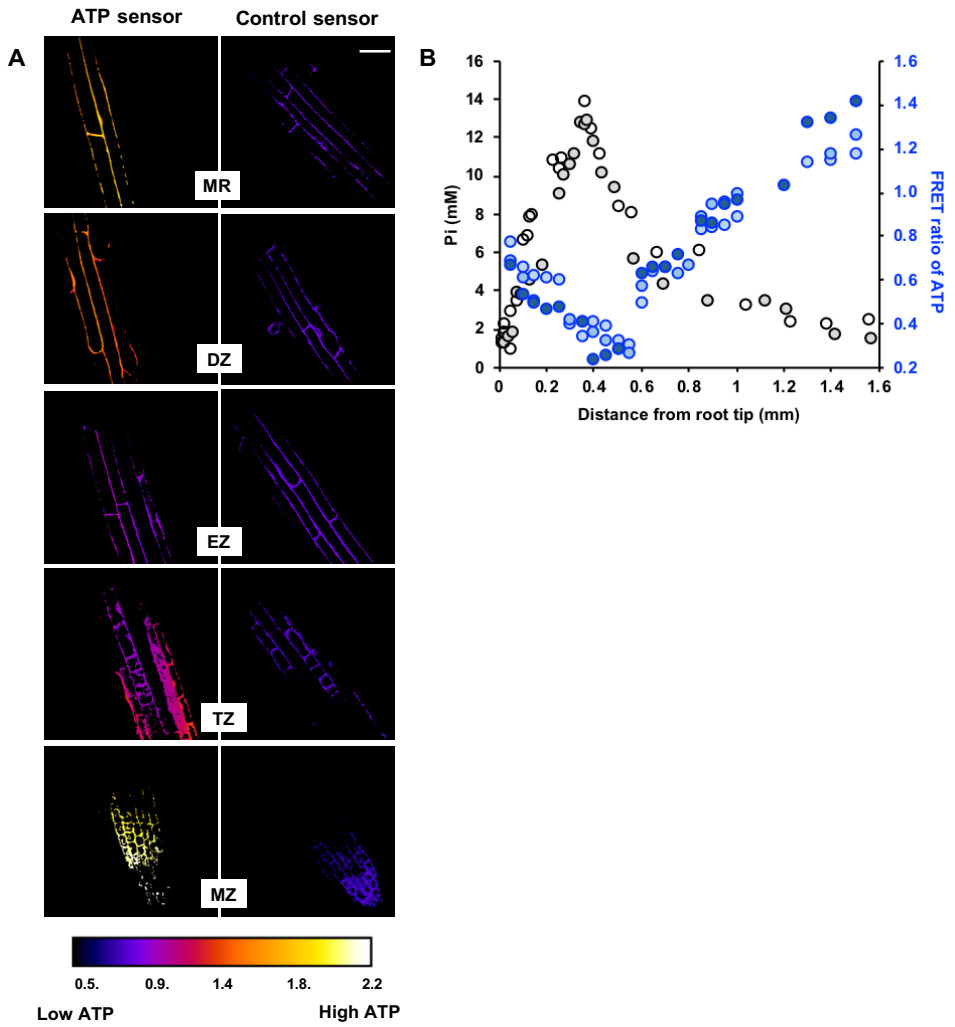

Figure 34. Spatial profile of ATP in Arabidopsis roots. (A) FRET/CFP micrographs for meristematic zone (MZ), transition zone (TZ), elongation zone (EZ), differentiation zone (DZ) and mature root (MR) in plants expressing AT1.03 (left) and AT1.03_R122K_R126K (right). Scale bar: 50 µm. (B) Plot represents Pi concentrations (black circles) and FRET ratios denoting relative ATP levels (blue circles) in root epidermis.

higher in cotyledons and root tip than in hypocotyl, shoot to root transition, and roots. This gradient was abolished by treatment with a protonophore, suggesting that the(17)se observations reflected changes in ATP concentrations. This sensor was also used to explore ATP dynamics in chloroplasts and mitochondria (275). However, these studies lacked a control sensor to distinguish changes in ATP concentration from non-specific changes in the cellular environment.

I demonstrated that the AT1.03_R122K_R126K sensor is suitable for this purpose. It is insensitive to ATP both *in vitro* and *in vivo*, and thus will be an important tool for future experiments that probe ATP dynamics in plants.

Pi acquisition from soil is rapidly followed by its assimilation to ATP, as observed previously with radioactivity assays (276). In this study, I demonstrated the interdependence of Pi and ATP concentrations in Arabidopsis roots. Cyanide treatment reduced ATP levels as expected, while turnover of existing ATP occurs at a rate equivalent to that for the increase in Pi levels. Thus, complex dynamics for both ATP and Pi can be monitored with high spatial and temporal resolution.

ATP concentration is an indicator of cellular metabolic status. For example, more ATP may be needed in cells in the EZ to support rapid cell wall synthesis and other structural processes associated with cell elongation than in the mature root where cells have reached their final size. The rates of ATP synthesis and hydrolysis determine steady-state cytosolic ATP concentration. This study provides a high-resolution map of cytosolic ATP concentrations throughout primary Arabidopsis roots. Interestingly, the pattern of cytosolic ATP distribution in the root is the opposite of Pi. Further experimentation is required to unravel why ATP levels are lowest in the TZ. It is possible that this reflects a high rate of ATP hydrolysis associated with actin polymerization and extensive cytoskeletal remodeling (100). This can be tested by treating plants with Latrunculin-B to sequester G-actin and inhibit F-actin assembly and thereby inhibit actin polymerization. As a result, ATP concentrations should increase in the TZ more than other zones. By contrast, a similar treatment in plants expressing a Pi-sensor should exhibit a maximal decrease in Pi levels in the TZ.

4.4 Materials and Methods

4.4.1 Plasmid construction and generation of transgenic lines

The ATeam1.03-nD/nA with CFP and cp173Venus was amplified from ATeam1.03-nD/nA/pENTR1A (Addgene plasmid #51959) (271) to introduce 5'*Bam*HI and 3'*Hin*dIII sites, then cloned into the pRSET vector for bacterial expression. To make AT1.03_R122K_R126K, lysine codons at position 122 and 126 were replaced with the arginine codon (270). This was done by site-directed mutagenesis of pRSET/ATeam1.03-nD/nA using primers 5'-gccgagctggcactgcagaaggccctgaacaagctggacgtggctgggaagg- 3' and 5'- ccttcccagccacgtccagcttgttcagggccttctgcagtgccagctcggc-3'. The mutations were confirmed by sequencing. I cloned this sensor gene into the pCN binary vector under the control of the *UBQ10* promoter. The insert was obtained by digesting pRSET/AT1.03_R122K_R126K with *Bam*HI and *Hin*dIII then cloned into the same sites of pCN/cpFLIPPi-null (166), replacing the 2461 bp cpFLIPPi-null sensor coding sequence. This construct was introduced into the Arabidopsis *sgs3-13* mutant (224) by *Agrobacterium*-mediated floral dip transformation (277). T1 seeds were selected for phosphinothricin resistance and then fluorescent seedlings were grown to collect T2 seeds.

4.4.2 *In vitro* characterization of ATP sensor AT1.03-nD/nA and control sensor AT1.03_R122K_R126K

4.4.2.1 Bacterial expression and protein purification

Electrocompetent *E.coli* BL21 cells were transformed with pRSET plasmid clones for ATP sensors (AT1.03-nD/nA, AT1.03_R122K_R126K) and single fluorophore controls (eCFP, cpVenus). Fluorescent colonies were cultured in LB medium with antibiotic selection, then harvested and lysed as described previously (165). Proteins were purified by His-affinity

chromatography and eluted in 20 mM Tris-HCl, pH 7.5, 150 mM K-gluconate and 400 mM imidazole. 20 mM Tris-HCl (pH 7.5) was used to dialyze the eluent at 4°C, then the eluent was centrifuged briefly before transferring to a new tube and stored at 4°C.

4.4.2.2 Confocal ATP-dependent FRET assay

Sensor protein concentrations were determined by Bradford assay then 3 μM protein was mixed with buffer containing 50 mM MOPS-KOH pH 7.5, 50 mM KCl, 0.5 mM $MgCl_2$ and 1 mg/ml BSA. A droplet containing sensor, ATP, and buffer was placed on a 43 X 50 mm cover slip and imaged using an inverted spinning disk confocal Olympus IX81 microscope and EMCCD camera (Andor Technology, USA). A 445 nm laser was used for CFP excitation and a 515 nm laser was used for direct cpVenus excitation. A 483/32 nm filter was used to detect CFP emission and a 542/27 nm filter for FRET emission and cpVenus emission. EM gain was set at 10, pre-amplifier gain at 2.4X and exposure time at 1000 ms. Imaging was conducted at 40X magnification using an oil immersion objective (NA 1.3). Image acquisition parameters were kept constant for all *in vitro* and *in vivo* imaging using these sensors. FRET response was measured at 10 different ATP concentrations ranging from 0-10 mM. Sensitized FRET was calculated based on the following formula:

Sensitized FRET = CY – (CC*a) – (YY*b)

CC is CFP excitation with CFP emission, CY is CFP excitation with YFP emission (FRET signal), and YY is YFP excitation with YFP emission. For this purpose, cpVenus is equivalent to YFP.

a and b are correction factors

a is CY/CC with CFP alone [donor bleed-through into yellow emission channel]

b is CY/YY with cpVenus alone [cross excitation of acceptor in yellow emission channel]

Sensitized FRET/CFP ratios were plotted versus ATP concentrations and curve fitting to estimate B_{max} and K_d using the Hill equation was done with Kaleidagraph.

Hill equation, $R-R0=Rmax * [L]^n / Kd^n + [L]^n$

n is the Hill coefficient, which is a measure of the number of ligand binding sites.

4.4.2.3 Plant growth and imaging

Arabidopsis seeds were germinated and grown in 96-well microplates containing 0.5x Murashige and Skoog (MS) medium with 0.25% (w/v) sucrose and 0.25 mM Pi (Pi-replete). Plates were incubated in a growth chamber (60% relative humidity, 21°C, and 110 μmol/m^2/s light intensity for a 16 h photoperiod). Seedlings were mounted on a cover slip in 0.5x MS medium without Pi. A smaller cover slip was placed on top of the root to keep it flat against the larger cover slip and to limit its movement during imaging. Initial images were captured then the medium was replaced with 30 μl of medium containing 10 mM NaCN and the same cells were imaged after 14 s. Image settings were the same as those used for *in vitro* calibration.

CHAPTER V

CONCLUSIONS AND FUTURE DIRECTIONS

Our understanding of how plants sense, acquire, store, and use Pi has been limited by the inability to measure Pi with high spatiotemporal resolution in live plants. This limitation was partially resolved through the development of a genetically encoded FRET-based biosensor for Pi (165) and a closely-related control sensor to detect and quantify non-specific changes in FRET ratio, including pH, viscosity, and other ions (166). However, changes in Pi-dependent FRET ratios report relative, rather than absolute, changes in Pi concentration. *In vitro* calibration is unsuitable because it does not account for optical interference from the cell wall or other cell components. To circumvent this problem, *in vivo* calibration was conducted by microinjecting defined concentrations of Pi into the cell cytosol. I used this calibration curve to report absolute Pi concentration (mM) in the cytosol of root cells.

As shown in Chapter 2, cytosolic Pi is not uniformly distributed in the Arabidopsis root. Cells in the TZ have highest Pi concentrations in the root. This is surprising because cells in the TZ are symplastically connected with those in the flanking MZ and EZ. In order to identify the mechanism(s) responsible for this bi-directional Pi concentration gradient, I measured metabolic recycling, Pi uptake, and vacuolar sequestration in each developmental zone of the primary root. These processes occur too rapidly within a cell to easily distinguish them under steady-state conditions. I therefore used cyanide to block Pi assimilation into ATP, and this allowed detection of rapid changes in cytosolic Pi concentrations due to recycling or uptake with high spatiotemporal resolution. This Pi imaging approach is a significant advance over the previously available methods that relied on accumulation of ^{32}Pi or ^{33}Pi because they report total P accumulation rather than distinguish free Pi from assimilated organic-P, and lack cellular and

subcellular resolution. Nevertheless, Pi imaging has limitations. Because it reports changes in Pi concentrations, it is not possible to measure Pi uptake in cells with large cytosolic volumes, i.e., cells in the EZ, DZ, and MR. It is likely that Pi uptake occurs in these cells but the change in Pi-dependent FRET is below the detection limit of the sensor.

In wild-type plants, I detected spatial patterns for both metabolic recycling and Pi uptake in roots. Although these patterns did not correlate with the distribution of cytosolic Pi, the results can be used to infer underlying mechanisms. For example, higher levels of Pi recycling observed in the EZ than MZ may reflect greater metabolic demands for cell wall synthesis in the EZ than cell division in the MZ. It will be interesting to evaluate Pi recycling in these zones in mutants like *csld3-1* (124) and *cdc2a* (95), which are defective in cell wall synthesis and cell division, respectively. In addition, Pi transport mutants can be used to measure the contribution of each affected transporter on Pi uptake in each developmental zone. Preliminary data suggest that cytosolic Pi concentrations are significantly reduced in *pht1;1* in all developmental zones under steady-state growth conditions (**Figure 35)**. However, any potential spatial specificity may have been masked due to intercellular movement. Nevertheless, the effect of this mutation is encouraging because it suggests the possibility of applying the strategies described above to reveal insights into spatial, developmental, and/or kinetic contributions of PHT1 transporters in Arabidopsis roots.

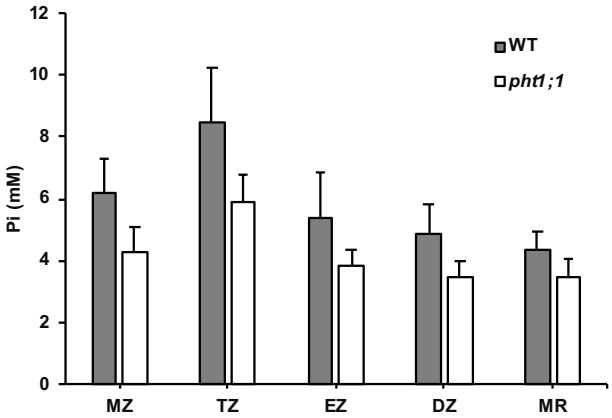

Figure 35: Cytosolic Pi distribution in WT and *pht1;1* seedlings. Seedlings were grown in Pi-replete conditions for 6 d before imaging. Pi concentrations (mean ± SD) were measured in epidermal cells of 5 independent plants. Pi concentrations in all developmental zones of *pht1;1* are significantly less than WT ($p<0.05$, Student's t-test).

This study also evaluated the effect of vacuolar sequestration on cytosolic Pi concentration. Vacuoles constitute 90% of plant cell volume and serve as a reservoir of Pi. However, cells in the TZ do not have fully developed, central vacuoles. Therefore, loading and unloading capacities of these vacuoles may differ from those of the adjoining zones. An ideal method of detecting changes in vacuolar Pi concentration would be to target a Pi-biosensor to vacuoles. Unfortunately, our current Pi sensors do not function in the vacuole, and this is partly due to the acidic environment of the vacuolar lumen. As a proxy, I measured cytosolic Pi concentrations in a vacuolar Pi import mutant *pht5;1*. I found that cytosolic Pi concentrations throughout *pht5;1* roots are elevated, except for cells in the TZ, which indicates vacuolar Pi sequestration is less active in these cells. In addition to lower vacuolar Pi import, these cells may also export more Pi from vacuoles to cytosol. This can be tested by measuring steady-state cytosolic Pi concentrations in mutants of vacuolar Pi exporters, VPE (40). If Pi export from vacuoles is high in the TZ, cytosolic Pi concentration in *vpe* mutants will be low in these cells.

This study provides a comprehensive view of the three main processes controlling cytosolic Pi homeostasis: metabolic recycling, Pi uptake, and vacuolar Pi sequestration. It also lays the foundation for further investigations to resolve cellular and/or developmental specificity of Pi transporters that catalyze vacuolar Pi export. Although this study established a role for vacuolar Pi sequestration in the distribution of Pi throughout the root, the significance of maintaining high Pi concentrations in the TZ for root/plant growth, or Pi sensing, remains unknown. Since cells in the TZ exhibit the greatest reduction in Pi concentration during Pi starvation, I speculate that changes in Pi concentration in TZ act as a signal to trigger Pi-starvation responses. It will therefore be interesting to monitor Pi concentrations in the Pi-insensitive mutant *lpr1* (73). Primary root growth is not inhibited in this mutant during Pi starvation (73), but total Pi accumulation in these roots is reduced (73). However, it is not known if cytosolic Pi concentration is affected in this mutant or if there are any spatial differences. If high Pi concentration in the TZ is responsible for signaling root growth, one might expect to see similar Pi concentrations in at least the TZ of the *lpr1* mutant.

Root hairs play a critical role in Pi acquisition in low-Pi environments. Therefore, they are important in regulating plant growth and development during nutrient stress. My work focused on quantification of cytosolic Pi in root hairs and analyzing Pi gradients within a root hair. My results showed that root hairs have non-uniform Pi distribution in the cytosol. While most root hairs showed highest Pi concentration at the tip, there were some that showed highest levels at the center or the base. I concluded from temporal assays and mutant studies that a combination of high Pi uptake and low vacuolar Pi sequestration activities is responsible for high Pi levels at the tip. However, why Pi is high in the center or base of some root hairs is unclear. I speculate that such differences reflect Pi movement from the tip to the base of the hair following

Pi uptake. This can be evaluated by time-lapse imaging of a root hair after exogenous Pi is provided. Tracking changes in FRET ratio over time will reveal if Pi moves through the root hair in a bolus as suggested by single time point measurements.

In addition to resolving spatial differences in Pi levels within root hairs, I also measured differences in Pi concentrations between root hairs and epidermal cells of the same developmental zone. Monitoring Pi at single cell level revealed that cell bodies of trichoblasts have higher Pi concentrations than atrichoblasts. This may be due to difference in Pi uptake or difference in xylem loading or both. If rate of Pi export from epidermis to the xylem is the same for trichoblasts and atrichoblasts, then the difference in cytosolic Pi levels in these cells can be attributed to higher Pi uptake in trichoblasts due to their extended root hairs. Since Pi uptake is not detectable in epidermal cells in the DZ using cyanide, an alternative strategy to test this hypothesis is to compare Pi concentrations in trichoblasts and atrichoblasts of mutants defective in root hair formation, e.g., *rhd2* and *rhd6* (136). I predict that Pi levels will be similar in all epidermal cells in these mutants since they lack root hairs. Another possible explanation for why Pi accumulation differs between trichoblasts and atrichoblasts is that the rate of Pi export to xylem is greater for atrichoblasts. This, of course, assumes that Pi uptake is equivalent. Thus, it will be possible to dissect the mechanisms responsible for the difference in Pi levels in trichoblasts and atrichoblasts.

Since root hair growth increases during Pi starvation, I wanted to assess the effect of starvation on internal Pi concentrations. Preliminary data suggest that cytosolic Pi concentration does not change in root hairs after 48 h of Pi starvation (**Figure 36**). This differs from the response observed for cells in the primary root cells where cytosolic Pi levels in all development zones decrease during Pi starvation. I speculate that when plants are subjected to nutrient

starvation, they allocate more resources to the growth and development of root hairs so that their net uptake capacity increases. Therefore, despite the increase in length and density of root hairs, cytosolic Pi concentration is unchanged. It will be interesting to test the effect of Pi starvation on the accumulation of Pi in root hairs of mutants that are insensitive to Pi starvation, e.g., *lpr1* (73).

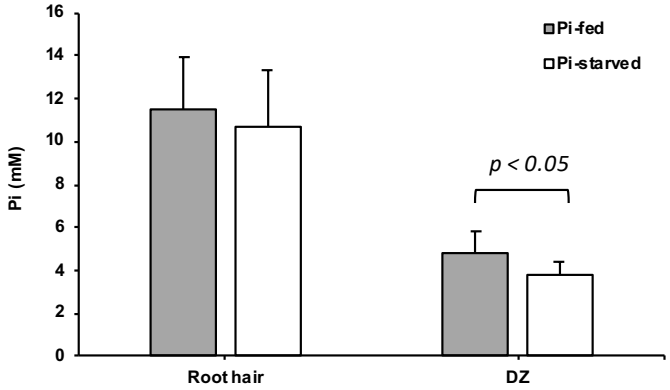

Figure 36. Change in cytosolic Pi in root hairs and epidermal cells of DZ in WT after Pi starvation. Seedlings were grown in Pi-replete conditions for 6 d then transferred to 0 Pi for 48 h before imaging. Pi concentrations (mean ± SD) were measured in epidermal cells of DZ and root hairs of 5 independent plants. Pi concentration in DZ cells is significantly lower in Pi-starved medium ($p<0.05$, Student's t-test). No significant difference is observed between Pi-fed and Pi-starved root hairs.

In this study, I also measured relative levels of cytosolic ATP in the root epidermis using an ATP sensor. Since ATP is the initial product of Pi assimilation, an integrated view of Pi and ATP distribution is critical to elucidate mechanisms governing Pi distribution and ATP production. One of the key contributions of this study is the construction and *in vivo* validation of an ATP-insensitive sensor that allows us to distinguish between ATP-specific and non-specific responses. In Chapter IV, I demonstrated that unlike the ATP sensor AT1.03, FRET ratio for the control sensor AT1.03_R122K_R126K does not change upon treatment with cyanide, which confirms its insensitivity to ATP *in vivo*. In addition, I established protocols to

calibrate FRET ratio measurements for AT1.03 and AT1.03_R122K_R126K under defined conditions and using different imaging platforms. This facilitated sharing of data with another research group that supported a study of ATP compartmentation in Arabidopsis leaves (168).

Preliminary data using the ATP sensor AT1.03 show that during cyanide treatment, cytosolic ATP levels decline at the same rate as Pi levels increase. This experiment confirmed that internal Pi and ATP levels are tightly coupled. It will be interesting to test how *in vivo* ATP concentrations change in response to changes in Pi supply. For example, do cytosolic ATP concentrations decline during Pi deprivation? If so, what is the magnitude of change and do these vary in different parts of the root?

Monitoring cytosolic ATP concentrations in the root revealed a spatial distribution pattern. Interestingly, cells in the TZ have the lowest ATP concentrations, which is the opposite pattern observed for Pi. I speculate that increased ATP hydrolysis in cells of this zone leads to lower ATP concentration. One of the characteristic features of the TZ is cytoskeletal remodeling, which involves F-actin polymerization and ATP hydrolysis. Therefore, monitoring the change in ATP levels after treatment with Latrunculin B, which inhibits F-actin polymerization, can test my hypothesis and gain a holistic view of both ATP and Pi dynamics.

My results in Chapter IV report FRET ratios that represent relative changes in ATP concentration. I could not estimate absolute concentrations of ATP due to the lack of an *in vivo* calibration curve. The same approach used for making the Pi calibration curve could be adopted for calibrating the ATP sensor. However, this may be confounded if ATP hydrolysis is rapid. In order to maintain a stable concentration of the injected ligand, we could inject a non-hydrolyzable version of ATP, e.g., ATP-γ-S. Before injection, intracellular ATP should be depleted to minimize the effect of endogenous ATP on the sensor. This can be achieved by

treating the cells with oligomycin to inhibit the proton channel of mitochondrial ATP synthase. Defined concentrations of ATP-γ-S would be injected into the cytosol of plants expressing the ATP sensor and then changes in FRET ratio would be measured. Although labor-intensive, this *in vivo* calibration process would allow quantification of cytosolic ATP concentration.

REFERENCES

1. S. Banerjee, Live Cell Imaging of Inorganic Phosphate Distribution in Multicellular Organisms Using a FRET Based Biosensor. Doctoral dissertation, Texas A & M University. Available electronically from http : / /hdl .handle .net /1969 .1 /165991. (2017).
2. D. P. Schachtman, R. J. Reid, S. M. Ayling, Phosphorus Uptake by Plants: From Soil to Cell. *Plant Physiology* **116**, 447-453 (1998).
3. R. L. Bieleski, Phosphate Pools, Phosphate Transport, and Phosphate Availability. *Annual Review of Plant Physiology* **24**, 225-252 (1973).
4. D. Cordell, J.-O. Drangert, S. White, The story of phosphorus: Global food security and food for thought. *Global Environmental Change* **19**, 292-305 (2009).
5. H. Shin, G. Dewbre, M. Harrison, Phosphate transport in Arabidopsis: Pht1;1 and Pht1;4 play a major role in phosphate acquisition from both low- and high-phosphate environments. *Plant journal* **39**, 629-642 (2004).
6. A. Ayadi *et al.*, Reducing the genetic redundancy of Arabidopsis Phosphate Transporter1 transporters to study phosphate uptake and signaling. *Plant Physiol* **167**, 1511-1526 (2015).
7. T.-J. Chiou, H. Liu, M. J. Harrison, The spatial expression patterns of a phosphate transporter (MtPT1) from Medicago truncatula indicate a role in phosphate transport at the root/soil interface. *The Plant Journal* **25**, 281-293 (2001).

8. P. Daram, S. Brunner, B. L. Persson, N. Amrhein, M. Bucher, Functional analysis and cell-specific expression of a phosphate transporter from tomato. *Planta* **206**, 225-233 (1998).

9. S. A. Arisz, C. Testerink, T. Munnik, Plant PA signaling via diacylglycerol kinase. *Biochim Biophys Acta* **1791**, 869-875 (2009).

10. S. Y. Yang, T. K. Huang, H. F. Kuo, T. J. Chiou, Role of vacuoles in phosphorus storage and remobilization. *J Exp Bot* **68**, 3045-3055 (2017).

11. L. Nussaume *et al.*, Phosphate Import in Plants: Focus on the PHT1 Transporters. *Front Plant Sci* **2**, 83 (2011).

12. C. I. Ullrich-Eberius, A. Novacky, A. J. E. van Bel, Phosphate uptake in Lemna gibba G1: energetics and kinetics. *Planta* **161**, 46-52 (1984).

13. T. Furihata, M. Suzuki, H. Sakurai, Kinetic Characterization of Two Phosphate Uptake Systems with Different Affinities in Suspension-Cultured Catharanthus roseus Protoplasts. *Plant and Cell Physiology* **33**, 1151-1157 (1992).

14. T.-Y. Liu *et al.*, Identification of plant vacuolar transporters mediating phosphate storage. *Nature Communications* **7**, 11095 (2016).

15. J. Misson, M.-C. Thibaud, N. Bechtold, K. Raghothama, L. Nussaume, Transcriptional regulation and functional properties of Arabidopsis Pht1;4, a high affinity transporter contributing greatly to phosphate uptake in phosphate deprived plants. *Plant Molecular Biology* **55**, 727-741 (2004).

16. U. S. Muchhal, K. Raghothama, Transcriptional regulation of plant phosphate transporters. *Proceedings of the National Academy of Sciences* **96**, 5868-5872 (1999).

17. Gonz *et al.*, Phosphate Transporter Traffic Facilitator1 Is a Plant-Specific SEC12-Related Protein That Enables the Endoplasmic Reticulum Exit of a High-Affinity Phosphate Transporter in Arabidopsis. *The Plant Cell* **17**, 3500-3512 (2005).

18. V. Bayle *et al.*, Arabidopsis thaliana high-affinity phosphate transporters exhibit multiple levels of posttranslational regulation. *Plant Cell* **23**, 1523-1535 (2011).

19. H. Jia *et al.*, The Phosphate Transporter Gene OsPht1;8 Is Involved in Phosphate Homeostasis in Rice. *Plant Physiology* **156**, 1164-1175 (2011).

20. C. I. Ullrich, A. J. Novacky, Extra-and intracellular pH and membrane potential changes induced by K+, Cl−, H2PO4−, and NO3− uptake and fusicoccin in root hairs of Limnobium stoloniferum. *Plant Physiology* **94**, 1561-1567 (1990).

21. K. Sakano, Proton/Phosphate Stoichiometry in Uptake of Inorganic Phosphate by Cultured Cells of Catharanthus roseus (L.) G. Don. *Plant Physiology* **93**, 479-483 (1990).

22. K. G. Raghothama, Phosphate Acquisition. *Annual Review of Plant Physiology and Plant Molecular Biology* **50**, 665-693 (1999).

23. A. S. Karthikeyan *et al.*, Regulated Expression of Arabidopsis Phosphate Transporters. *Plant Physiology* **130**, 221-233 (2002).

24. S. Kanno *et al.*, A novel role for the root cap in phosphate uptake and homeostasis. *eLife* **5**, e14577 (2016).

25. E. Gout, R. Bligny, R. Douce, A.-M. Boisson, C. Rivasseau, Early response of plant cell to carbon deprivation: in vivo 31P-NMR spectroscopy shows a quasi-instantaneous disruption on cytosolic sugars, phosphorylated intermediates of energy metabolism, phosphate partitioning, and intracellular pHs. *New Phytologist* **189**, 135-147 (2011).

26. P. Mukherjee *et al.*, Live imaging of inorganic phosphate in plants with cellular and subcellular resolution. *Plant Physiol* **167**, 628-638 (2015).

27. R. Fliege, U. I. Flügge, K. Werdan, H. W. Heldt, Specific transport of inorganic phosphate, 3-phosphoglycerate and triosephosphates across the inner membrane of the envelope in spinach chloroplasts. *Biochim Biophys Acta* **502**, 232-247 (1978).

28. U.-I. Flügge, Phosphate Translocator In Plastids. *Annual Review of Plant Physiology and Plant Molecular Biology* **50**, 27-45 (1999).

29. B. Guo, S. Irigoyen, T. B. Fowler, W. K. Versaw, Differential expression and phylogenetic analysis suggest specialization of plastid-localized members of the PHT4 phosphate transporter family for photosynthetic and heterotrophic tissues. *Plant Signaling & Behavior* **3**, 784-790 (2008).

30. B. Guo *et al.*, Functional analysis of the Arabidopsis PHT4 family of intracellular phosphate transporters. *New Phytologist* **177**, 889-898 (2008).

31. C. Guo *et al.*, Function of wheat phosphate transporter gene TaPHT2;1 in Pi translocation and plant growth regulation under replete and limited Pi supply conditions. *Planta* **237**, 1163-1178 (2013).

32. T. Miyaji *et al.*, AtPHT4;4 is a chloroplast-localized ascorbate transporter in Arabidopsis. *Nature Communications* **6**, 5928 (2015).

33. W. K. Versaw, M. J. Harrison, A Chloroplast Phosphate Transporter, PHT2;1, Influences Allocation of Phosphate within the Plant and Phosphate-Starvation Responses. *The Plant Cell* **14**, 1751-1766 (2002).

34. S. Irigoyen, P. M. Karlsson, J. Kuruvilla, C. Spetea, W. K. Versaw, The Sink-Specific Plastidic Phosphate Transporter PHT4;2 Influences Starch Accumulation and Leaf Size in Arabidopsis. *Plant Physiology* **157**, 1765-1777 (2011).

35. B. Cubero *et al.*, The Phosphate Transporter PHT4;6 Is a Determinant of Salt Tolerance that Is Localized to the Golgi Apparatus of Arabidopsis. *Molecular Plant* **2**, 535-552 (2009).

36. S. Hassler *et al.*, Function of the Golgi-located phosphate transporter PHT4;6 is critical for senescence-associated processes in Arabidopsis. *Journal of Experimental Botany* **67**, 4671-4684 (2016).

37. S. Hassler *et al.*, Lack of the Golgi phosphate transporter PHT4;6 causes strong developmental defects, constitutively activated disease resistance mechanisms and altered intracellular phosphate compartmentation in Arabidopsis. *The Plant Journal* **72**, 732-744 (2012).

38. G. C. Ferreira, P. L. Pedersen, Phosphate transport in mitochondria: Past accomplishments, present problems, and future challenges. *Journal of Bioenergetics and Biomembranes* **25**, 483-492 (1993).

39. A. Phelps, C. Briggs, L. Mincone, H. Wohlrab, Mitochondrial Phosphate Transport Protein. Replacements of Glutamic, Aspartic, and Histidine Residues Affect Transport and Protein Conformation and Point to a Coupled Proton Transport Path. *Biochemistry* **35**, 10757-10762 (1996).

40. L. Xu *et al.*, Identification of vacuolar phosphate efflux transporters in land plants. *Nature Plants* **5**, 84-94 (2019).

41. J. Liu *et al.*, Vacuolar SPX-MFS transporters are essential for phosphate adaptation in plants. *Plant Signal Behav* **11**, e1213474 (2016).

42. M. Luan *et al.*, Vacuolar Phosphate Transporters Contribute to Systemic Phosphate Homeostasis Vital for Reproductive Development in Arabidopsis. *Plant Physiol* **179**, 640-655 (2019).

43. I. Grotjohann, P. Gräber, The H+-ATPase from chloroplasts: effect of different reconstitution procedures on ATP synthesis activity and on phosphate dependence of ATP synthesis. *Biochimica et Biophysica Acta (BBA) - Bioenergetics* **1556**, 208-216 (2002).

44. H. W. Heldt *et al.*, Role of Orthophosphate and Other Factors in the Regulation of Starch Formation in Leaves and Isolated Chloroplasts. *Plant Physiology* **59**, 1146 (1977).

45. L. R. Pavon *et al.*, Arabidopsis ANTR1 is a thylakoid Na+-dependent phosphate transporter: functional characterization in Escherichia coli. *J Biol Chem* **283**, 13520-13527 (2008).

46. P. M. Karlsson *et al.*, The Arabidopsis thylakoid transporter PHT4;1 influences phosphate availability for ATP synthesis and plant growth. *The Plant Journal* **84**, 99-110 (2015).

47. M. Ferro *et al.*, Proteomics of the Chloroplast Envelope Membranes from Arabidopsis thaliana. *Molecular & Cellular Proteomics* **2**, 325 (2003).

48. M. Ferro *et al.*, AT_CHLORO, a Comprehensive Chloroplast Proteome Database with Subplastidial Localization and Curated Information on Envelope Proteins. *Molecular & Cellular Proteomics* **9**, 1063 (2010).

49. M. Tomizioli *et al.*, Deciphering Thylakoid Sub-compartments using a Mass Spectrometry-based Approach. *Molecular & Cellular Proteomics* **13**, 2147 (2014).

50. B. Schulz *et al.*, Expression of the triose phosphate translocator gene from potato is light dependent and restricted to green tissues. *Molecular and General Genetics MGG* **238**, 357-361 (1993).

51. G.-Y. Wang *et al.*, Circadian Clock-Regulated Phosphate Transporter PHT4;1 Plays an Important Role in Arabidopsis Defense. *Molecular Plant* **4**, 516-526 (2011).

52. H. E. N. and, M. J. Emes, Nonphotosynthetic Metabolism In Plastids. *Annual Review of Plant Physiology and Plant Molecular Biology* **51**, 111-140 (2000).

53. J. Reiser, N. Linka, L. Lemke, W. Jeblick, H. E. Neuhaus, Molecular Physiological Analysis of the Two Plastidic ATP/ADP Transporters from Arabidopsis. *Plant Physiology* **136**, 3524-3536 (2004).

54. P. Hamel *et al.*, Redundancy in the function of mitochondrial phosphate transport in Saccharomyces cerevisiae and Arabidopsis thaliana. *Molecular Microbiology* **51**, 307-317 (2004).

55. F. Jia *et al.*, Overexpression of Mitochondrial Phosphate Transporter 3 Severely Hampers Plant Development through Regulating Mitochondrial Function in Arabidopsis. *PLOS ONE* **10**, e0129717 (2015).

56. M. Monné *et al.*, Functional characterization and organ distribution of three mitochondrial ATP–Mg/Pi carriers in Arabidopsis thaliana. *Biochimica et Biophysica Acta (BBA) - Bioenergetics* **1847**, 1220-1230 (2015).

57. C. Tateda, K. Watanabe, T. Kusano, Y. Takahashi, Molecular and genetic characterization of the gene family encoding the voltage-dependent anion channel in Arabidopsis. *Journal of Experimental Botany* **62**, 4773-4785 (2011).

58. G. Neckelmann, A. Orellana, Metabolism of Uridine 5′-Diphosphate-Glucose in Golgi Vesicles from Pea Stems. *Plant Physiology* **117**, 1007 (1998).

59. B. Guo, S. Irigoyen, T. B. Fowler, W. K. Versaw, Differential expression and phylogenetic analysis suggest specialization of plastid-localized members of the PHT4 phosphate transporter family for photosynthetic and heterotrophic tissues. *Plant Signal Behav* **3**, 784-790 (2008).

60. M. Bucher, I. Fabianska, Long-Sought Vacuolar Phosphate Transporters Identified. *Trends Plant Sci* **21**, 463-466 (2016).

61. J. Liu *et al.*, A vacuolar phosphate transporter essential for phosphate homeostasis in Arabidopsis. *Proc Natl Acad Sci U S A* **112**, E6571-6578 (2015).

62. N. E. Robbins, C. Trontin, L. Duan, J. R. Dinneny, Beyond the Barrier: Communication in the Root through the Endodermis. *Plant Physiology* **166**, 551 (2014).

63. A. Sasaki, N. Yamaji, J. F. Ma, Transporters involved in mineral nutrient uptake in rice. *Journal of Experimental Botany* **67**, 3645-3653 (2016).

64. Y. Poirier, S. Thoma, C. Somerville, J. Schiefelbein, Mutant of Arabidopsis Deficient in Xylem Loading of Phosphate. *Plant Physiology* **97**, 1087-1093 (1991).

65. Y. Wang, C. Ribot, E. Rezzonico, Y. Poirier, Structure and expression profile of the Arabidopsis PHO1 gene family indicates a broad role in inorganic phosphate homeostasis. *Plant Physiol* **135**, 400-411 (2004).

66. D. Hamburger, E. Rezzonico, J. MacDonald-Comber Petetot, C. Somerville, Y. Poirier, Identification and characterization of the Arabidopsis PHO1 gene involved in phosphate loading to the xylem. *Plant Cell* **14**, 889-902 (2002).

67. A. B. Arpat *et al.*, Functional expression of PHO1 to the Golgi and trans-Golgi network and its role in export of inorganic phosphate. *The Plant Journal* **71**, 479-491 (2012).

68. S. Wege *et al.*, The EXS Domain of PHO1 Participates in the Response of Shoots to Phosphate Deficiency via a Root-to-Shoot Signal. *Plant Physiology* **170**, 385-400 (2016).

69. H. Rouached *et al.*, Uncoupling phosphate deficiency from its major effects on growth and transcriptome via PHO1 expression in Arabidopsis. *Plant J* **65**, 557-570 (2011).

70. Z. Fang, C. Shao, Y. Meng, P. Wu, M. Chen, Phosphate signaling in Arabidopsis and Oryza sativa. *Plant Science* **176**, 170-180 (2009).

71. J. López-Bucio *et al.*, Phosphate Availability Alters Architecture and Causes Changes in Hormone Sensitivity in the Arabidopsis Root System. *Plant Physiology* **129**, 244-256 (2002).

72. C. W. Lisa, P. C. P. R. Sebastien, A. H. Fitter, H. M. O. Leyser, Phosphate Availability Regulates Root System Architecture in Arabidopsis. *Plant Physiology* **126**, 875-882 (2001).

73. S. Svistoonoff *et al.*, Root tip contact with low-phosphate media reprograms plant root architecture. *Nature Genetics* **39**, 792-796 (2007).

74. C. A. Ticconi *et al.*, ER-resident proteins PDR2 and LPR1 mediate the developmental response of root meristems to phosphate availability. *Proceedings of the National Academy of Sciences* **106**, 14174-14179 (2009).

75. C. A. Ticconi, C. A. Delatorre, B. Lahner, D. E. Salt, S. Abel, Arabidopsis pdr2 reveals a phosphate-sensitive checkpoint in root development. *The Plant Journal* **37**, 801-814 (2004).

76. L. Sánchez-Calderón *et al.*, Characterization of low phosphorus insensitive Mutants Reveals a Crosstalk between Low Phosphorus-Induced Determinate Root Development and the Activation of Genes Involved in the Adaptation of Arabidopsis to Phosphorus Deficiency. *Plant Physiology* **140**, 879-889 (2006).

77. X. Wang *et al.*, The Function of LPR1 is Controlled by an Element in the Promoter and is Independent of SUMO E3 Ligase SIZ1 in Response to Low Pi Stress in Arabidopsis thaliana. *Plant and Cell Physiology* **51**, 380-394 (2010).

78. T. R. Bates, J. P. Lynch, Stimulation of root hair elongation in Arabidopsis thaliana by low phosphorus availability. *Plant, Cell & Environment* **19**, 529-538 (1996).

79. Z. Ma, D. G. Bielenberg, K. M. Brown, J. P. Lynch, Regulation of root hair density by phosphorus availability in Arabidopsis thaliana. *Plant, Cell & Environment* **24**, 459-467 (2001).

80. D. K. Varadarajan, A. S. Karthikeyan, P. D. Matilda, K. G. Raghothama, Phosphite, an Analog of Phosphate, Suppresses the Coordinated Expression of Genes under Phosphate Starvation. *Plant Physiology* **129**, 1232-1240 (2002).

81. J. R. Pratt *et al.*, Effects of Methylphosphonate, a Phosphate Analogue, on the Expression and Degradation of the High-Affinity Phosphate Transporter Pho84, in Saccharomyces cerevisiae. *Biochemistry* **43**, 14444-14453 (2004).

82. C. A. Ticconi, C. A. Delatorre, S. Abel, Attenuation of Phosphate Starvation Responses by Phosphite in Arabidopsis. *Plant Physiology* **127**, 963-972 (2001).

83. S. H. Burleigh, M. J. Harrison, The Down-Regulation of Mt4-Like Genes by Phosphate Fertilization Occurs Systemically and Involves Phosphate Translocation to the Shoots. *Plant Physiology* **119**, 241-248 (1999).

84. E. Delhaize, P. J. Randall, Characterization of a Phosphate-Accumulator Mutant of Arabidopsis thaliana. *Plant Physiology* **107**, 207-213 (1995).

85. K. Aung *et al.*, pho2, a Phosphate Overaccumulator, Is Caused by a Nonsense Mutation in a MicroRNA399 Target Gene. *Plant Physiology* **141**, 1000-1011 (2006).

86. B. Dong, Z. Rengel, E. Delhaize, Uptake and translocation of phosphate by pho2 mutant and wild-type seedlings of Arabidopsis thaliana. *Planta* **205**, 251-256 (1998).

87. M. W. Jones-Rhoades, D. P. Bartel, B. Bartel, MicroRNAs And Their Regulatory Role In Plants. *Annual Review of Plant Biology* **57**, 19-53 (2006).

88. T.-J. Chiou *et al.*, Regulation of Phosphate Homeostasis by MicroRNA in Arabidopsis. *The Plant Cell* **18**, 412-421 (2006).

89. R. Bari, B. Datt Pant, M. Stitt, W.-R. Scheible, PHO2, MicroRNA399, and PHR1 Define a Phosphate-Signaling Pathway in Plants. *Plant Physiology* **141**, 988-999 (2006).

90. B. D. Pant, A. Buhtz, J. Kehr, W.-R. Scheible, MicroRNA399 is a long-distance signal for the regulation of plant phosphate homeostasis. *The Plant Journal* **53**, 731-738 (2008).

91. J. M. Franco-Zorrilla *et al.*, Target mimicry provides a new mechanism for regulation of microRNA activity. *Nature Genetics* **39**, 1033-1037 (2007).

92. H. Shin, H.-S. Shin, R. Chen, M. J. Harrison, Loss of At4 function impacts phosphate distribution between the roots and the shoots during phosphate starvation. *The Plant Journal* **45**, 712-726 (2006).

93. M. Iijima, S. Morita, P. W. Barlow, Structure and Function of the Root Cap. *Plant Production Science* **11**, 17-27 (2008).

94. L. Dolan *et al.*, Cellular organisation of the Arabidopsis thaliana root. *Development* **119**, 71-84 (1993).

95. A. Hemerly, C. Bergounioux, M. Van Montagu, D. Inzé, P. Ferreira, Genes regulating the plant cell cycle: isolation of a mitotic-like cyclin from Arabidopsis thaliana. *Proceedings of the National Academy of Sciences* **89**, 3295-3299 (1992).

96. A. Colón-Carmona, R. You, T. Haimovitch-Gal, P. Doerner, Spatio-temporal analysis of mitotic activity with a labile cyclin–GUS fusion protein. *The Plant Journal* **20**, 503-508 (1999).

97. P. C. Ferreira *et al.*, Developmental expression of the arabidopsis cyclin gene cyc1At. *The Plant Cell* **6**, 1763-1774 (1994).

98. F. Baluška, Š. Kubica, M. Hauskrecht, Postmitotic 'isodiametric' cell growth in the maize root apex. *Planta* **181**, 269-274 (1990).

99. J.-P. Verbelen, T. De Cnodder, J. Le, K. Vissenberg, F. Baluška, The Root Apex ofArabidopsis thaliana Consists of Four Distinct Zones of Growth Activities. *Plant signaling & behavior* **1**, 296-304 (2006).

100. F. Baluska, S. Vitha, P. W. Barlow, D. Volkmann, Rearrangements of F-actin arrays in growing cells of intact maize root apex tissues: a major developmental switch occurs in the postmitotic transition region. *Eur J Cell Biol* **72**, 113-121 (1997).

101. F. Baluska, J. S. Parker, P. W. Barlow, Specific patterns of cortical and endoplasmic microtubules associated with cell growth and tissue differentiation in roots of maize Zea mays. *Journal of Cell Science* **103**, 191-200 (1992).

102. D. Ludevid, H. Höfte, E. Himelblau, M. J. Chrispeels, The Expression Pattern of the Tonoplast Intrinsic Protein γ-TIP in Arabidopsis thaliana Is Correlated with Cell Enlargement. *Plant Physiology* **100**, 1633-1639 (1992).

103. K. Vissenberg, I. M. Martinez-Vilchez, J.-P. Verbelen, J. G. Miller, S. C. Fry, In Vivo Colocalization of Xyloglucan Endotransglycosylase Activity and Its Donor Substrate in the Elongation Zone of Arabidopsis Roots. *The Plant Cell* **12**, 1229-1237 (2000).

104. S. C. Fry *et al.*, Xyloglucan endotransglycosylase, a new wall-loosening enzyme activity from plants. *Biochemical Journal* **282**, 821-828 (1992).

105. D.-K. Lee, J. H. Ahn, S.-K. Song, Y. D. Choi, J. S. Lee, Expression of an Expansin Gene Is Correlated with Root Elongation in Soybean. *Plant Physiology* **131**, 985-997 (2003).

106. N. Zhang, K. H. Hasenstein, Distribution of Expansins in Graviresponding Maize Roots. *Plant and Cell Physiology* **41**, 1305-1312 (2000).

107. L. McCartney, C. G. Steele-King, E. Jordan, J. P. Knox, Cell wall pectic (1→4)-β-d-galactan marks the acceleration of cell elongation in the Arabidopsis seedling root meristem. *The Plant Journal* **33**, 447-454 (2003).

108. G. Schindelman *et al.*, COBRA encodes a putative GPI-anchored protein, which is polarly localized and necessary for oriented cell expansion in Arabidopsis. *Genes Dev* **15**, 1115-1127 (2001).

109. F. Baluška, D. Volkmann, P. W. Barlow, A Polarity Crossroad in the Transition Growth Zone of Maize Root Apices: Cytoskeletal and Developmental Implications. *Journal of Plant Growth Regulation* **20**, 170-181 (2001).

110. W. G. T. Willats, J. P. Knox, A role for arabinogalactan-proteins in plant cell expansion: evidence from studies on the interaction of β-glucosyl Yariv reagent with seedlings of Arabidopsis thaliana. *The Plant Journal* **9**, 919-925 (1996).

111. A. J. Van Hengel, K. Roberts, Fucosylated arabinogalactan-proteins are required for full root cell elongation in arabidopsis. *The Plant Journal* **32**, 105-113 (2002).

112. F. Baluška, J. Jasik, H. G. Edelmann, T. Salajová, D. Volkmann, Latrunculin B-Induced Plant Dwarfism: Plant Cell Elongation Is F-Actin-Dependent. *Developmental Biology* **231**, 113-124 (2001).

113. S. Kerstens, J.-P. Verbelen, Cellulose orientation at the surface of the Arabidopsis seedling. Implications for the biomechanics in plant development. *Journal of Structural Biology* **144**, 262-270 (2003).

114. C. M. Duckett, K. J. Oparka, D. A. M. Prior, L. Dolan, K. Roberts, Dye-coupling in the root epidermis of Arabidopsis is progressively reduced during development. *Development* **120**, 3247-3255 (1994).

115. T.-J. Wen, P. S. Schnable, Analyses of mutants of three genes that influence root hair development in Zea mays (Gramineae) suggest that root hairs are dispensable. *American Journal of Botany* **81**, 833-842 (1994).

116. F. Hochholdinger *et al.*, The maize (Zea mays L.) roothairless3 gene encodes a putative GPI-anchored, monocot-specific, COBRA-like protein that significantly affects grain yield. *The Plant Journal* **54**, 888-898 (2008).

117. M. Kwasniewski, A. Janiak, B. Mueller-Roeber, I. Szarejko, Global analysis of the root hair morphogenesis transcriptome reveals new candidate genes involved in root hair formation in barley. *Journal of Plant Physiology* **167**, 1076-1083 (2010).

118. M. Kwasniewski *et al.*, Accumulation of peroxidase-related reactive oxygen species in trichoblasts correlates with root hair initiation in barley. *Journal of Plant Physiology* **170**, 185-195 (2013).

119. M. Marzec, I. Szarejko, M. Melzer, Arabinogalactan proteins are involved in root hair development in barley. *Journal of Experimental Botany* **66**, 1245-1257 (2014).

120. J. Verbančič, J. E. Lunn, M. Stitt, S. Persson, Carbon Supply and the Regulation of Cell Wall Synthesis. *Molecular Plant* **11**, 75-94 (2018).

121. J. K. Polko, J. J. Kieber, The Regulation of Cellulose Biosynthesis in Plants. *The Plant Cell* **31**, 282 (2019).

122. C. M. Kim *et al.*, OsCSLD1, a Cellulose Synthase-Like D1 Gene, Is Required for Root Hair Morphogenesis in Rice. *Plant Physiology* **143**, 1220-1230 (2007).

123. T. Yuo *et al.*, Root hairless 2 (rth2) mutant represents a loss-of-function allele of the cellulose synthase-like gene OsCSLD1 in rice (Oryza sativa L.). *Breeding Science* **61**, 225-233 (2011).

124. X. Wang *et al.*, AtCSLD3, A Cellulose Synthase-Like Gene Important for Root Hair Growth in Arabidopsis. *Plant Physiology* **126**, 575-586 (2001).

125. C. Wang *et al.*, Mutation in xyloglucan 6-xylosytransferase results in abnormal root hair development in Oryza sativa. *Journal of Experimental Botany* **65**, 4149-4157 (2014).

126. M. Kwasniewski, I. Szarejko, Molecular Cloning and Characterization of β-Expansin Gene Related to Root Hair Formation in Barley. *Plant Physiology* **141**, 1149-1158 (2006).

127. S.-K. Won *et al.*, Root hair-specific EXPANSIN B genes have been selected for graminaceae root hairs. *Molecules and Cells* **30**, 369-376 (2010).

128. Y. ZhiMing *et al.*, Root hair-specific expansins modulate root hair elongation in rice. *The Plant Journal* **66**, 725-734 (2011).

129. W. Guo *et al.*, A soybean β-expansin gene GmEXPB2 intrinsically involved in root system architecture responses to abiotic stresses. *The Plant Journal* **66**, 541-552 (2011).

130. T.-J. Wen, F. Hochholdinger, M. Sauer, W. Bruce, P. S. Schnable, The roothairless1 Gene of Maize Encodes a Homolog of sec3 Which Is Involved in Polar Exocytosis. *Plant Physiology* **138**, 1637-1643 (2005).

131. J. Huang *et al.*, Formin homology 1 (OsFH1) regulates root-hair elongation in rice (Oryza sativa). *Planta* **237**, 1227-1239 (2013).

132. W. Yang *et al.*, Bent Uppermost Internode1 Encodes the Class II Formin FH5 Crucial for Actin Organization and Rice Development. *The Plant Cell* **23**, 661-680 (2011).

133. J. Wang, X. Xue, H. Ren, New insights into the role of plant formins: regulating the organization of the actin and microtubule cytoskeleton. *Protoplasma* **249**, 101-107 (2012).

134. P. A. C. van Gisbergen, M. Bezanilla, Plant formins: membrane anchors for actin polymerization. *Trends in Cell Biology* **23**, 227-233 (2013).

135. S. Chen, D. W. Ehrhardt, C. R. Somerville, Mutations of cellulose synthase (CESA1) phosphorylation sites modulate anisotropic cell expansion and bidirectional mobility of cellulose synthase. *Proceedings of the National Academy of Sciences* **107**, 17188 (2010).

136. T. R. Bates, J. P. Lynch, Plant growth and phosphorus accumulation of wild type and two root hair mutants of Arabidopsis thaliana (Brassicaceae). *American Journal of Botany* **87**, 958-963 (2000).

137. M. E. Galway *et al.*, The TTG Gene Is Required to Specify Epidermal Cell Fate and Cell Patterning in the Arabidopsis Root. *Developmental Biology* **166**, 740-754 (1994).

138. A. R. Walker *et al.*, The Transparent Testa Glabra1 Locus, Which Regulates Trichome Differentiation and Anthocyanin Biosynthesis in Arabidopsis, Encodes a WD40 Repeat Protein. *The Plant Cell* **11**, 1337-1349 (1999).

139. J. D. Masucci *et al.*, The homeobox gene GLABRA2 is required for position-dependent cell differentiation in the root epidermis of Arabidopsis thaliana. *Development* **122**, 1253-1260 (1996).

140. M. Di Cristina *et al.*, The Arabidopsis Athb-10 (GLABRA2) is an HD-Zip protein required for regulation of root hair development. *The Plant Journal* **10**, 393-402 (1996).

141. W. G. Rerie, K. A. Feldmann, M. D. Marks, The GLABRA2 gene encodes a homeo domain protein required for normal trichome development in Arabidopsis. *Genes Dev* **8**, 1388-1399 (1994).

142. C.-Y. Hung *et al.*, A Common Position-Dependent Mechanism Controls Cell-Type Patterning and GLABRA2 Regulation in the Root and Hypocotyl Epidermis of Arabidopsis. *Plant Physiology* **117**, 73-84 (1998).

143. T. Wada, T. Tachibana, Y. Shimura, K. Okada, Epidermal Cell Differentiation in Arabidopsis Determined by a Myb Homolog, CPC. *Science* **277**, 1113-1116 (1997).

144. M. M. Lee, J. Schiefelbein, WEREWOLF, a MYB-Related Protein in Arabidopsis, Is a Position-Dependent Regulator of Epidermal Cell Patterning. *Cell* **99**, 473-483 (1999).

145. A. K. Wilson, F. B. Pickett, J. C. Turner, M. Estelle, A dominant mutation inArabidopsis confers resistance to auxin, ethylene and abscisic acid. *Molecular and General Genetics MGG* **222**, 377-383 (1990).

146. M. Tanimoto, K. Roberts, L. Dolan, Ethylene is a positive regulator of root hair development in Arabidopsis thaliana. *The Plant Journal* **8**, 943-948 (1995).

147. J. D. Masucci, J. W. Schiefelbein, The rhd6 Mutation of Arabidopsis thaliana Alters Root-Hair Initiation through an Auxin- and Ethylene-Associated Process. *Plant Physiology* **106**, 1335-1346 (1994).

148. J. W. Schiefelbein, C. Somerville, Genetic Control of Root Hair Development in Arabidopsis thaliana. *The Plant Cell* **2**, 235-243 (1990).

149. E. Ryan, C. S. Grierson, A. Cavell, M. Steer, L. Dolan, TIP1 is required for both tip growth and non-tip growth in Arabidopsis. *New Phytologist* **138**, 49-58 (1998).

150. C. S. Grierson, K. Roberts, K. A. Feldmann, L. Dolan, The COW1 Locus of Arabidopsis Acts after RHD2, and in Parallel with RHD3 and TIP1, to Determine the Shape, Rate of Elongation, and Number of Root Hairs Produced from Each Site of Hair Formation. *Plant Physiology* **115**, 981-990 (1997).

151. T. S. Gahoonia, N. E. Nielsen, Direct evidence on participation of root hairs in phosphorus (32P) uptake from soil. *Plant and Soil* **198**, 147-152 (1998).

152. D. Föhse, N. Claassen, A. Jungk, Phosphorus efficiency of plants. *Plant and Soil* **132**, 261-272 (1991).

153. S. R. Mudge, A. L. Rae, E. Diatloff, F. W. Smith, Expression analysis suggests novel roles for members of the Pht1 family of phosphate transporters in Arabidopsis. *The Plant Journal* **31**, 341-353 (2002).

154. R. Gordon-Weeks, Y. Tong, T. G. E. Davies, G. Leggewie, Restricted spatial expression of a high-affinity phosphate transporter in potato roots. *Journal of Cell Science* **116**, 3135-3144 (2003).

155. T. R. Bates, J. P. Lynch, Root hairs confer a competitive advantage under low phosphorus availability. *Plant and Soil* **236**, 243-250 (2001).

156. J. K. M. Roberts, P. M. Ray, N. Wade-Jardetzky, O. Jardetzky, Estimation of cytoplasmic and vacuolar pH in higher plant cells by 31P NMR. *Nature* **283**, 870-872 (1980).

157. R. B. Lee, R. G. Ratcliffe, Nuclear magnetic resonance studies of the location and function of plant nutrients in vivo. *Plant and Soil* **155**, 45-55 (1993).

158. R. B. Lee, R. G. Ratcliffe, T. E. Southon, 31P NMR Measurements of the Cytoplasmic and Vacuolar Pi Content of Mature Maize Roots: Relationships with Phosphorus Status and Phosphate Fluxes. *Journal of Experimental Botany* **41**, 1063-1078 (1990).

159. R. G. Ratcliffe, Y. Shachar-Hill, Probing Plant Metabolism With NMR. *Annual Review of Plant Physiology and Plant Molecular Biology* **52**, 499-526 (2001).

160. S. Kanno *et al.*, Development of real-time radioisotope imaging systems for plant nutrient uptake studies. *Philosophical Transactions of the Royal Society B: Biological Sciences* **367**, 1501-1508 (2012).

161. P. M. Kopittke *et al.*, Synchrotron-Based X-Ray Fluorescence Microscopy as a Technique for Imaging of Elements in Plants. *Plant Physiology* **178**, 507-523 (2018).

162. K. L. Moore *et al.*, Combined NanoSIMS and synchrotron X-ray fluorescence reveal distinct cellular and subcellular distribution patterns of trace elements in rice tissues. *New Phytologist* **201**, 104-115 (2014).

163. O. Shimomura, F. H. Johnson, Y. Saiga, Extraction, Purification and Properties of Aequorin, a Bioluminescent Protein from the Luminous Hydromedusan, Aequorea. *Journal of Cellular and Comparative Physiology* **59**, 223-239 (1962).

164. H. Gu *et al.*, A novel analytical method for in vivo phosphate tracking. *FEBS Letters* **580**, 5885-5893 (2006).

165. P. Mukherjee *et al.*, Live Imaging of Inorganic Phosphate in Plants with Cellular and Subcellular Resolution. *Plant Physiology* **167**, 628-638 (2015).

166. S. Banerjee, L. R. Garcia, W. K. Versaw, Quantitative Imaging of FRET-Based Biosensors for Cell- and Organelle-Specific Analyses in Plants. *Microsc Microanal* **22**, 300-310 (2016).

167. P. Gardeström, A. U. Igamberdiev, The origin of cytosolic ATP in photosynthetic cells. *Physiologia Plantarum* **157**, 367-379 (2016).

168. C. P. Voon *et al.*, ATP compartmentation in plastids and cytosol of Arabidopsis thaliana revealed by fluorescent protein sensing. *Proc Natl Acad Sci U S A* **115**, E10778-E10787 (2018).

169. M. Klingenberg, The ADP and ATP transport in mitochondria and its carrier. *Biochimica et Biophysica Acta (BBA) - Biomembranes* **1778**, 1978-2021 (2008).

170. N. Picault, M. Hodges, L. Palmieri, F. Palmieri, The growing family of mitochondrial carriers in Arabidopsis. *Trends in Plant Science* **9**, 138-146 (2004).

171. I. Haferkamp, J. H. P. Hackstein, F. G. J. Voncken, G. Schmit, J. Tjaden, Functional integration of mitochondrial and hydrogenosomal ADP/ATP carriers in the Escherichia coli membrane reveals different biochemical characteristics for plants, mammals and anaerobic chytrids. *European Journal of Biochemistry* **269**, 3172-3181 (2002).

172. T. Möhlmann *et al.*, Occurrence of two plastidic ATP/ADP transporters in Arabidopsis thaliana L. *European Journal of Biochemistry* **252**, 353-359 (1998).

173. J. Tjaden, C. Schwöppe, T. Möhlmann, P. W. Quick, H. E. Neuhaus, Expression of a Plastidic ATP/ADP Transporter Gene inEscherichia coli Leads to a Functional Adenine Nucleotide Transport System in the Bacterial Cytoplasmic Membrane. *Journal of Biological Chemistry* **273**, 9630-9636 (1998).

174. J. Reiser, N. Linka, L. Lemke, W. Jeblick, H. E. Neuhaus, Molecular Physiological Analysis of the Two Plastidic ATP/ADP Transporters from Arabidopsis. *Plant Physiology* **136**, 3524 (2004).

175. K. F. Kleppinger-Sparace, R. J. Stahl, S. A. Sparace, Energy Requirements for Fatty Acid and Glycerolipid Biosynthesis from Acetate by Isolated Pea Root Plastids. *Plant Physiology* **98**, 723 (1992).

176. H. E. Neuhaus, M. J. Emes, Nonphotosynthetic Metabolism in Plastids. *Annual Review of Plant Physiology and Plant Molecular Biology* **51**, 111-140 (2000).

177. M. Leroch *et al.*, Identification of a Novel Adenine Nucleotide Transporter in the Endoplasmic Reticulum of <em>Arabidopsis</em&gt. *The Plant Cell* **20**, 438 (2008).

178. F. Kellermeier *et al.*, Analysis of the Root System Architecture of Arabidopsis Provides a Quantitative Readout of Crosstalk between Nutritional Signals. *The Plant Cell* **26**, 1480 (2014).

179. H. Javot, N. Pumplin, M. Harrison, Phosphate in the arbuscular mycorrhizal symbiosis: transport properties and regulatory roles. *Plant, cell and environment* **30**, 310-322 (2007).

180. C. P. Vance, C. Uhde-Stone, D. L. Allan, Phosphorus Acquisition and Use: Critical Adaptations by Plants for Securing a Nonrenewable Resource. *The New Phytologist* **157**, 423-447 (2003).

181. W. C. Plaxton, H. T. Tran, Metabolic Adaptations of Phosphate-Starved Plants. *Plant Physiology* **156**, 1006-1015 (2011).

182. W. K. Versaw, L. R. Garcia, Intracellular transport and compartmentation of phosphate in plants. *Curr Opin Plant Biol* **39**, 25-30 (2017).

183. T. Mimura, Regulation of phosphate transport and homeostasis in plant cells. *Int. Rev. Cytol.* **191**, 149-200 (1999).

184. C. Balzergue *et al.*, Low phosphate activates STOP1-ALMT1 to rapidly inhibit root cell elongation. *Nature Communications* **8**, 15300 (2017).

185. J. Müller *et al.*, Iron-Dependent Callose Deposition Adjusts Root Meristem Maintenance to Phosphate Availability. *Developmental Cell* **33**, 216-230 (2015).

186. P.-S. Chien, C.-P. Chiang, S. J. Leong, T.-J. Chiou, Sensing and Signaling of Phosphate Starvation: From Local to Long Distance. *Plant and Cell Physiology* **59**, 1714-1722 (2018).

187. M. I. Puga *et al.*, SPX1 is a phosphate-dependent inhibitor of PHOSPHATE STARVATION RESPONSE 1 in Arabidopsis. *Proceedings of the National Academy of Sciences* **111**, 14947 (2014).

188. V. Rubio *et al.*, A conserved MYB transcription factor involved in phosphate starvation signaling both in vascular plants and in unicellular algae. *Genes Dev* **15**, 2122-2133 (2001).

189. M.-C. Thibaud *et al.*, Dissection of local and systemic transcriptional responses to phosphate starvation in Arabidopsis. *The Plant Journal* **64**, 775-789 (2010).

190. Z. Wang *et al.*, Rice SPX1 and SPX2 inhibit phosphate starvation responses through interacting with PHR2 in a phosphate-dependent manner. *Proceedings of the National Academy of Sciences* **111**, 14953 (2014).

191. L. Sun, L. Song, Y. Zhang, Z. Zheng, D. Liu, Arabidopsis PHL2 and PHR1 Act Redundantly as the Key Components of the Central Regulatory System Controlling Transcriptional Responses to Phosphate Starvation. *Plant Physiology* **170**, 499 (2016).

192. R. Jost *et al.*, Differentiating phosphate-dependent and phosphate-independent systemic phosphate-starvation response networks in Arabidopsis thaliana through the application of phosphite. *Journal of Experimental Botany* **66**, 2501-2514 (2015).

193. R. Wild *et al.*, Control of eukaryotic phosphate homeostasis by inositol polyphosphate sensor domains. *Science* **352**, 986 (2016).

194. B. Naim *et al.*, Passive and Facilitated Transport in Nuclear Pore Complexes Is Largely Uncoupled. *Journal of Biological Chemistry* **282**, 3881-3888 (2007).

195. H.-F. Kuo *et al.*, Arabidopsis inositol phosphate kinases IPK1 and ITPK1 constitute a metabolic pathway in maintaining phosphate homeostasis. *The Plant Journal* **95**, 613-630 (2018).

196. J. Zhu *et al.*, Two bifunctional inositol pyrophosphate kinases/phosphatases control plant phosphate homeostasis. *eLife* **8**, e43582 (2019).

197. J. Pratt *et al.*, Phosphate (Pi) starvation effect on the cytosolic Pi concentration and Pi exchanges across the tonoplast in plant cells: an in vivo 31P-nuclear magnetic resonance study using methylphosphonate as a Pi analog. *Plant Physiol.* **151**, 1646-1657 (2009).

198. F. Rebeille, R. Bligny, R. Douce, Is the cytosolic Pi concentration a limiting factor for plant cell respiration? *Plant Physiol.* **74**, 355-359 (1984).

199. Y. Benitez-Alfonso *et al.*, Symplastic Intercellular Connectivity Regulates Lateral Root Patterning. *Developmental Cell* **26**, 136-147 (2013).

200. C. M. Duckett, K. J. Oparka, D. A. M. Prior, L. Dolan, K. Roberts, Dye-coupling in the root epidermis of Arabidopsis is progressively reduced during development. *Development* **120**, 3247 (1994).

201. H. R. Lapis-Gaza, R. Jost, P. M. Finnegan, Arabidopsis Phosphate Transporter1 genes PHT1;8 and PHT1;9 are involved in root-to-shoot translocation of orthophosphate. *BMC plant biology* **14**, 334 (2014).

202. A. Stefanovic *et al.*, Members of the PHO1 gene family show limited functional redundancy in phosphate transfer to the shoot, and are regulated by phosphate deficiency via distinct pathways. *The Plant Journal* **50**, 982-994 (2007).

203. S. Kanno *et al.*, Performance and limitations of phosphate quantification: guidelines for plant biologists. *Plant Cell Physiol* **57**, 690-706 (2016).

204. F. Lai, J. Thacker, Y. Li, P. Doerner, Cell division activity determines the magnitude of phosphate starvation responses in Arabidopsis. *The Plant journal : for cell and molecular biology* **50**, 545-556 (2007).

205. R. Di Mambro *et al.*, Auxin minimum triggers the developmental switch from cell division to cell differentiation in the Arabidopsis root. *Proceedings of the National Academy of Sciences* **114**, E7641 (2017).

206. J. J. Petricka, C. M. Winter, P. N. Benfey, Control of Arabidopsis root development. *Annu. Rev. Plant Biol.* **63**, 563-590 (2012).

207. K. P. Carter, M. C. Carpenter, B. Fiedler, R. Jimenez, A. E. Palmer, Critical Comparison of FRET-Sensor Functionality in the Cytosol and Endoplasmic Reticulum and Implications for Quantification of Ions. *Analytical Chemistry* **89**, 9601-9608 (2017).

208. J. Shen *et al.*, Organelle pH in the Arabidopsis Endomembrane System. *Molecular Plant* **6**, 1419-1437 (2013).

209. W. E. Van Heyningen, The inhibition of respiration by cyanide. *Biochem J* **29**, 2036-2039 (1935).

210. T. R. Bates, J. P. Lynch, The efficiency of Arabidopsis thaliana (Brassicaceae) root hairs in phosphorus acquisition. *Am J Bot* **87**, 964-970 (2000).

211. S. M. Brady *et al.*, A High-Resolution Root Spatiotemporal Map Reveals Dominant Expression Patterns. *Science* **318**, 801 (2007).

212. L. Copeland, A. Zammit, Kinetic properties of NAD-dependent glyceraldehyde-3-phosphate dehydrogenase from the host fraction of soybean root nodules. *Archives of biochemistry and biophysics* **312**, 107-113 (1994).

213. M. Stitt, H. W. Heldt, Control of photosynthetic sucrose synthesis by fructose 2,6-bisphosphate : VI. regulation of the cytosolic fructose 1,6-bisphosphatase in spinach leaves by an interaction between metabolic intermediates and fructose 2,6-bisphosphate. *Plant Physiol.* **79**, 599-608 (1985).

214. K. Volkert *et al.*, Loss of the two major leaf isoforms of sucrose-phosphate synthase in Arabidopsis thaliana limits sucrose synthesis and nocturnal starch degradation but does not alter carbon partitioning during photosynthesis. *Journal of Experimental Botany* **65**, 5217-5229 (2014).

215. E. Gout, R. Bligny, R. Douce, A. M. Boisson, C. Rivasseau, Early response of plant cell to carbon deprivation: in vivo 31P-NMR spectroscopy shows a quasi-instantaneous disruption on cytosolic sugars, phosphorylated intermediates of energy metabolism, phosphate partitioning, and intracellular pHs. *New Phytol* **189**, 135-147 (2011).

216. F. Baluska, D. Volkmann, P. W. Barlow, Specialized zones of development in roots: view from the cellular level. *Plant physiology* **112**, 3-4 (1996).

217. X. Kong, G. Liu, J. Liu, Z. Ding, The Root Transition Zone: A Hot Spot for Signal Crosstalk. *Trends in Plant Science* **23**, 403-409 (2018).

218. F. Baluška, S. Mancuso, D. Volkmann, P. W. Barlow, Root apex transition zone: a signalling–response nexus in the root. *Trends in Plant Science* **15**, 402-408 (2010).

219. J. Mora-Macías *et al.*, Malate-dependent Fe accumulation is a critical checkpoint in the root developmental response to low phosphate. *Proceedings of the National Academy of Sciences* **114**, E3563 (2017).

220. D. Gutiérrez-Alanís *et al.*, Phosphate Starvation-Dependent Iron Mobilization Induces CLE14 Expression to Trigger Root Meristem Differentiation through CLV2/PEPR2 Signaling. *Developmental Cell* **41**, 555-570.e553 (2017).

221. L. Sánchez-Calderón *et al.*, Phosphate Starvation Induces a Determinate Developmental Program in the Roots of Arabidopsis thaliana. *Plant and Cell Physiology* **46**, 174-184 (2005).

222. R. Bustos *et al.*, A central regulatory system largely controls transcriptional activation and repression responses to phosphate starvation in Arabidopsis. *PLoS genetics* **6**, e1001102-e1001102 (2010).

223. T. Murashige, F. Skoog, A revised medium for rapid growth and bioassays with tobacco tissue cultures. *Physiol Plant* **15**, 473-497 (1962).

224. N. Kumakura *et al.*, SGS3 and RDR6 interact and colocalize in cytoplasmic SGS3/RDR6-bodies. *FEBS Letters* **583**, 1261-1266 (2009).

225. E. Truenit, J. Haseloff, A simple way to identify non-viable cells within living plant tissue using confocal microscopy. *Plant Methods* **4**, 15 (2008).

226. A. J. Lam *et al.*, Improving FRET dynamic range with bright green and red fluorescent proteins. *Nat. Methods* **9**, 1005-1012 (2012).

227. T. Kunkel, Microinjection into plant cells of etiolated seedlings using the Eppendorf Injectman4. Eppendorf Cell Technology application note No. 346 (2015).

228. F. J. Massey, The Kolmogorov-Smirnov Test for Goodness of Fit. *Journal of the American Statistical Association* **46**, 68-78 (1951).

229. A. G. Bengough, K. Loades, B. M. McKenzie, Root hairs aid soil penetration by anchoring the root surface to pore walls. *Journal of Experimental Botany* **67**, 1071-1078 (2016).

230. L. H. Stolzy, K. P. Barley, Mechanical Resistance Encountered By Roots Entering Compact Soils. *Soil Science* **105** (1968).

231. A. G. Bengough, B. M. McKenzie, P. D. Hallett, T. A. Valentine, Root elongation, water stress, and mechanical impedance: a review of limiting stresses and beneficial root tip traits. *Journal of Experimental Botany* **62**, 59-68 (2011).

232. H. F. Rosene, Quantitative Measurement Of The Velocity Of Water absorption In Individual Root Hairs By A Microtechnique. *Plant physiology* **18**, 588-607 (1943).

233. H. F. Rosene, Velocities of Water Absorption by Individual Root Hairs of Different Species. *Botanical Gazette* **111**, 11-21 (1949).

234. M. Cailloux, Metabolism and the absorption of water by root hairs. *Canadian Journal of Botany* **50**, 557-573 (1972).

235. W. D. Bauer, Infection of Legumes by Rhizobia. *Annual Review of Plant Physiology* **32**, 407-449 (1981).

236. A. Jungk, Root hairs and the acquisition of plant nutrients from soil. *Journal of Plant Nutrition and Soil Science* **164**, 121-129 (2001).

237. D. G. Lewis, J. P. Quirk, Phosphate diffusion in soil and uptake by plants. *Plant and Soil* **26**, 99-118 (1967).

238. I. Anghinoni, S. A. Barber, Phosphorus Influx and Growth Characteristics of Corn Roots as Influenced by Phosphorus Supply1. *Agronomy Journal* **72**, 685-688 (1980).

239. K. K. S. Bhat, P. H. Nye, Diffusion of phosphate to plant roots in soil. *Plant and Soil* **38**, 161-175 (1973).

240. D. Leitner *et al.*, A dynamic model of nutrient uptake by root hairs. *New Phytologist* **185**, 792-802 (2010).

241. J. Liu *et al.*, Closely related members of the Medicago truncatula PHT1 phosphate transporter gene family encode phosphate transporters with distinct biochemical activities. *J Biol Chem* **283**, 24673-24681 (2008).

242. D. Foehse, A. Jungk, Influence of phosphate and nitrate supply on root hair formation of rape, spinach and tomato plants. *Plant and Soil* **74**, 359-368 (1983).

243. Z. Ma, T. C. Walk, A. Marcus, J. P. Lynch, Morphological synergism in root hair length, density, initiation and geometry for phosphorus acquisition in Arabidopsis thaliana: A modeling approach. *Plant and Soil* **236**, 221-235 (2001).

244. J. Zhu, S. M. Kaeppler, J. P. Lynch, Mapping of QTL controlling root hair length in maize (Zea mays L.) under phosphorus deficiency. *Plant and Soil* **270**, 299-310 (2005).

245. H. J. Dittmer, Root Hair Variations in Plant Species. *American Journal of Botany* **36**, 152-155 (1949).

246. R. L. Green, J. B. Beard, M. J. Oprisko, Root Hairs and Root Lengths in Nine Warm-season Turfgrass Genotypes. *Journal of the American Society for Horticultural Science jashs* **116**, 965-969 (1991).

247. K. L. Nielsen, J. P. Lynch, A. G. Jablokow, P. S. Curtis, Carbon cost of root systems: an architectural approach. *Plant and Soil* **165**, 161-169 (1994).

248. T. S. Gahoonia, N. E. Nielsen, P. A. Joshi, A. Jahoor, A root hairless barley mutant for elucidating genetic of root hairs and phosphorus uptake. *Plant and Soil* **235**, 211-219 (2001).

249. T. S. Gahoonia, N. E. Nielsen, Barley genotypes with long root hairs sustain high grain yields in low-P field. *Plant and Soil* **262**, 55-62 (2004).

250. T. N. Bibikova, E. B. Blancaflor, S. Gilroy, Microtubules regulate tip growth and orientation in root hairs of Arabidopsis thaliana. *The Plant Journal* **17**, 657-665 (1999).

251. B. J. Sieberer, T. Ketelaar, J. J. Esseling, A. M. C. Emons, Microtubules guide root hair tip growth. *New Phytologist* **167**, 711-719 (2005).

252. C. M. Rounds, M. Bezanilla, Growth Mechanisms in Tip-Growing Plant Cells. *Annual Review of Plant Biology* **64**, 243-265 (2013).

253. N. H. Chua, K. Roberts, R. J. Carol, L. Dolan, Building a hair: tip growth in Arabidopsis thaliana root hairs. *Philosophical Transactions of the Royal Society of London. Series B: Biological Sciences* **357**, 815-821 (2002).

254. P. K. Hepler, L. Vidali, A. Y. Cheung, Polarized Cell Growth in Higher Plants. *Annual Review of Cell and Developmental Biology* **17**, 159-187 (2001).

255. S. E. H. Holstein, Clathrin and Plant Endocytosis. *Traffic* **3**, 614-620 (2002).

256. J. Šamaj *et al.*, Endocytosis, Actin Cytoskeleton, and Signaling. *Plant Physiology* **135**, 1150 (2004).

257. J. Šamaj, J. Müller, M. Beck, N. Böhm, D. Menzel, Vesicular trafficking, cytoskeleton and signalling in root hairs and pollen tubes. *Trends in Plant Science* **11**, 594-600 (2006).

258. S. Park, A. L. Szumlanski, F. Gu, F. Guo, E. Nielsen, A role for CSLD3 during cell-wall synthesis in apical plasma membranes of tip-growing root-hair cells. *Nature Cell Biology* **13**, 973-980 (2011).

259. A. J. Bernal *et al.*, Functional Analysis of the Cellulose Synthase-Like Genes CSLD1, CSLD2 and CSLD4 in Tip-Growing Arabidopsis Cells. *Plant Physiology* **148**, 1238 (2008).

260. F. Baluska *et al.*, Root hair formation: F-actin-dependent tip growth is initiated by local assembly of profilin-supported F-actin meshworks accumulated within expansin-enriched bulges. *Dev Biol* **227**, 618-632 (2000).

261. D. D. Miller, N. C. A. De Ruijter, T. Bisseling, A. m. C. Emons, The role of actin in root hair morphogenesis: studies with lipochito-oligosaccharide as a growth stimulator and cytochalasin as an actin perturbing drug. *The Plant Journal* **17**, 141-154 (1999).

262. S. Chen *et al.*, Anisotropic Cell Expansion Is Affected through the Bidirectional Mobility of Cellulose Synthase Complexes and Phosphorylation at Two Critical Residues on CESA3. *Plant Physiology* **171**, 242 (2016).

263. P. A. Oude Weernink, M. López de Jesús, M. Schmidt, Phospholipase D signaling: orchestration by PIP2 and small GTPases. *Naunyn-Schmiedeberg's Archives of Pharmacology* **374**, 399-411 (2007).

264. H. Kusano *et al.*, The Arabidopsis Phosphatidylinositol Phosphate 5-Kinase PIP5K3 Is a Key Regulator of Root Hair Tip Growth. *The Plant Cell* **20**, 367 (2008).

265. M. Hollander, D. A. Wolfe, E. Chicken, *Nonparametric statistical methods* (John Wiley & Sons, 2013), vol. 751.

266. M. Marzec, E. Kurczynska, Importance of symplasmic communication in cell differentiation. *Plant signaling & behavior* **9**, e27931-e27931 (2014).

267. D. I. Arnon, D. R. Hoagland, Crop production in artificial culture solutions and in soils with special reference to factors influencing yields and absorption of inorganic nutrients. *Soil Science* **50**, 463-483 (1940).

268. H. J. Kennedy *et al.*, Glucose Generates Sub-plasma Membrane ATP Microdomains in Single Islet β-Cells: Potential Role For Strategically Located Mitochondria. *Journal of Biological Chemistry* **274**, 13281-13291 (1999).

269. J. Berg, Y. P. Hung, G. Yellen, A genetically encoded fluorescent reporter of ATP:ADP ratio. *Nature Methods* **6**, 161-166 (2009).

270. H. Imamura *et al.*, Visualization of ATP levels inside single living cells with fluorescence resonance energy transfer-based genetically encoded indicators. *Proceedings of the National Academy of Sciences* **106**, 15651 (2009).

271. I. Kotera, T. Iwasaki, H. Imamura, H. Noji, T. Nagai, Reversible Dimerization of Aequorea victoria Fluorescent Proteins Increases the Dynamic Range of FRET-Based Indicators. *ACS Chemical Biology* **5**, 215-222 (2010).

272. T. Tsuyama *et al.*, In vivo fluorescent adenosine 5'-triphosphate (ATP) imaging of Drosophila melanogaster and Caenorhabditis elegans by using a genetically encoded fluorescent ATP biosensor optimized for low temperatures. *Anal Chem* **85**, 7889-7896 (2013).

273. V. De Col *et al.*, ATP sensing in living plant cells reveals tissue gradients and stress dynamics of energy physiology. *Elife* **6** (2017).

274. M. Nakano, H. Imamura, T. Nagai, H. Noji, Ca2+ Regulation of Mitochondrial ATP Synthesis Visualized at the Single Cell Level. *ACS Chemical Biology* **6**, 709-715 (2011).

275. C. P. Voon *et al.*, ATP compartmentation in plastids and cytosol of Arabidopsis thaliana revealed by fluorescent protein sensing. *Proceedings of the National Academy of Sciences* **115**, E10778 (2018).

276. S. A. Arisz, C. Testerink, T. Munnik, Plant PA signaling via diacylglycerol kinase. *Biochimica et Biophysica Acta (BBA) - Molecular and Cell Biology of Lipids* **1791**, 869-875 (2009).

277. X. Zhang, R. Henriques, S.-S. Lin, Q.-W. Niu, N.-H. Chua, Agrobacterium-mediated transformation of Arabidopsis thaliana using the floral dip method. *Nature Protocols* **1**, 641-646 (2006).